# Control Strategies for Grasping and Holding Deformable Items Using a Gripper on a Robotic Arm

Joris Pijnacker

Master of Science Thesis

TU Delft Delft University of Technology

Delft Center for Systems and Control

# Control Strategies for Grasping and Holding Deformable Items Using a Gripper on a Robotic Arm

Master of Science Thesis

For the degree of Master of Science in Systems and Control at Delft University of Technology

Joris Pijnacker

September 9, 2018

Faculty of Mechanical, Maritime and Materials Engineering (3mE) · Delft University of Technology

# Abstract

Because of the increasing e-commerce volume, resulting in increasing demands on the speed of delivery, logistical processes become more and more automated. Order picking is one of the last tasks that is done by humans in warehouses, because humans are flexible with respect to the large variability and changeability in items. However, it is a labour intensive and monotonous task, resulting in fatigue and a shortage of order picking personnel. This motivates the development of automated pick-and-place systems.

One of the challenges for such systems is the heterogeneity of items. In warehouses there is a big diversity in items so the system has to be able to deal with all of them. Another challenge is dealing with items that are deformable. Current systems often make use of suction cups but integrating sensors that can be used to handle deformable items is hard. Fingered robotic grippers have more potential in grasping these kind of items, but grasping deformable items is one of the least addressed topics in robotics. Therefore, the objective of this thesis is to design a control strategy for a fingered robotic gripper to grasp and hold deformable items in a pick-and-place task.

Inspired by the underlying principles that humans use to execute a pick-and-place task, a multi-level controller is proposed for a three-fingered gripper with capacitive pressure pads. The multi-level controller consists of a low-level computed torque controller and a high-level numerical optimisation based extremum seeking controller. The computed torque controller uses an internal model of the kinematics and dynamics, which is derived with screw theory, to compute the torques required to comply with the fundamental grasping constraint and the setpoint on the gripping force. The controller is tuned in such a way that the grasp quality is maximised, given a constant reference gripping force. Because of the fact that the properties of the items are unknown, an intelligent control system has to be able to determine the gripping force setpoint autonomously. This is the task of the high-level controller, that uses tactile sensors to derive the slip. This slip is used to determine the setpoint on the gripping force that the low-level controller has to follow, while maximising the grasp quality and not damaging the products as a result of applying excessive gripping force.

The proposed control strategy is tested and tuned in a simulation environment. The pick-and-place task is executed for the products from a virtual product inventory. The controller

is optimised with respect to the control goal on a wide variety of deformable items. Designing controllers according to the proposed principle will increase the diversity of items that can be handled in a pick-and-place environment, while increasing the quality of the grasp and minimising the risk of damaged products.

# Table of Contents

# List of Figures

# List of Tables

# Preface

This document is the final delivery of my Master of Science graduation thesis. The idea of doing my thesis on this subject came after a discussion at Vanderlande. By explaining my background (Systems&Control and BioRobotics) they proposed to focus on Smart Item Robotics (SIR). This was perfect for me because the topic is on the boundary of both Masters. The focus within SIR up till then was on the implementation of suction cups but not all products can be picked and sensing and identification of items is limited. Examples of difficult products are non-rigid and porous items. The challenge for now is to conceive a robotic gripping system that is capable of picking the items that already can be picked with the suction cup, extended with deformable items, in a stable and controlled way. This thesis describes the design of a control architecture that is able to do this with a fingered robotic gripper.

# Acknowledgements

During this project I received support from a lot of people. I would like to thank them all. Specifically, I would like to thank Erik Steur, my supervisor at Delft University of Technology from Systems&Control for the weekly discussions that kept me focussed and helped me in prioritising my tasks. Also thanks to Martijn Wisse at Delft University of Technology from BioRobotics for the constructive feedback on the early versions of the assignment descriptions and the reports. Besides that, I would also thank all the people at Vanderlande for their time and the knowledge they shared with me. Special thanks to Evert van de Plassche within Vanderlande for the weekly meetings that helped me viewing the system from a higher level. Also the out of the box thinking during some brainstorm sessions helped me funding my choices. Also thanks to Robbert Dijkstra from Vanderlande for taking me up in his team and the feedback on reports and presentations. Finally, I would like to thank all the other graduation students and colleagues from Vanderlande for the nice discussions we had about my project and other subjects, I really enjoyed my time.

Delft, University of Technology — Joris Pijnacker
September 9, 2018

# Chapter 1

# Introduction

## 1-1 Background

Because of the increasing e-commerce volume, the increasing demands on the speed of delivery and technological advancements, logistical processes become more and more automated. In production environments like car manufacturing, items have to be displaced from a stock to the assembly. This is a very repetitive task and because of the fact that the items are always the same, a customised robotic solution is devised for this. This contrasts to a warehouse environment that contains automatic storage and retrieval systems that consists of storage racks with shuttles in between in order to facilitate order picking, with limited robotic applications due to the complexity of the problem.

## 1-2 Problem Description

In order picking, a box with items is transported to an order picking station (in warehouses this box is called a Transport Storage Unit (TSU), see Figure 1-1). There one or multiple of the objects from the box need to be placed in the order box. This is the pick-and-place task. A schematic overview of the pick-and-place set-up is shown in Figure 1-2. The pick-and-place station needs to be able to handle the big diversity of items that the warehouse contains. Besides that, the inventory of the warehouse can change on a daily basis. This requires flexibility in item picking. These are the reasons why order picking is one of the last tasks that is done by humans in a warehouse. However, this is one of the most labour intensive tasks in internal logistics [11]. Besides that, it is a very monotonous task that induces fatigue [12]. Finally, there is a global shortage of order picking personnel [13]. This all induces high costs: Vanderlande calculated that the average labour costs of one single pick in a robotic solution is only 50% of the costs of a manual solution. So, as within the production environments, higher degrees of autonomy are also introduced in warehouses [2], to lower the costs and increase the capacity and efficiency of warehouses.

**Figure 1-1:** A TSU with a product placed at the center.

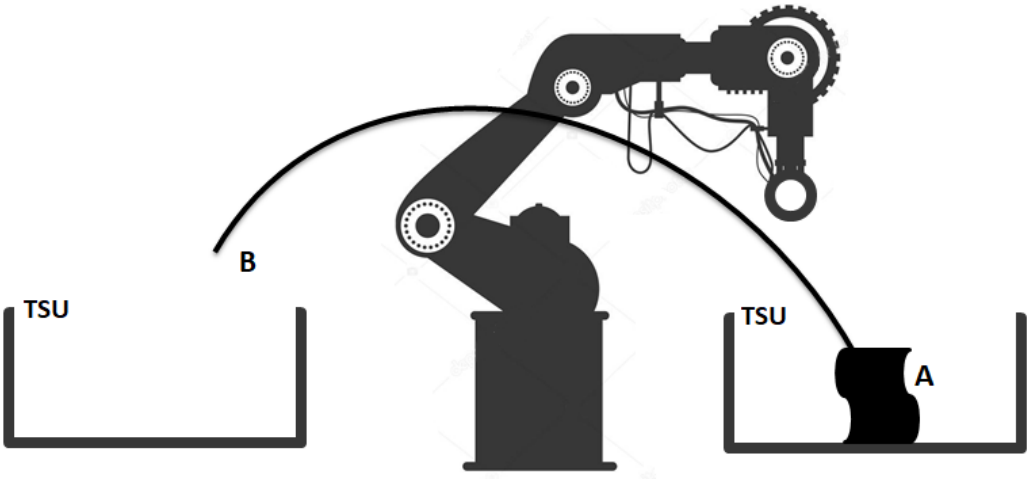


**Figure 1-2:** The schematic overview of the system: items have to be displaced from A to B using a gripper on a robotic arm.

## 1-3 Challenges

Typically, robotic applications are effective if tailored grippers are developed for a specific task. This holds for homogeneous environments in which parts are always the same, for example in car manufacturing. One of the challenges in the application of order picking in a warehouse is the heterogeneity because, ideally, all items present in the warehouse can be picked by one single gripper, which currently is a human, also if new items are added to the inventory or if existing items change dimensions. Because of this uncertainty in the environment, the system needs to be autonomous and intelligent [14]. The robotic gripping system can be made autonomous by making use of adaptive strategies.

Categorisation of the wide variety of items is needed in order to identify the challenges of specific categories. GS1 is an international organization that provides standards for companies working in retail, healthcare and transport and logistics [15]. The standard from GS1 is a commonly adopted categorisation in industry and will therefore be used here. The Global Product Classification (GPC) from GS1 classifies products by grouping them into categories

based on their relationships to other products [16]. Products in a warehouse form a subset of this. The classification within this subset is shown in Appendix A. There the product categories are described, examples are shown and the codes according to the GPC are displayed.

The robotic gripping system needs to be able to pick up all items within these categories. A commonly adopted solution in industry is the use of a suction cup to pick-and-place objects. Previous research showed that suction cups are relatively cheap, easy to implement and capable of lifting a modest number of different items [17]. However, it is hard to manipulate the suction cup, once it is detected that items are slipping or close to a release. It is required to detect these events by making use of sensors, and additionally act on it such that the items are not lost. Attempts to introduce these sensor modalities in suction cups can be found in literature [18] [19], but still not all items can be picked up. Boxes with lids can for example not be picked up. Also, porous items give problems because the vacuum cannot be maintained. Nets give problems because of the nature of the surface that does not allow for a closed sealing. Finally bags give problems because of the high deformability during movement; the inertial effects and single contact point with the suction cup causes the grasp to fail [2]. So, to handle all item categories from the list, the suction cup alone is not a good candidate. The ultimate goal is to be able to pick up all items with a single dedicated gripping solution. One of the challenges is to find a gripping solution that is capable of coping with this wide variety in items, especially deformable items. Deformability here means that the object changes volume and shape once an external force is applied [20]. Crushable objects are not regarded as deformable items because they can be regarded as rigid after crushing. Grasping deformable objects is one of the least addressed topics in robotics and is a very active research field in the past years [20] [21] [22] [23].

## 1-4 Requirements of the system

Based on industry standards and application specific demands, the following general requirements (G) for the robotic pick-and-place station are set up:

G1. All categories from the GS1-GPC list need to be picked up.

G2. The size of the items is between 25 $mm \times 25\ mm \times 1\ mm$ and 400 $mm \times 400\ mm \times 200\ mm$ (length $\times$ width $\times$ height).

G3. The items weigh between 0.050 $kg$ and 2 $kg$.

G4. The items are picked from a TSU as shown in Figure 1-1, which has outer dimensions 600 $mm \times 400\ mm \times 300\ mm$ (length $\times$ width $\times$ height).

G5. The trajectory of the gripper is fixed and given. It is designed such that the cycle time of one pick-and-place action is under 3 seconds.

G6. Constant monitoring of the grasp is required. In this way the loss of a product can immediately detected instead of finishing the task without a product being attached.

G7. Minimal a priori knowledge of the products is used in the system. The reason for this is that the inventory of the warehouse can change on a daily basis.

G8. In order to not damage the products, the gripper has to apply minimal gripping force on the item. Given the properties of the item, the contact surface and the trajectory, a theoretical minimum gripping force can be calculated. This value is unknown to the controller but it can be used to calculate the excess of gripping force that the system uses. This excess has to be minimal.

Next to the application specific requirements, an extra requirement is added with respect to the performance of a grasp. This requirement allows the devised control strategy to be tuned optimally with respect to a qualitative measure.

G9. The *grasp quality* should be maximised. The *grasp quality* is a measure that indicates the relation between the disturbing forces and moments on the grasped object that can be withstood by the gripper. If higher disturbances can be withstood, the quality of the grasp is higher.

## 1-5 Research Focus

To increase the quality of this contribution, this research has to focus on a subset of the general requirements from Section 1-4. This thesis therefore only focusses on a selected part of the complete system as will be explained next. The requirements for this specific project are listed after that because these are different compared to the requirements of the complete system.

This research only focusses on deformable items because these are the items that give problems in current industrial applications. The item categories from the GPC are classified on deformability in Figure 1-3. The non-packed category both contains non-deformable and deformable items, therefore it is present in both squares. Examples in this category are shown. Because the focus is on deformable items, this project will only focus on the nets, bags and deformable items from the non-packed category.

Vanderlande showed that small items can best be handled by suction cups. The potential for fingered grippers lies in the medium sized items. Therefore, only medium sized objects are taken into account. Medium items have a size between 60 $mm \times 60\ mm \times 60\ mm$ and 120 $mm \times 120\ mm \times 120\ mm$. The lower boundary is based on the item list used within Vanderlande that devises between small and medium items. The upper boundary is derived from the workspace of the human hand, that, on average, can pick up items with a transverse area of up to 120 $mm \times 120\ mm$ [24].

Medium items from the item list used within Vanderlande do not weigh more than 1 $kg$ so this is the maximum weight that is taken into account.

This research only investigates fingered grippers because previous research shows that this is a good alternative for suction cups [17]. Also, this type of grippers is widely used in industry when suction cups do not suffice. The focus on only one gripping principle is required to investigate the full potential of that principle, before looking at possible combinations with other gripper principles.

In order for the robot to follow the predefined trajectory, it is not required to have a wrist joint. A wrist joint would add an extra degree of freedom to the system. This extra degree

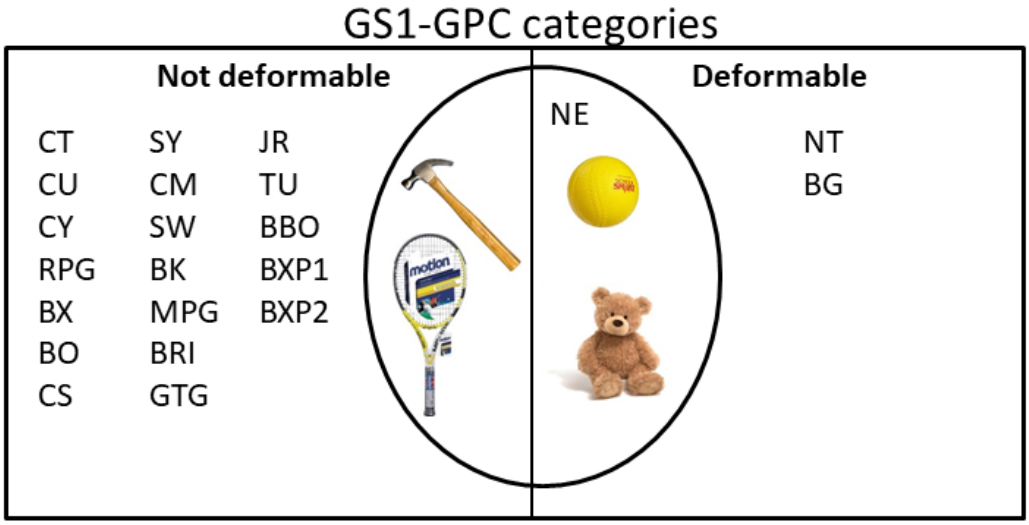


**Figure 1-3:** The GS1-GPC categories classified by deformability.

of freedom is not required to execute the pick-and-place task and explore the potential of the smart gripping system, so a wrist joint is not considered. The result of this focus is that items can only be picked from above.

The items are present at the center of the TSU. If multiple items are present at the pick location, the system selects the most accessible product that will be at the center of the TSU. If no item is present at the center of the TSU, systems exist that displace items to the center again. So, this assumption does not limit the operation of the system.

The vision algorithm is put outside the scope of this project. It is assumed that the system knows where the item is located and the approximate size of the item such that the gripper can be opened accordingly. Besides that, vision algorithms are investigated thoroughly and much more improvements in grasping can be made by investigating the use of other sensor modalities at the contact locations [21] [22].

Placement of the items is not considered, it is only about grasping and holding of objects. According to Ken Goldberg, director of the Autolab at Berkeley, grasping is the most critical part of the manipulation process [22]. If the item cannot be grasped, it is impossible to execute the other components of the pick-and-place task. However, it has to be noted the the sensors present in the gripper can be beneficial during placement because the moment of touch-down can be sensed.

Because of this focus, some of the general requirements for the system are adapted for this project. The numbers of the adapted specific requirements (S) correspond to the general ones. Besides that, new requirements arose:

S1. The deformable categories from the GS1-GPC list need to be picked up.

S2. The size of the items is between 60 $mm \times 60$ $mm \times 60$ $mm$ and 120 $mm \times 120$ $mm \times 120$ $mm$ (length $\times$ width $\times$ height).

S3. The items weigh between 0.050 $kg$ and 1 $kg$.

S10. A fingered gripper will be used.

S11. The gripper does not have a wrist joint.

S12. The objects need to be picked from the center of the pick TSU which is a known location. Because of the fact that this location in known, there is no need to use vision sensors.

S13. Only the grasping and holding phases of the pick-and-place task need to be performed.

## 1-6 Research Objective

Given the challenges and the requirements, the following research objective is set up:

*Design a control strategy for a fingered robotic gripper to grasp and hold deformable items with minimal gripping force and maximal grasp quality while moving over a desired trajectory using active feedback*

## 1-7 Contribution

This thesis shows how a human inspired multi-level control strategy is used to pick and place unknown, deformable items. The control strategy uses a low-level, model based reference follower and a high-level gripping force setpoint generator that makes use of tactile sensory information. The separation between the low-level and high-level controller allows for individual optimisation of controller parameters with respect to distinct control goals. The integration of a sensor based setpoint generator allows for controlled grasping without damage. The focus on deformable items in this thesis is one of the main contributions because grasping deformable items is one of the least addressed topics in robotics. Finally, the fact that unknown items can be handled makes this a perfect control strategy to be utilised in pick-and-place tasks because of the variability and changeability of items in warehouses. Designing controllers according to the proposed principle will increase the diversity of items that can be handled in a pick-and-place environment, while increasing the quality of the grasp and minimising the risk of damaged products.

## 1-8 Outline

The robotic gripping system consists of a gripper with sensors and a controller. Details on the hardware are explained in Chapter 2. The goal of the controller is to actuate the gripper based on sensory information such that it can pick up and hold the items without damaging them. The control system uses an internal model and a controller that is able to follow setpoints on positions and gripping force. The part of the controller that is responsible for that requires a model. The modelling approach is given in Chapter 3. Besides this part of the controller, there needs to be a part that is responsible for determining the setpoints that have to be followed by the first part. This is based on sensory information and has the goal of adapting to specific objects. The control architecture is further elaborated on in Chapter

4. To be able to judge the controller with respect to the requirements, there is a need for a testing environment. The development of this environment is explained in Chapter 5. The description of the experiments that are performed in the test environment can be found in Chapter 6. This chapter also discusses the results of these experiments and discusses them. Finally, Chapter 7 covers the conclusions and recommendations.

# Chapter 2

# Background on the Robotic Gripping System

This chapter introduces the robotic grasping system that is considered. First the grasping process is analysed. After that grippers and sensors are described. In the last section of this chapter the connection with biology, especially the human, is made. The underlying principles in the human brain are an inspiration for robotic applications.

## 2-1 Grasping

A grasp can be described as an object that is being gripped by the end-effector of a robotic gripper [25]. Grasping indicates an action of a gripper on an object by preventing its motions relative to the gripper, possibly in the face of disturbance forces acting on the object [26]. Grasping thus aims at firmly stabilising the object with respect to the gripper, in contrast to manipulation, which is the ability to move objects from one equilibrium point to another [27].

The different phases in grasping can best be illustrated for the case of a fingered gripper because the different phases can be visualised individually. The grasping process starts when the object is positioned nearby the fingered gripper. The first phase in grasping is approaching the item with the gripper. After that the gripper closes by reducing the distance between the fingers. This results in a contact with the object. After the first contact is made the force can be increased (third phase) up to a certain value where the object is secured. Once the object is secured, the gripper together with the object can start to move. Once at its destination the last phases of the grasping process can be initiated: decreasing the force, releasing and moving away. During all phases sensors can provide information to monitor the grasping process. A similar description of the grasping process is presented in [2], but then for grasping in general. A visualization of the grasping phases can be found in Figure 2-1. This thesis only focusses on stage 2 until 5.

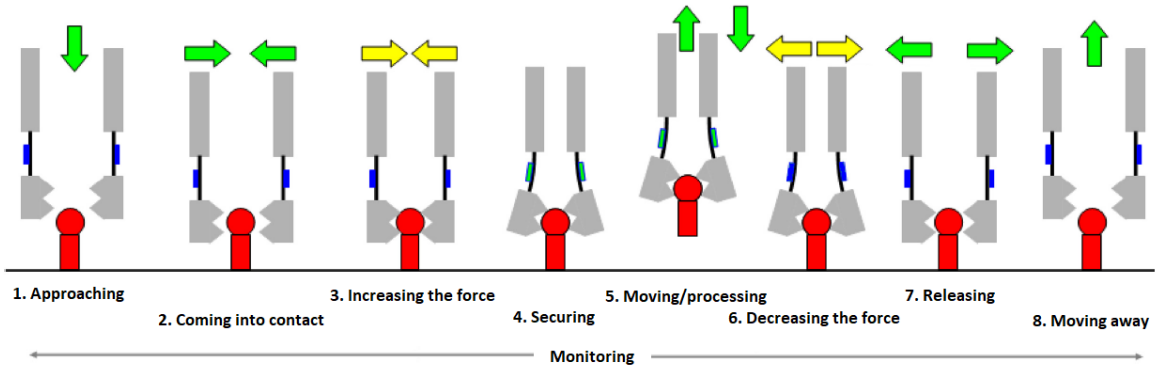


**Figure 2-1:** Phases of the grasp process, adapted from [1].

## 2-2 Gripper

### 2-2-1 Gripping Principle

A gripping principle can be defined as "the physical principle which causes the force effect necessary to get and maintain the part in a relative position with respect to the gripping device" [28]. Fingered robotic grippers are mechanical grippers, in contrast to, for example, magnetic grippers. Within mechanical gripping there is a division between force closure and form closure. Force closure can be accomplished by using a friction gripper. A jaw gripper is used to do form closure. Both principles are shown in Figure 2-2 and explained below:

1. Friction gripper: applies a normal force on the object that has to be grasped. Friction at the surface of the object results in a force that compensates for gravity and dynamical forces resulting from accelerations. The grasp fails if the normal force applied by the gripper is not sufficient.

2. Jaw gripper: is formed such that the object is not falling, independent of the applied forces by the gripper.

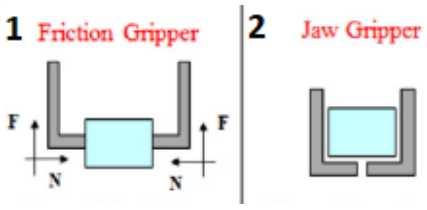


**Figure 2-2:** Two forms of mechanical grippers, adapted from [2].

The difference between force closure and form closure is explained by referring to Figure 2-2. The way a gripper prevents the object from moving depends on the working principle of the gripper. In a force closure, the gripper clamps the object being grasped actively. "A fixed set of contacts on a rigid body is said to exhibit force closure if the maintenance of the body's equilibrium requires the application of an externally applied forces" [29]. So for any external force on the object, there exists a set of gripper forces such that all friction constraints are

fulfilled [30]. This is a theoretical description because nothing is said about the physical limits of the fingers. So theoretically it is true that ANY external wrench can be withstood but this may require infinite actuation forces.

In contrast, form closure does not depend on the applied forces of the gripper but on the shape of the gripper. "Form-closure is the ability of a hand to prevent motions of the object, relying only on unilateral, frictionless contact constraints" [26]. This type of grasp is stable regardless of the external force applied to the object [29].

Jaw grippers offer higher process reliability and positioning accuracy compared to friction grippers, at the cost of low shape flexibility because the shape of the fingertip is customised with respect to the item shape. For the pick-and-place application of this project, it is not doable to make a gripper for every product present in the warehouse because of the diversity of items present there. Therefore it is necessary to use friction grippers in situations with high item heterogeneity [31]. This finishes the motivation for using a gripper with force closure (a friction gripper) in the sequel of this project.

### 2-2-2 Number of Fingers

The more fingers a robotic hand has, the bigger the hand becomes. A big hand is not desired because versatility is required in the warehouse application. Besides the size argument, also the costs increase when the number of fingers increase [32]. On the other hand, more fingers increase the number of products that can be picked. A balance has to be found between the number of fingers and performance. [33] tries to quantify this. It is stated that if one classifies the gripping abilities of a five-finger hand as 100%, a four-finger hand has 99% of this ability, a three-finger hand 90% and a two-finger hand only 40%. These numbers are just a quantitative description of a classification. The improvement in gripping ability by using a three-finger hand instead of a two-finger hand is greater than the improvement when going from a gripper with three to four fingers. It has to be noted that the scale from [33] is a poor quantification and does not have any connection with the item list, but it is an attempt to quantify the intuition that goes with this argument.

Next to this, [34] states that grippers with three fingers generally have more than enough contacts points to manipulate the object and to withstand external wrenches on the object. This is based on practical experience of the authors and can not be regarded as a general statement. However, it is a second argument to use a three-finger gripper.

In the case of picking up deformable items, having three fingers is advantageous compared to having two fingers because the contact area between the fingers and the product is higher when applying the same gripping force because the deformable product can wrap itself around the fingers. This is not possible with a two-finger gripper. The contact area per finger for a four-finger gripper with respect to a three-finger gripper is more or less the same so there is no advantage of using a four-finger gripper over a three-finger gripper in this context. This is shown in Figure 2-3. Besides that, four fingered grippers are not very common in industry so a five fingered gripper is the next option. This is even more complex while having the same relative contact area. The control is far more complex so this is not suited for this problem.

The arguments mentioned above try to maximise functionality with a minimal number of fingers. This can be seen as a minimalistic approach: "the realization of some desirable

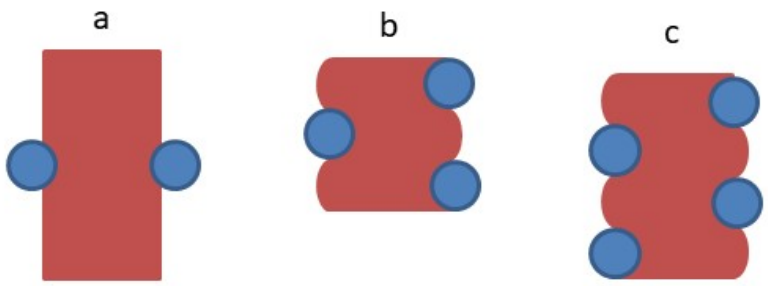


**Figure 2-3:** Contact area for different number of fingers: a)two, b)three and c)four fingers.

grasping or manipulation features by purposeful design of mechanisms that have no intentional resemblance with any biological system" [30]. This opposes the anthropomorphic approach which aims at replicating the capabilities of the human by imitating the mechanical structure. The latter suffers from problems with accuracy and the size of the actuators while the former is much more in line with the current research to optimally make use of the limited hardware capabilities. Besides that, by mimicking the human hand, one also gets other functions which are not desired for the task. This implicates that a human also would require only three fingers for basic tasks such as pick-and-place tasks.

### 2-2-3 Type of Actuation

Within fingered robotic grippers there is a branch with fully actuated hands (one motor for every joint) and underactuated hands (less Degrees of Actuation (DOA) compared to Degrees of Freedom (DOF)). Flexibility in grasping can be achieved by having full control of a fully actuated hand or having less control on underactuated hands. The underactuated hand is self-solvable in this case because the fingers passively form around the object whereas in the first case the control system is actively controlling this. This can also be described as "mechanical intelligence" [35], whereas a fully actuated hand has controller intelligence. In order to introduce this intelligence to the gripper, full knowledge of the system states is required, as well as it should be able to control all joints individually. This opposes the idea of underactuated grippers.

Previous research regarding gripping in warehouse environments considered fully actuated grippers [17]. Together with the supervisory team it was decided to further develop knowledge regarding this type of actuation and hence use a fully actuated gripper.

### 2-2-4 Conclusion

Force closure in the application of deformable items with unknown properties is needed because form closure requires customised grippers which is not possible. Mechanical grippers are able to do this, specifically the friction gripper.

**Figure 2-4:** The Schunk Dextrous Hand (SDH), from [3].

Because of the balance between number of fingers and capability, human inspiration and relative contact area, three fingers turn out to be best suited for this application.

The Schunk SDH is a three fingered, fully actuated friction gripper. Contacts within Schunk within Vanderlande led to the choice of Schunk in order to be able to quickly perform experiments in a later phase of the project. This gripper will be used as a reference in the sequel of this thesis. The gripper is shown in Figure 2-4.

## 2-3 Sensors

Tactile sensing is essential for automating industrial tasks, such as the pick-and-place task, currently done by humans [36]. Because vision is not considered, there is a need for local detection of contacts and shapes in case of gripping deformable items. The importance of local sensors can be explained by looking at the task of opening or closing buttons when your hands are cold. It becomes clear that this is hardly possible. This is not, as one might think, because of the muscles that are anaesthetised, it are the sensors present in the human hand that are not working properly any more [34]. From this one can already feel that tactile sensing is required. These sensors can also be used to identify the (mechanical) properties of the objects, which is essential if robots have to handle unknown objects reliably in unstructured environments [10], which is the goal of this project.

### 2-3-1 Sensing Principles

Figure 2-5 shows two sensing principles to measure contact forces. The fingertip sensor is an external sensor and measures the contact forces directly. The finger sensor in an internal sensor and measures this forces indirectly. Internal sensors are very well suited for monitoring forces outside the gripper's (or finger's) system boundary like gravity, acceleration and contact forces. However, forces inside the gripper cannot be detected [2]. The external sensor (fingertip) is better suited for this. Besides that, the accuracy of internal sensors is lower [33]. This comes from the fact that transformations are needed to convert the measured information from a local to a global coordinate frame because inertial terms are involved. External sensors further have the advantage that they cover larger areas and that the point of contact is explicitly measured. Internal force sensors are not required because the torques inside the joints of the gripper are known.

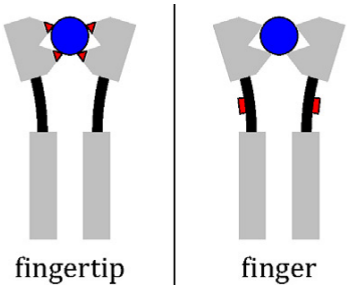


**Figure 2-5:** Two principles of tactile sensing, adapted from [2].

### 2-3-2 Transducer Principles

The transducer principles that are available for the arrays of tactile sensors are capacitive, piezoelectric and resistive [37]. [37] gives arguments to use capacitive sensor pads: the bandwidth is less compared to the other two, but it is easier to integrate and they are widely used in distributed tactile sensors. Besides that, the chip needed for acquisition and conditioning is commercially available and small, whereas the chip for a piezoelectric sensor has to be custom made and cannot be integrated on small devices. A final disadvantage is that it is frail compared to the piezoelectric variant [38]. The resistive variant is also cheap, easy to construct and requires only little amount of simple electronics [10]. However, it is also frail and temperature sensitive [38]. [39] uses a resistive sensor array with low complexity, low cost and easy electronics to classify which products from a set of 10 products is being gripped. This was possible because the products were very diverse and the information from the resistive pads sufficed to classify the products in such diverse product groups. In case of a wider variety of products and higher demands on sensor quality the capacitive array offers increased performance. Because of these advantages, and the fact that capacitive pressure pads are present at the Schunk SDH gripper, these sensors are selected to be used.

### 2-3-3 Measurable quantities

Measuring shear (for example by means of strain gauges) is often considered very to be important but it is not clear how this information could be used in manipulation [10]. This

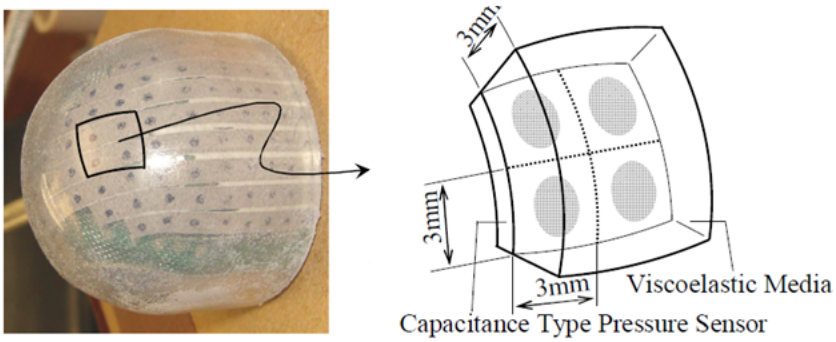


**Figure 2-6:** A schematic overview of a capacitive pressure cell, from [4].

probably originates from the desire to imitate the design of the human skin. An example of a bio-inspired implementation of shear sensor based on the nailbed of human fingers can be found in [40]. Slip and contact point information are information types that are much more important because they give information about the grasp kinematics. Shear could be used to determine the friction coefficient. However, this is also possible by vibration sensing and more simple, by inducing small slips while measuring the resulting forces, just as humans do (see Section 2-4).

By using an array of capacitive sensors, it is possible to measure the total normal force acting on the finger. Also, the normal direction of the contact area can be determined. The size of the contact area is an indication for the amount of external torque that is needed to rotate the object (rotational slip). The wider this area, the more torque can be sustained by the contact [10]. Besides that, the Center of Pressure (COP) can be calculated as being the average location of all individual pressure components. A method for extracting the slip based on the variations in this COP is presented in [4]. Slip can also be defined as the time derivative of the tangential force [41]. Intuitively this can be explained by the fact that generally there is a sudden drop in the shear force between static friction and dynamic friction. This indicates that there is a delay. Therefore slip detection is relatively slow and it is better to use the change of the COP for example. [42] tries to solve this by determining the so called initial slip using the change in voltage between two conductive plates. This is called initial slip because it is the partial slip between an object and the gripper fingers just before the object actually starts to slip [43]. It is required to post-process the signal to determine if a contact is slipping or not. Besides that, a threshold on the intensity of this transform is required which is very material dependent and has to be determined by trial and error. In [42] it is shown that the change in the COP detects slip at the same moments as the initial slip sensor, but with a high-speed response. This makes this sensor much better suited for real-time control applications. The working principle of such a sensor is shown in Figure 2-6. The array consisting of capacitive pressure cells is present on the fingertip. One cell is depicted next to it. The cell contains a viscoelastic medium. Once the pressure on the cell is increased, the capacitance of the cell changes. The measurement of the single capacitances over the fingertip gives the distribution of normal forces on the finger.

### 2-3-4 Conclusion

To determine the properties of the unknown objects, presence detection is not enough. External fingertip sensors will be used for tactile sensing. It is not required to measure shear. The normal force vector, COP and slip based on the COP are much more important to measure. The capacitive tactile array is capable of doing this and is therefore selected to be used in this thesis.

## 2-4 Human Grasping and Manipulation

Because of the fact that humans also have tactile sensors on the fingers that register variables such as place of contact, contact force and slip, a look at principles that humans use to handle this is useful [42]. High manipulation performance for a great diversity of objects can be achieved by making use of behaviour-based control algorithms and biologically-inspired concepts regarding sensing and actuation in mechanical grippers [44]. Therefore this section describes the principles used by humans to grasp and manipulate, which can serve as inspiration for controller design.

### 2-4-1 Human Cognition

In biology the following mechanisms are important when executing motion tasks [45]:

1. multi-level, hierarchical control: acting based on a planning to achieve higher level goals
2. Learned activities: activities that become automatic over time
3. Reflex actions: unconsciously controlled actions

Grasping and holding of objects with unknown shapes, is a new situation for every object. The learned activities can only partly be used, because some of the learned activities are generalisable and can be transferred over multiple objects. Reflex actions can be beneficial when an object is slipping out of hands: a reflex action then is the increase of the grasping force.

### 2-4-2 Human Sensors

In order for a gripper to reach the same dexterity level as humans, the gripper needs to be able to 'feel' and to adapt to a variety of objects [44]. Table 2-1 gives an overview of the tactile receptors in the human skin. FA stands for Fast Adapting and SA for Slow Adapting [10], this can also be seen in the Frequency Range column. The Field Diameter indicates the size of the active area. One can infer that different types of sensors are used to detect different types of information. Signals from multiple tactile afferents provide information about the direction, timing, magnitude and spatial distribution of fingertip forces, the local shape of the contact surface, and the friction between the skin and the object [46]. [47] showed that the earliest stages of slip were detected by the FAI receptors. The FAII receptors were

**Table 2-1:** Properties of the mechanoreceptors in the human skin, adapted from [10].

| Receptor type | Field Diameter [mm] | Frequency Range [Hz] | Sensed Parameter |
|---|---|---|---|
| FAI | 3-4 | 10-60 | skin stretch |
| SAI | 3-4 | 0-30 | compressive stretch |
| FAII | >20 | 50-1000 | vibration |
| SAII | >10 | 0-15 | directional skin stretch |

responsible for detecting the breaking of contact. It is worth noting that the specifications of these sensors, in technological terms, is quite low. For example, the latency in the Central Nervous System (CNS) is much higher compared to the latency in robotic systems [48]. The human has to account for this aspect by using an intelligent control strategy based on a good internal model. This feature of the human brain is discussed next.

### 2-4-3 Grip Force Adjustments

Humans use an initial estimate of the weight based on the size-weight principle: the smallest of two equally weighted objects is assumed to be lighter [46]. Based on this estimate a first approximation of the required normal forces is applied. This can however be incorrect so a second mechanism is required. [49] showed that humans adjust the grip force such that the resulting lifting force is slightly greater than that is required to compensate for the gravitational force of the object. Also in case of different frictional surfaces on the same object, the applied normal force is adjusted to the local friction coefficient [50]. This is all accomplished before lift-off. The underlying principle of this is the fast estimation of the friction coefficient. This is partly based on pre-knowledge: from the visual information it is possible to make a rough estimate of the frictional properties of the object to be grasped. Besides that, we update this estimate based on small controlled frictional slips in an early part of the load phase [51]. To this extend the normal force is increased until the object is lifted. After this the normal force is increased a little bit more up to the safety margin [52]. This safety margin is constant over a large range of object weights (more than 0.050 $kg$) [53]. For the robotic application, the use of pre-knowlegde is limited and also not considered in this project. However, the controller in this project could benefit from the approach of humans to estimate the local friction coefficient.

Even more strikingly, [54] showed that humans also adapt to acceleration dependent inertial loads. During upward accelerations (when the total load is increased by the inertial load) the grip force increases, during downward movement (when the inertial load compensates the gravitational load) the grip force decreased, as shown by [52]. [55] even showed that the increase and decrease of the grip force persisted when the initial grip force was set much higher than required to compensate gravity (when it actually is not required because the force is already high enough). This shows that the CNS is able to predict the forces that are induced by the motion and compensates for that based on an internal model. These grip force adjustments are also called Anticipatory Postural Adjustments (APAs) [56]. This specification of motor commands in advance of the movement can be seen as feed-forward control. Some [57] even say that this is the only way to achieve motion of objects because the reflexes of the human are too slow, but there is no consensus on this issue yet. This

principle can be an inspiration for the control principles in the application of this project where the dynamic model of the gripper and object are updated and used to anticipate on coming actions. Feedback control can subsequently be used to increase the precision. The principle of the parametric adaptation of the internal model based on errors detected between predicted feedback and received feedback is also used by the CNS [46].

### 2-4-4 Conclusion

For grasping unknown objects, it is beneficial for the robotic application to imitate the multi-level control of humans to set high level goals. Learning is not considered in this project. Reflex actions certainly are needed in the robotic application to prevent falling while estimating the properties of the object.

The CNS compensates for the high latency in the sensor network by making use of an internal model. This approach has potential to greatly improve the performance of the robotic application.

The way humans acquire information between the first contact and lift-off is partly based on visual information, hence this is not possible for this project as the visual system is out of scope. However, the way the knowledge is updated during movement, for example by inducing small slips to estimate the friction coefficient, will be an inspiration for the controllers in this project. Also, the APAs can be imitated to act based on the estimated information.

## 2-5 Conclusion

Concerning the question on what type of fingered gripper is desirable, it can be concluded that a three fingered, fully actuated gripper will be used. The Schunk SDH hand will be used as a reference. The sensors that will be used are capacitive pressure sensors. By placing multiple of those cells on the fingertip, the distribution of forces over the finger can be determined. Inspired by the human control strategy during grasping, a multi-level control approach is ideally used on the robotic gripping system. Also, the anticipatory actions that the human utilises can be used in the robotic gripping system by making use of model knowledge and feedforward actions.

# Chapter 3

# Modelling

Inspired by the human controller, the controller of the robotic gripping system relies on a model of the system that it controls. Therefore, the kinematics and dynamics of the system need to be described. First the modelling approach will be described. After that the kinematics and dynamics of the system will be derived.

## 3-1 Modelling Approach

Screw theory will be used to describe the kinematics and dynamics of the grasp. Screw theory is often used in literature on grasping [58] [59] [25] [60] [61] [62], mainly because of two reasons [59]. The first is that is gives a global description without singularities because local coordinates are used. Secondly, it provides a geometric description which simplifies mechanical analysis in an intuitive way.

The fundamental principle used in screw theory is the idea that any movement of a rigid body can be described as a movement consisting of a rotation about a straight line followed by a translation parallel to that line. This idea was first published in 1900 [63]. This motion looks like a screw so it is called a screw motion. The instantaneous velocity of this screw motion is called a twist. The dual of speed is force and the dual of a twist is called a wrench. Hence, a wrench is a vector consisting of forces and moments acting on a rigid body.

In grasping, there is a need to describe the kinematics and dynamics of both the object and the gripper. Besides that, there is a interconnection between these two because there is a contact and a constraint that the object needs to be held. Using screw theory, both the grasping constraint and the contact models can be incorporated. The derivation of the kinematics and dynamics of the object, gripper and the interconnection is shown next.

## 3-2 Kinematics

In order to be able to derive the dynamic equations that can be used for control, information on the positions and velocities of the system is required. Screw theory is used to derive the

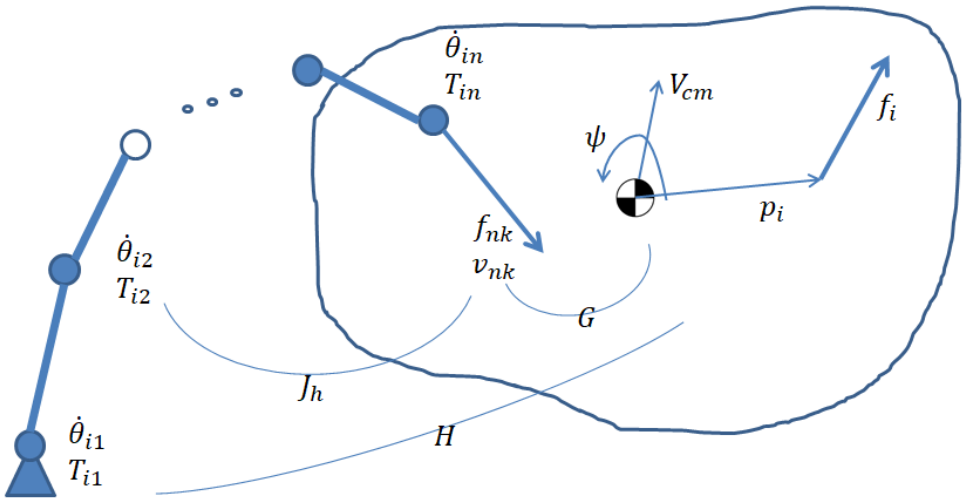


**Figure 3-1:** Schematic of the grasp kinematics.

kinematic equations of the gripper and the object. Besides that, a constraint is derived that combines the two.

### 3-2-1 Hand and Object Kinematics in General

The discussion in this section refers to Figure 3-1. An object is depicted with a Center of Mass (CM). The object is grasped with $n$ fingers that all have $m$ joints. At point $p_i$ a force $f_i$ is applied. This generates a torque around the CM of $\tau_i = p_i \times f_i$. A wrench vector $F_o$ is defined at the CM:

$$F_o = \begin{bmatrix} f_i \\ \tau_i \end{bmatrix}, \tag{3-1}$$

with $F_o \in \mathbb{R}^d$ where $d = 3$ for 2D modelling and $d = 6$ for 3D modelling.

The movement of the CM is defined by a translational velocity $V_{CM}$ and a rotational velocity $\psi$. Both are captured in a twist defined as:

$$\zeta = \begin{bmatrix} V_{CM} \\ \psi \end{bmatrix} \in \mathbb{R}^d. \tag{3-2}$$

The forces and velocities at the contact points (the fingertips) are defined as:

$$f = \begin{bmatrix} f_{1k}^T ... f_{nk}^T \end{bmatrix}^T \in \mathbb{R}^{nr} \text{ where } k = 1, ...r. \tag{3-3}$$

$$v = \begin{bmatrix} v_{1k}^T ... v_{nk}^T \end{bmatrix}^T \in \mathbb{R}^{nr} \text{ where } k = 1, ...r, \tag{3-4}$$

with $r$ the number of contact points per finger.

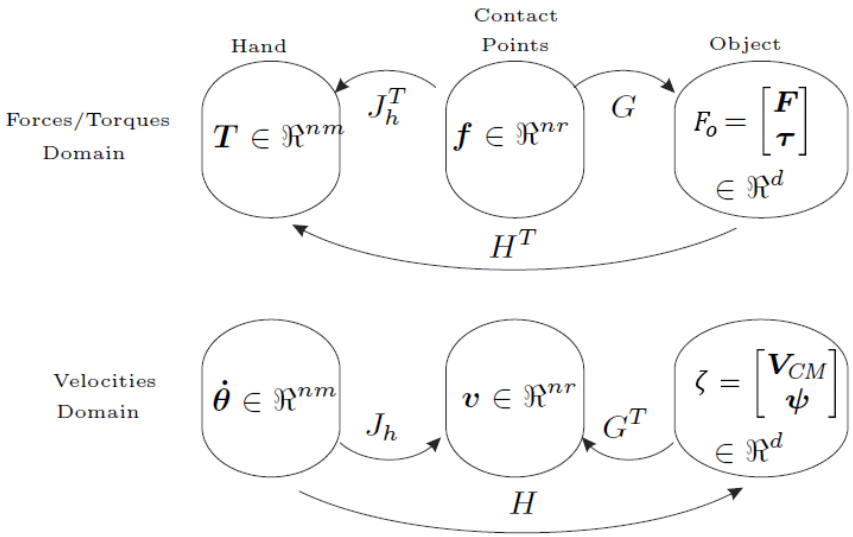


**Figure 3-2:** The kinematic relations for forces and velocities, from [5].

The fingertip force $f_i$ comes from the torques that are produced in all $m$ joints of finger $i$. If $j = 1, ..., m$, these torques can be captured in the following vector:

$$T = \left[T_{1j}^T ... T_{nj}^T\right]^T \in \mathbb{R}^{nm}. \tag{3-5}$$

The velocities in the finger joints are defined in a similar way:

$$\dot{\theta} = \left[\dot{\theta}_{1j}^T ... \dot{\theta}_{nj}^T\right]^T \in \mathbb{R}^{nm}. \tag{3-6}$$

The properties mentioned above are related, this is shown in Figure 3-2. The fingertip forces $f$ and velocities $v$ are related to the torques and velocities of the finger joints via the following equations:

$$T = J_h^T f, \tag{3-7}$$
$$v = J_h \dot{\theta}, \tag{3-8}$$

where $J_h$ is called the hand Jacobian composed of $n$ Jacobians (one for each finger $i$) as follows:

$$J_h = \text{diag}[J_1, ..., J_n] \in \mathbb{R}^{nr \times nm} \text{ with } J_i \in \mathbb{R}^{r \times n}. \tag{3-9}$$

The relation between the fingertip velocities and forces and the net wrench and twist applied on the object are:

$$F_o = Gf, \tag{3-10}$$
$$v = G^T \zeta, \tag{3-11}$$

where $G$ is the grasp matrix [62] $\in \mathbb{R}^{d \times nr}$.

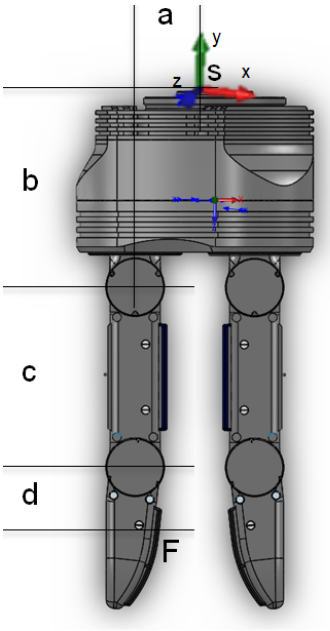


**Figure 3-3:** The Schunk SDH gripper with typical dimensions.

The hand Jacobian and the grasp matrix form the mapping between finger joint velocities and torques and object twist and wrench as follows:

$$T = H^T F_o, \tag{3-12}$$

$$\zeta = H\dot{\theta}, \tag{3-13}$$

with $H$ being the hand-object Jacobian defined as:

$$H = (G^+)^T J_h \in \mathbb{R}^{d \times nm}, \tag{3-14}$$

with $G^+$ the Moore-Penrose inverse of matrix $G$ because the latter in general is not a square matrix.

### 3-2-2 Hand Kinematics

The derivation of the hand kinematics as shown next applies on fingered grippers in general. However, because the reference gripper used in this thesis is the Schunk SDH gripper, the specific kinematics will be derived for this gripper here. The Schunk SDH gripper in reference configuration is shown in Figure 3-3. The typical dimensions are indicated. The value of the dimensions are shown in Table 3-1 but the subsequent calculations will make use of the symbols for sake of clarity. $F$ is defined as the contact point of the left finger with the object. $s$ indicates the spatial frame where the red arrow is the x-axis, the green arrow the y-axis and the blue arrow the z-axis. The goal is to describe the location and speed of this point as a function of the joint torques and velocities of the left finger. The kinematics are now described for finger 1 which is the left finger.

The rotational axis of both joints is pointing out of the paper. This means that a positive rotation results in a movement of the finger contact point $F$ to the right, i.e. a closing action.

**Table 3-1:** Dimensions of the Schunk SDH gripper, from Figure 3-3.

| Parameter | Value [mm] |
|---|---|
| a | 28.58 |
| b | 98.00 |
| c | 86.50 |
| d | 26.28 |

The rotational axis hence is:

$$\omega_1 = \begin{bmatrix} 0 \\ 0 \\ 1 \end{bmatrix}. \tag{3-15}$$

The value of rotation is defined by $\theta_{11}$ for the proximal joint and $\theta_{12}$ for the distal joint. The axis point of the proximal joint with respect to the spatial frame in reference configuration is:

$$q_{11} = \begin{bmatrix} -a \\ -b \\ 0 \end{bmatrix}. \tag{3-16}$$

These are the ingredients required to calculate the twist corresponding to the proximal joint of finger 1 in reference configuration. It is defined and calculated as follows:

$$\zeta_{11} = \begin{bmatrix} -\omega_1 \times q_{11} \\ \omega_1 \end{bmatrix} = \begin{bmatrix} -b \\ a \\ 0 \\ 0 \\ 0 \\ 1 \end{bmatrix}. \tag{3-17}$$

This can be interpreted as the movement of a point attached to the proximal joint, moving through origin $s$ with a unit rotation, expressed in origin frame $s$. This is also the way to read the common notation for this twist: $\zeta^s_{s,11}$.

For the distal joint, the contact point in reference configuration is:

$$q_{12} = \begin{bmatrix} -a \\ -b-c \\ 0 \end{bmatrix}. \tag{3-18}$$

The twist now is:

$$\zeta_{12} = \zeta^s_{s,12} = \begin{bmatrix} -\omega_1 \times q_{12} \\ \omega_1 \end{bmatrix} = \begin{bmatrix} -b-c \\ a \\ 0 \\ 0 \\ 0 \\ 1 \end{bmatrix}. \tag{3-19}$$

These twists only describe the motions in reference configuration. A powerful feature of screw theory is that this can be transformed to an orientation that is dependent on the angle of the joint. Still, only the twist in reference configuration is required. The matrix exponential is used to transform the twists in order to work with homogeneous matrices. The twists of both joints can then be combined by multiplying the matrix exponentials of the individual joints, as discovered by Brockett [64]. A homogeneous matrix describes the rotation and translation between two frames. It is structured as follows:

$$H = \begin{bmatrix} R & q \\ 0 & 1 \end{bmatrix}, \tag{3-20}$$

where $R$ is a matrix indicating the rotation and $q$ is the position vector. The homogeneous matrix from spatial frame $s$ to distal joint in zero configuration needs to be determined. The reference position is chosen such that this is convenient. There is no rotation between the frames and therefore the displacement is logical to set up, resulting in the following matrix:

$$H_2^s(0) = \begin{bmatrix} 1 & 0 & 0 & -a \\ 0 & 1 & 0 & -b-c \\ 0 & 0 & 1 & 0 \\ 0 & 0 & 0 & 1 \end{bmatrix}. \tag{3-21}$$

The matrix exponential transforms a general twist $\zeta$ as follows:

$$e^{\tilde{\zeta}\theta_{ij}} = \begin{bmatrix} e^{\tilde{\omega}\theta_{ij}} & (I - e^{\tilde{\omega}\theta_{ij}})(\omega \times v) + \omega\omega^T v\theta_{ij} \\ 0 & 1 \end{bmatrix}, \tag{3-22}$$

with $\tilde{\zeta}$ the tilde form of the twist:

$$\tilde{\zeta} = \begin{bmatrix} \tilde{\omega} & v \\ 0 & 0 \end{bmatrix}, \tag{3-23}$$

where $v = -\omega \times q$ and $\tilde{\omega}$ is the tilde form defined as:

$$\tilde{\omega} = \begin{bmatrix} 0 & -\omega_3 & \omega_2 \\ \omega_3 & 0 & -\omega_1 \\ -\omega_2 & \omega_1 & 0 \end{bmatrix} \text{ with } \omega = \begin{bmatrix} \omega_1 \\ \omega_2 \\ \omega_3 \end{bmatrix}. \tag{3-24}$$

$e^{\tilde{\omega}\theta_{ij}}$ is defined as (Rodriguez formula [65]):

$$e^{\tilde{\omega}\theta_{ij}} = I + \tilde{\omega}\sin(\theta_{ij}) + \tilde{\omega}^2(1 - \cos(\theta_{ij})). \tag{3-25}$$

Using these general results, the transformation between spatial and distal frame can be calculated by filling in the correct values for the twists. The homogeneous matrix of the distal joint with respect to the spatial frame is now defined as the multiplication of the individual matrix exponentials times the initial homogeneous matrix as follows:

$$H_2^s(\theta_{11}, \theta_{12}) = e^{\tilde{\zeta}_{11}\theta_{11}} e^{\tilde{\zeta}_{12}\theta_{12}} H_2^s(0). \tag{3-26}$$

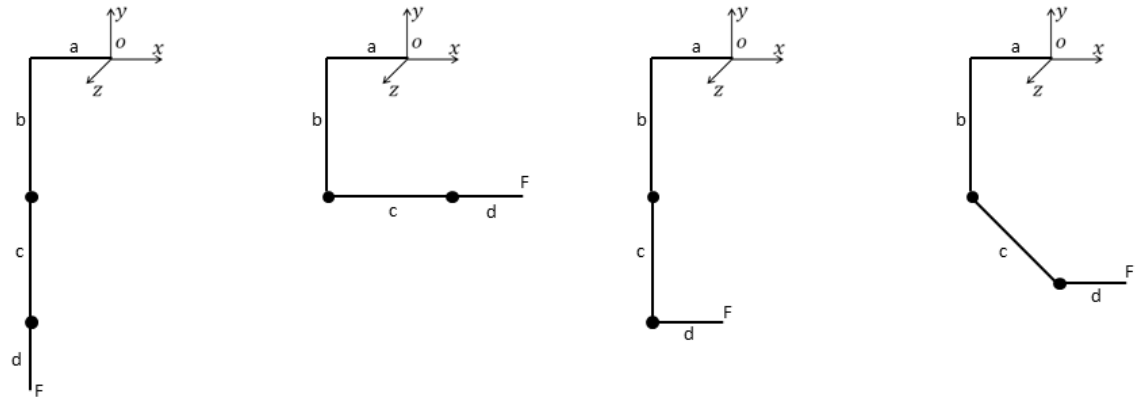


**Figure 3-4:** An abstraction of the first finger in different configurations.

To check the result, a position in the frame of the distal joint can be expressed in the spatial frame by making use of $H_2^s$. In reference configuration, the line of contact location $F$ can be described in the local frame of the distal joint as follows:

$$q_F^2 = \begin{bmatrix} 0 \\ -d \\ 0 \end{bmatrix}. \tag{3-27}$$

This position can be expressed in the spatial frame, as a function of the angles of the joints, as follows:

$$q_F^s = H_2^s(\theta_{11}, \theta_{12}) q_F^2. \tag{3-28}$$

By filling in some values for the angles of the joints, it can be checked that the results are correct. Remember that the joint is rotating counter-clockwise in case of a positive angle.

$$H_d^s(0,0) q_F^d = \begin{bmatrix} -a \\ -b-c-d \\ 0 \\ 1 \end{bmatrix}. \tag{3-29}$$

$$H_d^s(\tfrac{\pi}{2},0) q_F^d = \begin{bmatrix} -a+c+d \\ -b \\ 0 \\ 1 \end{bmatrix}. \tag{3-30}$$

$$H_d^s(0,\tfrac{\pi}{2}) q_F^d = \begin{bmatrix} -a+d \\ -b-c \\ 0 \\ 1 \end{bmatrix}. \tag{3-31}$$

$$H_d^s(\tfrac{\pi}{4},\tfrac{\pi}{4}) q_F^d = \begin{bmatrix} -a+c/\sqrt{2}+d \\ -b-c/\sqrt{2} \\ 0 \\ 1 \end{bmatrix}. \tag{3-32}$$

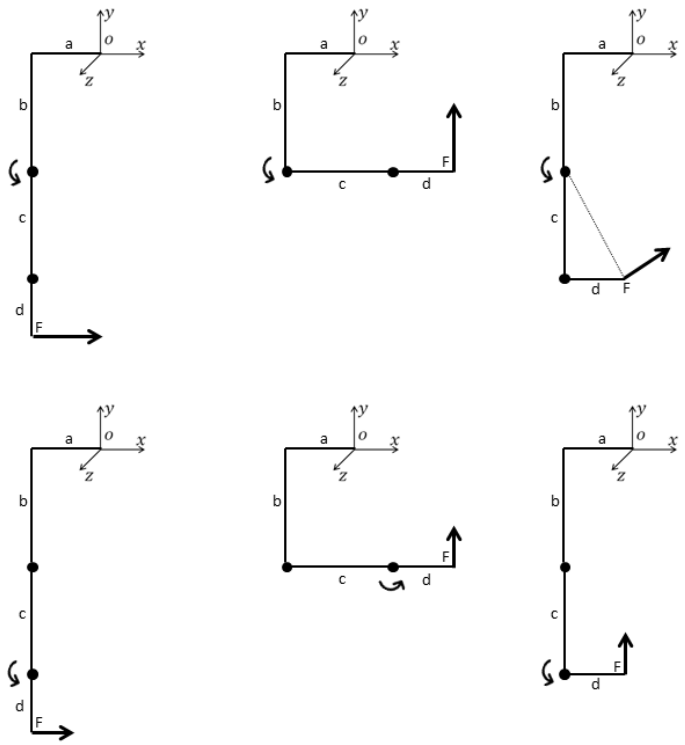


**Figure 3-5:** An abstraction of the first finger in different configurations with indicated speeds.

An abstraction of the first finger in these configurations is shown in Figure 3-4. By visual inspection it can be checked that the results are correct.

As described in the previous section, the hand Jacobian $J_h$ describes the relation between joint velocities and end-effector velocities of the hand. The derived twists can be used to easily create the Jacobian (for the first finger) because twists already describe the motion with respect to the spatial frame. If the twists would have been expressed in local coordinates, a transformation would be required to express all twists in the spatial frame s. This is not required now so:

$$J_1 = \begin{bmatrix} \zeta_{11} & \zeta_{12}(\theta_{11}) \end{bmatrix}. \tag{3-33}$$

Note that these twists are now dependent on the angles of the joints, in contrast to the twists defined in (3-17) and (3-19) for the reference configuration. This is not a problem now because the positions of the joints as a function of the angles are derived via the homogeneous matrix previously. The result can be checked by calculating the speed of the contact point $F$ by making use of this Jacobian and check it for configurations that are simple to interpret geometrically. The speed of the contact point is:

$$\dot{q}_F^s = \left( J_1 \tilde{\dot{\theta}}_1 \right) q_F^s, \tag{3-34}$$

with

$$\dot{\theta}_1 = \begin{bmatrix} \dot{\theta}_{11} \\ \dot{\theta}_{12} \end{bmatrix}. \tag{3-35}$$

This is dependent on both the angles and the angular velocities, as expected. By filling in some values for these parameters, it can be checked that the result is correct because the results match with visual inspection. For example in the first test, an angular velocity of 1 $rad/s$ for the first joint in reference configuration should result in a movement of $(c+d)[m] \cdot 1[rad/s] = (c+d)[m/s]$ in positive x-direction, which is also the result of the calculation. The other results can be checked in a similar way. The second to last shows that the speed is perpendicular to the axis of the finger, which is logical. The configurations and speeds are indicated in Figure 3-5 and show that the results are correct.

$$\dot{q}_F^s(0,0,1,0) = \begin{bmatrix} c+d \\ 0 \\ 0 \\ 0 \end{bmatrix}. \tag{3-36}$$

$$\dot{q}_F^s(0,0,0,1) = \begin{bmatrix} d \\ 0 \\ 0 \\ 0 \end{bmatrix}. \tag{3-37}$$

$$\dot{q}_F^s(\tfrac{\pi}{2},0,1,0) = \begin{bmatrix} 0 \\ c+d \\ 0 \\ 0 \end{bmatrix}. \tag{3-38}$$

$$\dot{q}_F^s(\tfrac{\pi}{2},0,0,1) = \begin{bmatrix} 0 \\ d \\ 0 \\ 0 \end{bmatrix}. \tag{3-39}$$

$$\dot{q}_F^s(0,\tfrac{\pi}{2},1,0) = \begin{bmatrix} c \\ d \\ 0 \\ 0 \end{bmatrix}. \tag{3-40}$$

$$\dot{q}_F^s(0,\tfrac{\pi}{2},0,1) = \begin{bmatrix} 0 \\ d \\ 0 \\ 0 \end{bmatrix}. \tag{3-41}$$

The orientation and speeds of selected contact points, expressed in the frame attached to the distal finger, is now described by making use of twists and the Jacobian. The kinematics of the right finger (finger 2) are derived in a similar way and can be found in Appendix B. In the next section these results will be used to derive the dynamics of the gripper. Finally it is noted that the hand Jacobian is composed of the Jacobian of the first finger and the second finger as follows:

$$J_h = \text{diag}[J_1, J_2]. \tag{3-42}$$

### 3-2-3 Object Kinematics

A schematic representation an object, a block, is shown in Figure 3-6. The origin frame of the object is chosen exactly in the middle of the two contact points, denoted by $o$. The distance

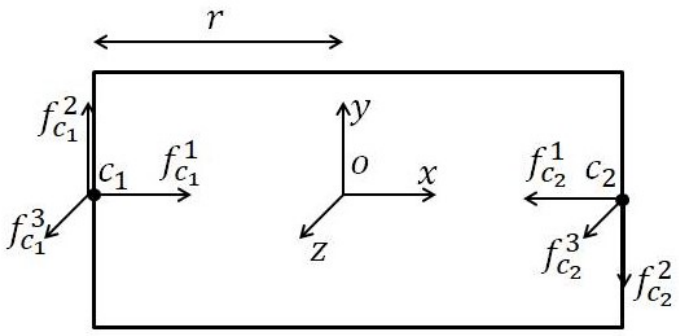


**Figure 3-6:** Schematic representation of a block, including frames in the origin and the contact points.

from the object origin to the left contact point, $c_1$, is $r$. The forces acting at $c_1$ are also indicated: one normal and two tangential components. The distance from the origin to the right contact point, $c_2$, is also equal to $r$. The frame at $c_2$ is created by rotating the displaced frame over $180^o$. This is done in order to let the first component of the force vector at this contact point, the normal force, be positive when pushing against the object. A point contact with friction can now be formalised by making use of screw theory. The wrench applied at $c_i$ is $F_{c_i}$ defined by a contact type specific wrench basis and a force as follows for a point contact with friction:

$$F_{c_i} = \begin{bmatrix} 1 & 0 & 0 \\ 0 & 1 & 0 \\ 0 & 0 & 1 \\ 0 & 0 & 0 \\ 0 & 0 & 0 \\ 0 & 0 & 0 \end{bmatrix} f_{c_i} = B_{c_1} f_{c_i} \quad f_{c_i} \in FC_{c_i}, \tag{3-43}$$

where $B_{c_i}$ is called the wrench basis that selects the components of the force that are taken into account (in this case one normal and two tangential) and $FC_{c_i}$ is the friction cone constraint explained next. The maximum amount of tangential force is defined by the friction coefficient $\mu$ according to Coulomb's friction law [5]. If the required force is outside of this boundary in any direction, the finger starts to slip relative to the object. This region is indicated with the friction cone which is represented as follows:

$$f_t < \mu f_n, \tag{3-44}$$

where $f_t$ is the tangential force and $f_n$ the normal force. This can be translated into the friction cone corresponding to the frames at the contact locations as follows:

$$FC_{c_i} = \left\{ f_{c_i} \in \mathbb{R}^3 : \sqrt{\left(f_{c_i}^2\right)^2 + \left(f_{c_i}^3\right)^2} \leq \mu f_{c_i}^1, f_{c_i}^1 \geq 0 \right\}. \tag{3-45}$$

The wrench with respect to the object center then is:

$$F_{oi} = Ad^T_{H_{c_i}^{o^{-1}}} F_{c_i} = Ad^T_{H_{c_i}^{o^{-1}}} B_{c_i} f_{c_i} = G_i f_{c_i}, \tag{3-46}$$

with $H_{c_i}^{o^{-1}}$ the homogeneous matrix expressing the contact point $c_i$ in the origin frame $o$ and $G_i$ the grasp map for contact $i$. The adjoint matrix transforms twists between different

coordinate frames. The adjoint matrix belonging to a homogeneous matrix $H$ is defined as follows:

$$Ad_H = \begin{bmatrix} R & 0 \\ \tilde{q}R & R \end{bmatrix}. \tag{3-47}$$

The transpose of this matrix does the same for wrenches because the dual of a twist is a wrench. Because of the fact that a wrench needs to change basis here, the transpose is used. Besides that, the inverse of the homogeneous matrix is used because the contact point has to be displaced to the object origin.

For the object in Figure 3-6 the homogeneous matrices for the contact points are defined as follows:

$$H^o_{c_1} = \begin{bmatrix} 1 & 0 & 0 & -r \\ 0 & 1 & 0 & 0 \\ 0 & 0 & 1 & 0 \\ 0 & 0 & 0 & 1 \end{bmatrix}, \quad H^o_{c_2} = \begin{bmatrix} -1 & 0 & 0 & r \\ 0 & -1 & 0 & 0 \\ 0 & 0 & 1 & 0 \\ 0 & 0 & 0 & 1 \end{bmatrix}. \tag{3-48}$$

The friction cone and wrench basis for each contact are the same as the generic ones described above. The grasp maps are:

$$G_1 = Ad^T_{H^{o^{-1}}_{c_1}} B_{c_1}, \quad G_2 = Ad^T_{H^{o^{-1}}_{c_2}} B_{c_2}. \tag{3-49}$$

Stacking the individual components $G_i$ give the full grasp matrix $G$:

$$G = \begin{bmatrix} G_1 & G_2 \end{bmatrix}. \tag{3-50}$$

The wrench on the object center can now be calculated, given the individual contact forces at the contact locations. These need to be in accordance with the friction cones. A simple test calculation can be performed by assuming a positive gripping force on the left contact point $c_1$ of $X1$ and a positive normal force on the right contact point $c_2$ of $X2$. According to the friction constraint, assuming no forces in z-direction, the contact force then are:

$$f_{c_1} = \begin{bmatrix} X1 \\ \mu X1 \\ 0 \end{bmatrix}, \quad f_{c_2} = \begin{bmatrix} X2 \\ \mu X2 \\ 0 \end{bmatrix}. \tag{3-51}$$

Now the individual components of the contact forces are stacked as follows:

$$f = \begin{bmatrix} f_{c_1} \\ f_{c_2} \end{bmatrix}. \tag{3-52}$$

The total wrench acting on the object center now is:

$$F_o = Gf = \begin{bmatrix} X1 - X2 \\ \mu X1 + \mu X2 \\ 0 \\ 0 \\ 0 \\ -\mu X1 r + \mu X2 r \end{bmatrix}. \tag{3-53}$$

This result is correct because the forces in x-direction of the origin are subtracted. This also holds for the forces in y-direction, but because of the fact that $X2$ works in negative direction when it is positive, a lifting force in positive y-direction results. The moments are counteracting each other.

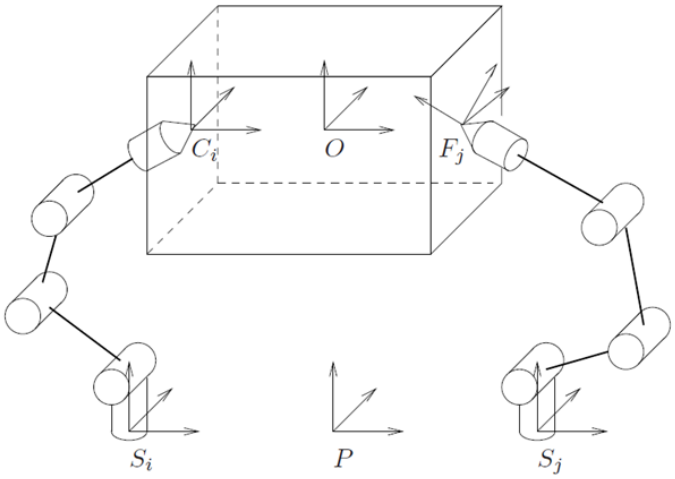


**Figure 3-7:** Overview of the frames in a grasp, from [5].

### 3-2-4 Fundamental Grasping Constraint

The subsequent section describes how the kinematics of the gripper and the object are connected in a grasp. Refer to Figure 3-7 for the description of the frames in a grasp. $O$ is again the origin of the object frame and $C_i$ is the contact point on the object. $S_i$ is the spatial reference frame of one finger. The description of the kinematics of one of the fingers used $s$ as reference frame, which was chosen at the palm of the hand. $P$ in Figure 3-7 indicates the palm reference frame, but in this case this is equal to $S_i$ and $S_j$. $F_j$ is the contact point on the finger of the $j$-th finger.

The constraint is described by setting the twist at the contact point of the finger, expressed in the spatial reference frame, equal to the twist of the contact point on the object, expressed in the same frame. The twist of the object reference frame is given by $\zeta$, the twist at $O$. The twist at the contact location $C_i$ can be calculated by making use of the grasp matrix $G$ as follows because it transforms twists between object center and contact points:

$$\dot{q}^s_{C_i} = G_i^T \zeta. \tag{3-54}$$

Now the twist at the same contact point, in the same coordinate frame, needs to be described as seen from the fingers. The previously derived Jacobian can partly be used for that. $J_h$ describes the twist of the contact point frame, expressed in the spatial frame:

$$\dot{q}^s_{F_i} = J_{h,i}\dot{\theta}. \tag{3-55}$$

The transformation between the two contact reference frames $F_i$ and $C_i$ is required to align the frames in order to match the forces and velocities. The homogeneous matrix that expresses $C_i$ with respect to $s$ is $H^s_{C_i}$. The twist can now be transformed as follows:

$$\dot{q}^s_{C_i} = Ad^{-1}_{H^s_{C_i}} J_{h,i}\dot{\theta}. \tag{3-56}$$

Finally the constraint can only act in the direction of the wrench basis. If, for example, only normal forces and no tangential force are taken into account, there can only be a constraint

regarding forces and velocities in the normal direction. Here both normal and tangential forces are taken into account, so the wrench basis as defined in (3-43) can be used:

$$\dot{q}^s_{C_i} = B^T_{C_i} Ad^{-1}_{H^s_{C_i}} J_{h,i}\dot{\theta}. \tag{3-57}$$

Now the twist are expressed in the same frame and the constraint can be formalised:

$$\dot{q}^s_{C_i} = B^T_{C_i} Ad^{-1}_{H^s_{C_i}} J_{h,i}\dot{\theta} = G^T_i \zeta. \tag{3-58}$$

This is still for contact point $i$. By defining

$$J_{h,con} = \text{diag}\left( B^T_{C_1} Ad^{-1}_{H^s_{C_i}} J_{h,i} \ \ldots \ B^T_{C_k} Ad^{-1}_{H^s_{C_n}} J_{h,n} \right), \tag{3-59}$$

the overall grasping constraint can be defined as:

$$J_{h,con}\dot{\theta} = G^T \zeta. \tag{3-60}$$

This is called the Fundamental Grasping Constraint (FGC) [59]. It couples the gripper and the object because it sets the speeds of the finger contact points equal to the speeds of the object contact points. This result will be used in the next section to couple the dynamics of the gripper and the object in the dynamic equations.

## 3-3 Dynamics

Now that the kinematics are known, the dynamic equations of both the gripper and the object can be derived. After that these individual dynamic equations can be combined to define the dynamics of the system consisting of the gripper and the object.

### 3-3-1 Gripper Dynamics

It is assumed that the gripper cannot rotate the fingers at the base, hence the fingers are moving in the plane. The generalised coordinates of the gripper are the angles of the two fingers.

$$\theta = \begin{bmatrix} \theta_{11} \\ \theta_{12} \\ \theta_{21} \\ \theta_{22} \end{bmatrix}. \tag{3-61}$$

Using the kinematic equations, the locations and velocities can be calculated. These can be used to derive the kinetic and potential energy.

$$T(\theta,\dot{\theta}) = \frac{1}{2}\dot{q}^{s^T}(\theta,\dot{\theta})\mathcal{M}\dot{q}^s(\theta,\dot{\theta}), \tag{3-62}$$

$$V(\theta) = Mgq^s_* = m_1 g y_{11} + m_2 g y_{12} + m_1 g y_{21} + m_2 g y_{22}, \tag{3-63}$$

with $\mathcal{M}$ the generalised inertia matrix containing the masses and moments of inertia because the twist $\dot{q}^s$ both contains linear and angular velocities of all phalanges. $q^s_*$ is only the part

of the positions in y-direction of frame $S$ because this is the direction of gravity. $m_1$ is the mass of the proximal phalange, $m_2$ that of the distal, these are equal for both fingers. The equations of motion are now derived by making use us Lagrangian equations [66]:

$$\frac{d}{dt}\left(\frac{\partial T}{\partial \dot{\theta}}\right) - \frac{\partial T}{\partial \theta} + \frac{\partial V}{\partial \theta}. \tag{3-64}$$

This is done in the m-file that is shown in Appendix C, it can be written as follows:

$$M_g(\theta)\ddot{\theta} + C_g(\theta, \dot{\theta})\dot{\theta} + N_g(\theta) = T, \tag{3-65}$$

with $T$ being the vector with the torques in the joints as follows:

$$T = \begin{bmatrix} \tau_{11} \\ \tau_{12} \\ \tau_{21} \\ \tau_{22} \end{bmatrix}, \tag{3-66}$$

and $M_g$ the inertia matrix of the gripper, $C_g$ the matrix containing the centrifugal and Coriolis terms of the gripper and $N_g$ the matrix containing the gravitational terms of the gripper. The structure of the gripper matrices is shown below. It can be seen that the dynamics of finger 1 (called finger now) and finger 2 (called thumb for now) are decoupled. This is logical because there is not yet interaction between them.

$$\begin{bmatrix} M_f & 0 \\ 0 & M_{th} \end{bmatrix} \begin{bmatrix} \ddot{\theta}_f \\ \ddot{\theta}_{th} \end{bmatrix} + \begin{bmatrix} C_f & 0 \\ 0 & C_{th} \end{bmatrix} \begin{bmatrix} \dot{\theta}_f \\ \dot{\theta}_{th} \end{bmatrix} + \begin{bmatrix} N_f \\ N_{th} \end{bmatrix} = \begin{bmatrix} \tau_f \\ \tau_{th} \end{bmatrix}. \tag{3-67}$$

Looking for example at the matrices belonging to the finger, the following structural properties should hold:

- $M_f$ is symmetric and positive definite
- $\dot{M}_f - 2C_f$ is skew symmetric and has zero trace

When running the m-file in Appendix C it can be seen that the structure of $M_f$ is:

$$M_f = \begin{bmatrix} j + k + l + m & l + \frac{1}{2}m \\ l + \frac{1}{2}m & l \end{bmatrix}. \tag{3-68}$$

This shows that the matrix is symmetric. In order to check the positive definiteness, the determinant is calculated:

$$\det(M_f) = p(1 - \cos(\theta_{12})^2) + r \text{ with } p > 0, r > 0. \tag{3-69}$$

This will always be greater than zero. Besides that, $c$ is greater than zero so the first principal minor is greater than zero. This proves that the matrix is positive definite. The second property is checked by calculating:

$$\dot{M}_f - 2C_f = \begin{bmatrix} 0 & s\sin(\theta_{12})\left(2\dot{\theta}_{11} + \dot{\theta}_{12}\right) \\ -s\sin(\theta_{12})\left(2\dot{\theta}_{11} + \dot{\theta}_{12}\right) & 0 \end{bmatrix}. \tag{3-70}$$

This shows that the second property also holds. The properties for the equations of the thumb and the overall equations of the gripper can be proven in a similar way.

### 3-3-2 Object Dynamics

The unconstrained object dynamics are simple to evaluate. Referring to Figure 3-6, it is just a block under gravity moving in free space. The general equation is:

$$M_o\ddot{x} + C_o\dot{x} + N_o = F_o, \tag{3-71}$$

with $M_o$ the inertia matrix of the object, $C_o$ the matrix containing the centrifugal and Coriolis terms of the object, $N_o$ the matrix with the gravitational terms and $F_o$ the wrench working on the object center. In case of the block this looks like:

$$\begin{bmatrix} m & 0 & 0 & 0 & 0 & 0 \\ 0 & m & 0 & 0 & 0 & 0 \\ 0 & 0 & 0 & 0 & 0 & 0 \\ 0 & 0 & 0 & 0 & 0 & 0 \\ 0 & 0 & 0 & 0 & 0 & 0 \\ 0 & 0 & 0 & 0 & 0 & \frac{m}{12}((2r)^2 + h^2) \end{bmatrix} \ddot{x} + \begin{bmatrix} 0 \\ mg \\ 0 \\ 0 \\ 0 \\ 0 \end{bmatrix} = F_o. \tag{3-72}$$

If the forces in the wrench from (3-53) are chosen such that they cancel the gravitational forces as follows:

$$X1 = X2 = \frac{mg}{2\mu}. \tag{3-73}$$

it can be seen that there is no displacement in x-direction and no net moment because the forces and moment cancel each other. Regarding the resultant lifting force, it can be seen that this is exactly equal to $mg$ so the object is held at place. In case of other wrenches at the object center, it can be seen that the dynamics describe what is expected.

### 3-3-3 Combined Dynamics

The object is grasped by the gripper so the dynamics need to be coupled. The FGC of (3-60) is used to describe the combined dynamics [59]:

$$\tilde{M}(q)\ddot{x} + \tilde{C}(q,\dot{q})\dot{x} + \tilde{N}(q,\dot{q}) = \tilde{F}, \tag{3-74}$$

with

$$q = \begin{bmatrix} \theta \\ x \end{bmatrix}, \tag{3-75}$$

$$\tilde{M} = M_o + GJ_h^{-T}M_gJ_h^{-1}G^T, \tag{3-76}$$

$$\tilde{C} = C_o + GJ_h^{-T}\left(C_gJ_h^{-1}G^T + M_g\frac{d}{dt}(J_h^{-1}G^T)\right), \tag{3-77}$$

$$\tilde{N} = N_o + GJ_h^{-T}N_g, \tag{3-78}$$

$$\tilde{F} = GJ_h^{-T}\tau. \tag{3-79}$$

$\theta$ is not present in this equation because it is eliminated via the constraints. These dynamics only hold when the controller is able to maintain contact. Now assume that a controller

action results in a value for $\tilde{F}$. This has to be converted to torques that have to be applied on the finger joints. The relation between the two is:

$$GJ_h^{-T}\tau = \tilde{F}. \tag{3-80}$$

The solution to this is:

$$\tau = J_h^T G^+ \tilde{F} + J_h^T f_n. \tag{3-81}$$

The first part ensures that the the FGC is fulfilled. The second part accounts for the internal forces: these have to be chosen such that they lie in the friction cone. The value of the gripping force $f_n$ can be chosen freely without influencing the first part. This decoupling is beneficial for control, this will be shown in Chapter 4.

## 3-4 Conclusion

Screw theory is used to formalise the kinematics, dynamics and contact models because the grasping constraint and contact models can easily be described in this framework. The individual kinematics of the gripper and the object are derived. The equation that connects these kinematics is the FGC, which is derived. Finally, the individual dynamics of the gripper and the object are derived and connected via this FGC into the overall dynamic equation that can be used for control purposes. Small intuitive tests are performed on the individual components of the kinematics and dynamics to show that the results are correct. Chapter 4 will elaborate on the combined kinematics and dynamics because first a controller needs to be defined that calculates the torques that are required in this equation.

# Chapter 4

# Control

Literature shows that a lot of good results can be accomplished by using intuition or knowledge based controllers [67], [68] and [69]. Research either focusses on modelling of the gripper or on control of it [70]. The models are typically used to generate a feedforward signal but no feedback is used to anticipate on deformation of items. The fact that the item properties are unknown and variable gives rise to the use of more advanced control methods. This thesis uses both models and feedback. The model of the system is already derived, this chapter now focusses on the controller approaches that utilise feedback. It describes how human intuition, modelling and feedback signals can be combined to create a control strategy to increase the grasp quality for the application of the pick-and-place task.

## 4-1 Control Goal

The control goal is to grasp and hold deformable items with minimal gripping force and maximal *grasp quality*, as will be defined in Section 4-1-1. The measurable quantities are the angles and velocities of the finger joints, the force on the fingers and the Center of Pressure (COP) on the fingers. The slip $\eta$ can be deducted from the change of COP over time.

The challenge is to determine the value of the reference gripping force. Slip will be used as a basis for this setpoint determination because slip indicates that the item is not being held. In order to not damage the products, a limit on the gripping force is introduced. The maximum gripping force is dependent on the type of product that is being grasped so this can be used during tuning of the controller on a known product. This theoretical maximum gripping force is calculated in Section 4-1-2. The following high-level control goal can now be formulated:

$$\begin{aligned} &\max \textit{ grasp quality} \\ &\text{s.t. } 0 < f_n(\eta) < f_{n,max}. \end{aligned} \tag{4-1}$$

The high-level controller relies on a controller that is able to apply the reference gripping force that is set by the high-level controller while maximising the grasp quality. This controller has

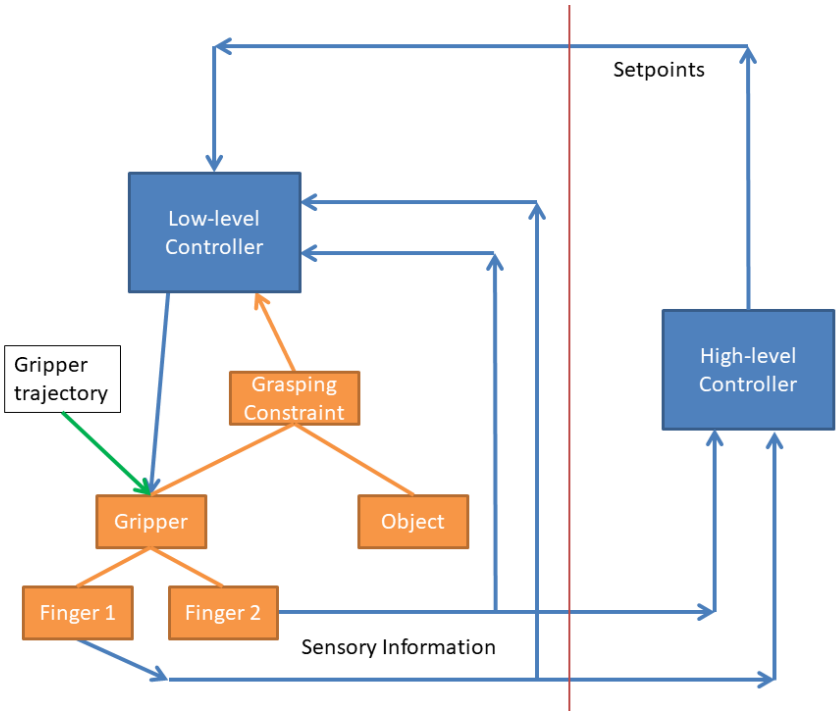


**Figure 4-1:** A visualisation of the control architecture. The red indicates the division between low-level and high-level control.

to work for arbitrary values of the reference gripping force. So the low-level control goal is:

$$\begin{aligned} &\max \textit{ grasp quality} \\ &\text{s.t. } f_n = \text{constant.} \end{aligned} \tag{4-2}$$

The division between high-level and low-level control naturally arose when decomposing the control goal. Because there is a separation of time scales between low-level reference following and high-level setpoint determination, there is a decoupling between the two levels of control. The decoupling is beneficial because the separate control levels can be optimised individually. From the division between a high-level and a low-level control goal, a control architecture with the same division can be derived. The gripper with its fingers are connected to the object via the grasping constraint that was derived in Section 3-2-4. This combined model is taken into account by the low-level controller. This controller can control the gripper while it is executing the predefined trajectory. Sensory information is used for this. Sensory information is also used by the high-level controller to determine the setpoint the low-level controller has to follow. This is all visualised in Figure 4-1.

Before diving into the controller approaches, first it is explained what *grasp quality* entails and how the value of the maximum amount of excess in gripping force is determined.

### 4-1-1 Grasp Quality Measure

The grasp quality, as used in the control goal, will be described here. The measure for grasp quality uses the knowledge of the states of both the gripper and the object to judge the

quality of the grasp. The hand-object Jacobian $H$ defines the overall mapping from gripper to object and thus can be used for this. A grasp is defined to have high quality if external moments and forces on the object in all directions can be withstood. If the gripper is not able to withstand a force or moment in a specific direction, $H$ becomes singular and hence one or more of the singular values of $H$ become zero [5]. The lower the smallest singular value, the closer the system is to a singular situation. The direction belonging to this lowest singular value indicates the direction in which no force or moment can be withstood, which is the physical interpretation of a singular value decomposition [71]:

$$Q_1 = \sigma_{min}(H). \tag{4-3}$$

To have a more bounded version of this quality measure, the minimum singular value can be compared to the maximum singular value. This gives a value between 0 and 1, where 0 indicates a singular configuration and 1 indicates an isotropic configuration [5]. Therefore this measure is the grasp isotropy index:

$$Q_2 = \frac{\sigma_{min}(H)}{\sigma_{max}(H)}. \tag{4-4}$$

The ability to withstand external forces and moments can also be determined by plotting the direction of the forces and moments corresponding to all singular values of $H$. Generally, this is an ellipsoid and therefore it is called the manipulability ellipsoid. In the special case that the forces and moments that can be withstood in all directions are equal (this is the isotropic configuration belonging to a $Q_2$ of 1), then all singular values are equal and the manipulability ellipsoid becomes a sphere. The volume of the ellipsoid is a measure for the quality of the grasp [72]:

$$Q_3 = \sqrt{\det(HH^T)} = \sigma_1\sigma_2...\sigma_d. \tag{4-5}$$

Physically, a larger volume of the manipulability ellipsoid means that for the same velocities in the finger joints, a larger velocity of the object can be obtained [62]. By duality this means that larger external forces on the object can be withstood by smaller torques in the fingers joints if the volume of the manipulability ellipsoid is higher.

$Q_1$ only provides a measure to compare grasps and is not an absolute measure because only the smallest singular value is taken into account. $Q_3$ takes into account the intermediate singular values but the additional information that is captured with this is poor because the ratio between the largest and smallest singular values is the same as the ratio between the intermediate values because they all indicate the relation between a maximum moment and a maximum force in a certain direction. Maximising the smallest singular value of $H$ with respect to the largest singular value achieves the other quality measures because they depend, directly or indirectly, on the singular values of $H$ [25]. So, this quality measure, $Q_2$, stands out as the most promising quality measure to be used in comparing the controllers.

An extra feature of the grasp quality measure is that the direction in which the largest forces can be withstood belongs to the largest singular value. This could be used in control to align the largest force that can be withstood with the direction of maximum acceleration. By taking the trajectory of the gripper into account, a lower grasp isotropy is required while executing the same trajectory by rotation of the gripper. This is only possible if the gripper has a wrist joint, which is not the case in this project.

### 4-1-2 Gripping Force Excess

In order to compute the excess in gripping force that is used, it is required to know properties of the item such as mass and material. The controllers are tuned on items of which the properties are known. The tuned controllers can then be applied in the real application, in which the item properties are not known. The maximum gripping force for a known item is calculated next. First the static case is examined. An object with two components of a gripping force is shown in Figure 4-2. The normal force exerted by each finger on the object results in a corresponding lifting force. In the static case, the static friction coefficient relates these two:

$$f_{l,i} = \mu_{stat} f_{n,i}. \tag{4-6}$$

The total gripping force is defined as the sum of the individual forces. In the static case, these forces are equal so it results in:

$$f_n = 2f_{n,i} = f_{n,1} + f_{n,2}. \tag{4-7}$$

In order to have static equilibrium, the lifting forces at the contacts should be equal to the gravitational force:

$$f_{l,1} + f_{l,2} = mg. \tag{4-8}$$

Given the relations in (4-6) and (4-7) this leads to:

$$2f_{l,i} = mg, \tag{4-9}$$
$$2\mu_{stat} f_{n,i} = mg, \tag{4-10}$$
$$\mu_{stat} f_n = mg. \tag{4-11}$$

So the minimum required gripping force can be calculated as:

$$f_{n,min,stat} = \frac{mg}{\mu_{stat}}. \tag{4-12}$$

Until now only the static case is treated. Because the robot is moving over a given trajectory, it also accelerates. The maximum acceleration in the direction of gravity is known. This acceleration is added to the gravitational acceleration. The gripper is also accelerating in the direction perpendicular to gravity so there will always be some swaying motion which results in a lower contact force. This induces slip so the kinetic friction coefficient needs to be used in the calculation for the minimum gripping force. Besides that, slip is a measurement that is used by the controller so it will definitely occur. The formula for the minimum gripping force now becomes:

$$f_{n,min,kin} = \frac{m(g + a_{y,max})}{\mu_{kin}}. \tag{4-13}$$

This is the theoretical minimum gripping force that only takes into account accelerations and perfect contacts. In case of deformable items, inertial effects from swaying and deforming can occur so it is not expected that a controller that applies this gripping force will succeed. The

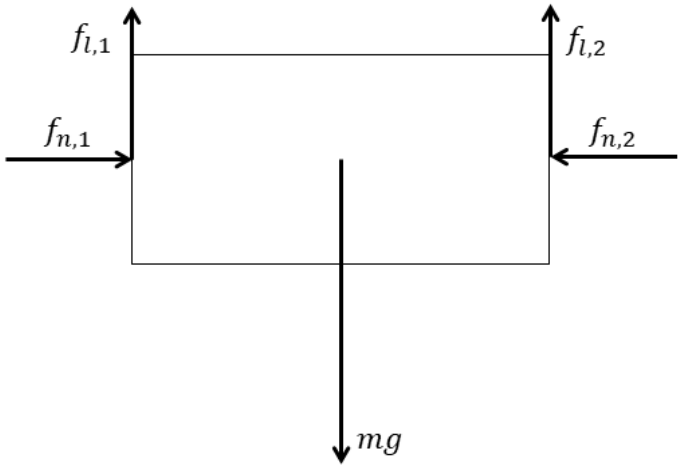


**Figure 4-2:** Static analysis of an object under gripping forces.

gripping force cannot be increased infinitely because then the objects are damaged, while the goal is to minimise this. Humans are able to pick up the items without crushing them, so the products are suited to be picked up by humans. Therefore, the upper boundary of the excess of gripping force comes from human factors research. As discussed in Section 2-4, humans have the ability to estimate the minimum required gripping force and apply a gripping force that is slightly higher to be safe. For items with a weight higher than 0.050 $kg$, this safety margin is 50% [53]. This motivates the use of an upper boundary on the gripping force that will be used by the controller:

$$f_{n,max,kin} = 1.5\frac{m(g + a_{y,max})}{\mu_{kin}}. \tag{4-14}$$

## 4-2 Low-level Control

Recall that the overall dynamic equation for the gripper and the object from (3-74) is:

$$\tilde{M}(q)\ddot{x} + \tilde{C}(q,\dot{q})\dot{x} + \tilde{N}(q,\dot{q}) = \tilde{F}. \tag{4-15}$$

Low-level controllers that are able to deal with these dynamics are presented next.

### 4-2-1 Controller Selection

In this section a low-level control strategy will be selected. Most of the controllers used in industry do not make use of any model knowledge [73]. The controller used here will make use of a model. Only relatively simple model based controllers are considered in this section. Other advanced controller approaches suffer from high computational load which is not desired because it may result in slow responses. Besides that, the low-level controller is just a reference follower so there is no need for advanced controllers such as impedance control because these type of controllers add functionalities to the system that are not required. The controllers elaborated on in this section are Open-loop Control, Computed Torque Control

**Table 4-1:** Low-level controller approaches weighted against the criteria.

| | 1. Tracking | 2. Stability | 3. Robustness |
|---|---|---|---|
| Open-loop Controller | 1 | 1 | 1 |
| Computed Torque Controller | 5 | 5 | 4 |
| PD Controller | 3 | 3 | 2 |

and PD Control. The selection is based on the performance of the controllers with respect to criteria. The criteria are explained next.

1. The controller needs to be able to track a desired profile of the states. This ensures that the gripper retains its pose and that the item has the desired location.
2. The controller needs to be stabilising.
3. The controller needs to be able to deal with inaccurate model knowledge. In this way, the controller can deal with unknown and deformable items. This is called robustness.

A score in the range from 1 to 5 is assigned to the different controller approaches, as shown in Table 4-1. It can be seen that the Computed Torque Controller scores best on all criteria. This controller will be used as the low-level controller. The considered low-level controller approaches and the motivation for the scores on the different criteria will be explained next.

### Open-loop Controller

In case of perfect model knowledge, open-loop control can be used [59]:

$$\tilde{F} = \tilde{M}(q_d)\ddot{x}_d + \tilde{C}(q_d, \dot{q}_d)\dot{x}_d + \tilde{N}(q_d, \dot{q}_d). \tag{4-16}$$

This controller needs to be provided with all desired states. No feedback is used within this controller so the tracking performance will be low in case of modelling errors. This controller is highly dependent on the knowledge of the initial conditions because no feedback is used to measure the actual value of the states. This also degrades the tracking performance, therefore it scores 1 at the first criterion. The open-loop controller cannot guarantee stability, therefore it scores 1 on the second criterion. Because of the fact that this controller completely relies on perfect model knowledge, it cannot cope with modelling errors so it also scores 1 at the third criterion.

### Computed Torque Controller

The computed torque approach uses only the reference of the acceleration in the feedforward part of the controller. The position and velocity of the joints are used as state feedback as follows [59]:

$$\tilde{F} = \tilde{M}(q)\ddot{x}_d + \tilde{C}(q, \dot{q})\dot{x} + \tilde{N}(q, \dot{q}). \tag{4-17}$$

A feedback law, that uses the reference values on the position and velocity, can be added to this:

$$\tilde{F} = \tilde{M}(q)(\ddot{x}_d - K_v\dot{e} - K_p e) + \tilde{C}(q,\dot{q})\dot{x} + \tilde{N}(q,\dot{q}), \tag{4-18}$$

with $e = x - x_d$. This computed torque approach is a form of feedback linearisation because the compensation term renders the system linear so a linear control law can be applied. The computed torque controller, supplemented with the stabilizing control law is also called Inverse Dynamics Control [74]. This controller can be tuned to be always stable if the tuning matrices are positive definite. Therefore this controller scores 5 on the second criterion. Because of this incorporation of the error terms, it is capable of tracking a desired state profile. Besides that it uses feedback on the states to determine the control action. This all contributes to high tracking performance so it scores 5 on the first criterion. Because of the fact that the system uses sensory information, it is capable of dealing with parametric uncertainties in the model. Besides that it can operate at all operating point so it scores 4 on the third criterion.

#### PD Controller

PD control can be applied at a linearised operating point.

$$\tilde{F} = -K_v\dot{e} - K_p e. \tag{4-19}$$

The augmented PD controller also uses the knowledge from the model [59]:

$$\tilde{F} = \tilde{M}(q)\ddot{x}_d + \tilde{C}(q,\dot{q})\dot{x}_d + \tilde{N}(q,\dot{q}) - K_v\dot{e} - K_p e. \tag{4-20}$$

The difference with the computed torque control law is that the error is directly compensated for via the applied torques instead of via the inertia matrix. This can lead to larger overshoots. Besides that, the Coriolis terms are computed based on the desired velocity instead of the measured velocity in case of the Computed Torque Controller. The possible overshoot and the use of only feedback on the state and not its derivative degrades the tracking performance of this controller (3). Because of the fact that less sensory information is taken into account and that the controller needs to be tuned for a linearised operating point, the robustness is relatively low (2). If the conditions change such that the operating point is different than the point at which the controller is tuned, the controller can fail. The stability is guaranteed at the linearised operating point, but outside this point it is not, therefore it scores 3.

### 4-2-2 Computed Torque Details

The Computed Torque Controller computes the forces that are required to cancel the dynamics and to follow a desired state profile as follows:

$$\tilde{F} = \tilde{M}(q)(\ddot{x}_d - K_v\dot{e} - K_p e) + \tilde{C}(q,\dot{q})\dot{x} + \tilde{N}(q,\dot{q}). \tag{4-21}$$

The result of this calculation, $\tilde{F}$, needs to be translated to the torques that have to be applied on the joints of the gripper. This follows from the derivation of the dynamics and results in the following, as shown in Section 3-3-3:

$$\tau = J_h^T G^+ \tilde{F} + J_h^T f_n. \tag{4-22}$$

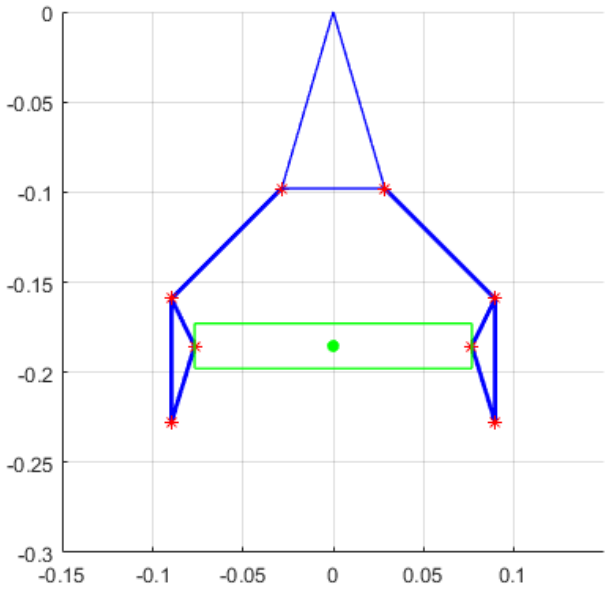


**Figure 4-3:** A visualisation of the gripper and the object.

The first part on the right-hand side of the equation accounts for the Fundamental Grasping Constraint (FGC) and the second part accounts for the reference gripping force. The second part does not influence the first part because $f_n$ lies in the nullspace of $G$.

The functionality of this decoupling will be demonstrated here by means of an example. The item that has to be picked is a block with a mass of $m_{block} = 0.25\ kg$. The width of the block is chosen such that the initial angles of the joints of the gripper are $45^o$. The friction coefficient between the gripper and the block is set to $\mu = 1$. The state profile that has to be followed is set equal to the initial state, in this way the task of the controller is to maintain the position of the block. The hand Jacobian $J_h$ and the grasp matrix $G$ for this specific gripper pose and object are included in Appendix D.

The first part calculates the torques that are required to maintain the configuration of the gripper such that contact with the object is maintained. A visualisation of the gripper with the object is shown in Figure 4-3. The constant value of the torques is calculated as follows:

$$\tau = J_h^T G^+ \tilde{F} = \begin{bmatrix} -0.1727 \\ 0.0458 \\ -0.1727 \\ 0.0458 \end{bmatrix}. \tag{4-23}$$

Recall the definition of positive torques from Section 3-2-2: positive torques result in a closing action. It is convenient to interpret this result. The negative torque on the proximal joints means that the proximal fingers are lifted upwards. This is required to compensate for gravity. The smaller positive torque on the distal joint is required to maintain contact with the object. This torque is positive to compensate for the upward torque of the proximal finger.

Next the part corresponding to the reference on the gripping force is added to the controller. The required gripping force can be calculated given the information on the mass and friction

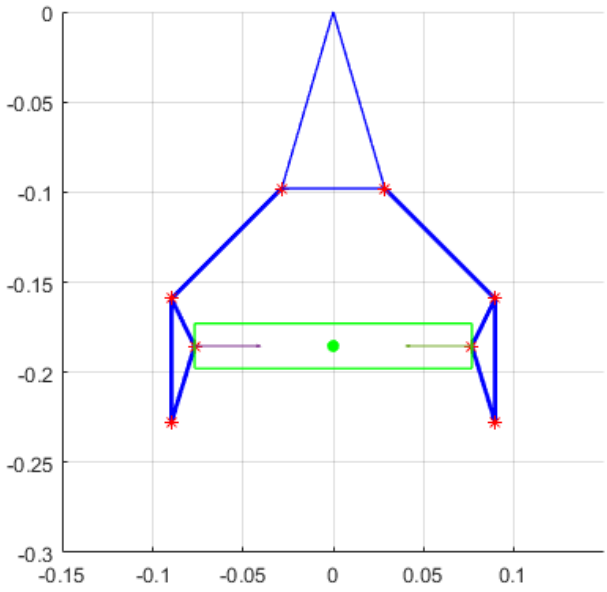


**Figure 4-4:** A visualisation of the gripper and the object, the arrows indicate the gripping force acting on the object.

coefficient of the object as follows:

$$f_{n,ref} = \frac{m_{block} g}{\mu} = \frac{0.250 \cdot 9.81}{1} = 2.45 \ N. \tag{4-24}$$

Filling in this value gives the following values for the torques:

$$\tau = J_h^T G^+ \tilde{F} + J_h^T f_n = \begin{bmatrix} -0.1727 \\ 0.0458 \\ -0.1727 \\ 0.0458 \end{bmatrix} + \begin{bmatrix} 0.1072 \\ 0.0322 \\ 0.1072 \\ 0.0322 \end{bmatrix} = \begin{bmatrix} -0.0655 \\ 0.0781 \\ -0.0655 \\ 0.0781 \end{bmatrix}. \tag{4-25}$$

The part that is accountable for maintaining the FGC is still the same, this follows from the decoupling. The contribution of the second part ensures that the force acts in horizontal direction and does not influence the other directions. These torques are both positive in order to increase the gripping force on the object. The sum of both components still shows a negative torque in the proximal joint, this is required to compensate for gravity. It is less negative compared to the first case, this is because the gripping force is higher. The torque on the distal joints is higher compared to the first case, this is logical because the gripping force is higher. A visualisation of the gripper with the object is shown in Figure 4-4. The arrows indicate the direction and value of the gripping force on the object.

If the friction coefficient is now set to $\mu = 0.5$, the gripping force required to hold the object is twice as high.

$$f_{n,ref} = \frac{m_{block} g}{\mu} = \frac{0.250 \cdot 9.81}{0.5} = 4.91 \ N. \tag{4-26}$$

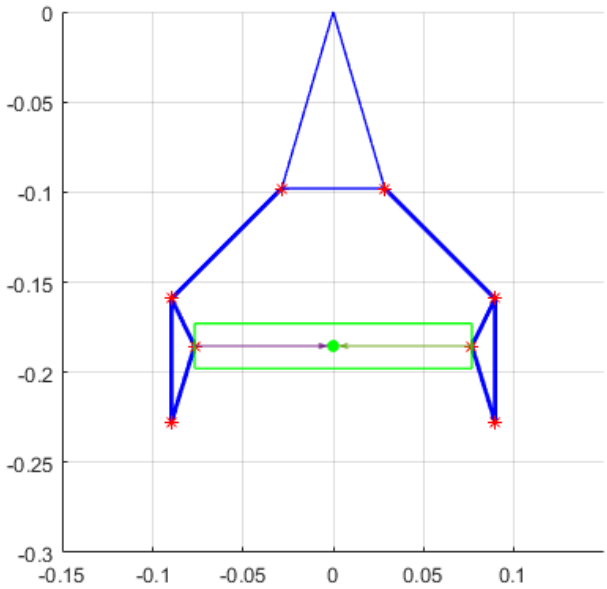


**Figure 4-5:** A visualisation of the gripper and the object, the arrows indicate the gripping force acting on the object.

Now the torques are:

$$\tau = J_h^T G^+ \tilde{F} + J_h^T f_n = \begin{bmatrix} -0.1727 \\ 0.0458 \\ -0.1727 \\ 0.0458 \end{bmatrix} + \begin{bmatrix} 0.2145 \\ 0.0645 \\ 0.2145 \\ 0.0645 \end{bmatrix} = \begin{bmatrix} -0.0418 \\ 0.1103 \\ -0.0418 \\ 0.1103 \end{bmatrix}. \tag{4-27}$$

The first part is again the same, which is logical. The torques of the second part are twice as high in order to be able to grip with a higher force. The ratio between the torques is the same in order to increase the gripping force only in horizontal direction. The hand Jacobian perfectly takes this into account. The sum of the torques show a less negative torque on both proximal joints and a higher torque on the distal joints. This is to take into account the FGC as well as the increase in gripping force. The visualisation for this case is shown in Figure 4-5

In the previous examples the controller calculates the static torques that are required to maintain the pose of the gripper and the object. This uses only the part of the computed torque controller that is on the cancelling of the dynamics. However, there is also a part in the computed torque controller that takes into account the regulation to the desired state. To demonstrate this, the gripper is desired to lift the object. The y-position in the state reference is set 0.01 $m$ higher compared to the initial state. The initial and final state are shown in Figure 4-6 [1]. The torque profiles along the run are shown in Figure 4-7. The required gripping force (still based on $\mu = 0.5$) is maintained during movement. The upper left plot in Figure 4-8 shows the y-position for this run. The controller parameters that were

[1]The corresponding video can be found at https://youtu.be/xGudKtGcPtY or on the USB-stick that is included with this thesis (Video1).

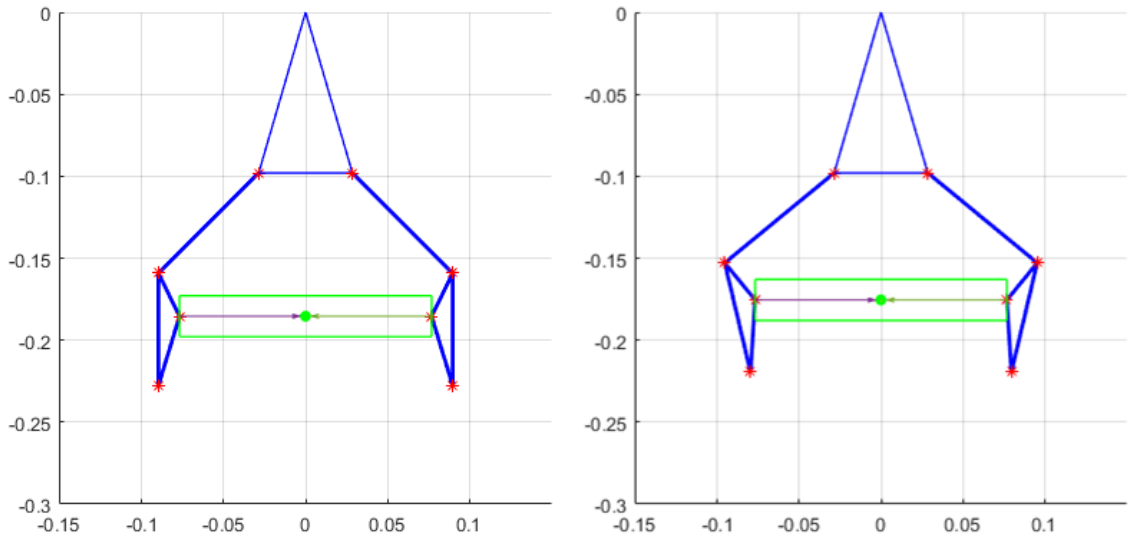


**Figure 4-6:** Configuration of the gripper at the start and end of the animation.

used during this run were $K_p = 100I$ and $K_d = 10I$. The influence of these parameters will be shown now. Their meaning is very intuitive, see Figure 4-8. Increasing the damping term ($K_d$) with respect to the nominal case eliminates the overshoot. Increasing the proportional term ($K_p$) of the controller introduces more overshoot but gives a faster response. Damping action can be added to this latter case in order to decrease the overshoot again, this is shown in the lower right figure. In Chapter 6 these parameters will be tuned with respect to the low-level control goal.

Appendix E and Appendix F contain the m-file and the function that implement this controller via integration in Matlab.

This ends the discussion on the working principle of this low-level controller applied on this project. This low-level controller will be implemented in Chapter 6.

## 4-3 High-level Control

In order to determine the setpoint on the reference gripping force that the low-level controller has to follow, a high-level controller is required. High-level controllers are controllers that account for the varying parameters by changing the setpoints for the low-level controller. One can think of the friction coefficient and the shape of the object that are unknown, so it is necessary to adjust the gripping force to those parameters [42]. They rely on the low-level controller to execute these commands. This controller does not require detailed information on the dynamics of the system, it only determines the setpoints based on sensory information.

### 4-3-1 Controller Selection

A controller that is able to comply with the high-level control goal needs to be selected. This controller needs to be able to determine the setpoints for the low-level controller based

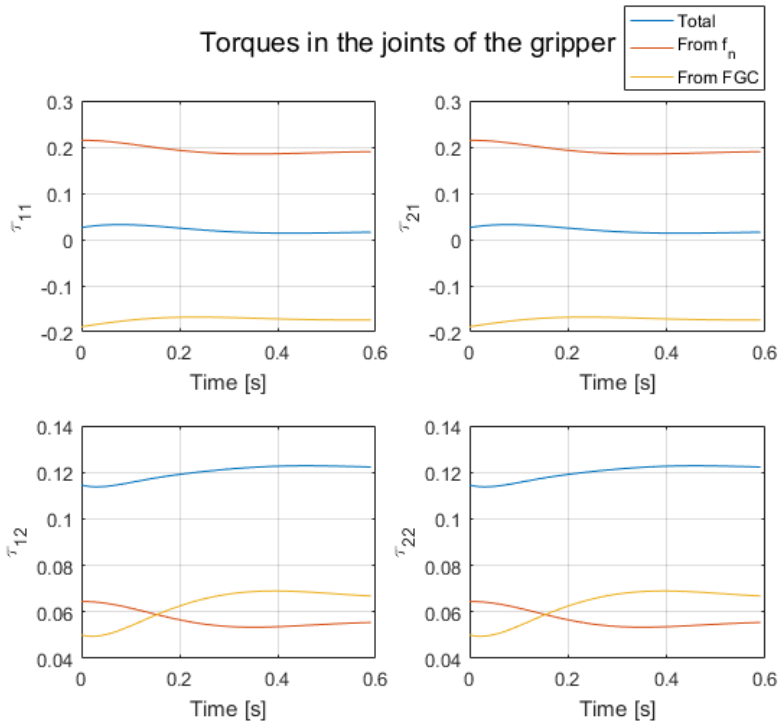


**Figure 4-7:** The torques in the gripper joints during the run.

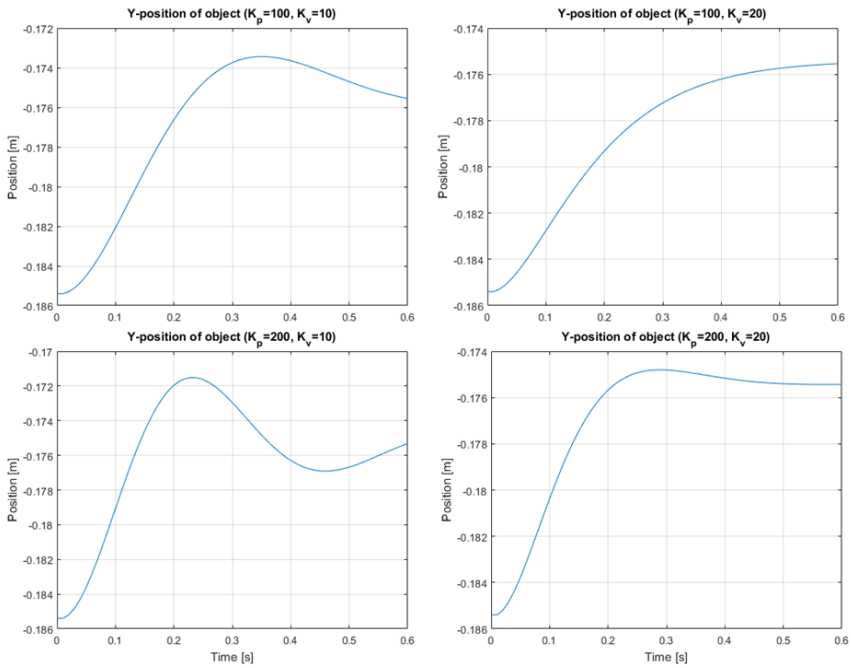


**Figure 4-8:** The response of the system, visualized by the height of the object, for different controller parameters.

**Table 4-2:** High-level controller approaches weighted against the criterion.

| | Score |
|---|---|
| Adaptive Control (AC) | |
| -Gain Scheduling | 2 |
| -Model Reference Adaptive Control (MRAC) | 1 |
| Extremum Seeking Control (ESC) | |
| -Analog Optimisation | 4 |
| -Numerical Optimisation | 5 |

on sensory information, i.e. it is a setpoint generator. The controller principles that will be explained here are versions of Adaptive Control (AC) and Extremum Seeking Control (ESC). These controller principles are selected because they are able to pass the gripping force setpoint to the the low-level controller. Besides that they are able to deal with instantaneous variations of item properties because item picking and releasing is a fast process. Finally they are selected because these are approaches when off-line calculation of the optimal parameters is impractical [8].

The performance of the different high-level controllers is determined with respect to a criterion:

- The controller needs to be able to deal with an unknown, wide variety of items.

The items are unknown to the high-level controller so the controller has to cope with this. Besides that, the items that have to be handled are very diverse so the controller also has to be able to deal with this wide variety.

A score on this criterion on a scale from 1 to 5 is assigned to the different controller approaches, as shown in Table 4-2. It can be seen that the Numerical Optimisation based ESC scores best on the criterion. This controller will be used as the high-level controller approach. The considered high-level controller approaches and the motivation for the scores on the criterion will be explained next.

### Adaptive Control

Adaptive control provides an adaptation mechanism that is able to adapt a controller based on parametric models. These models are only partly known in advance and adaptive control is, in contrast to traditional controllers like PID or pole placement, able to cope with these uncertainties because it adapts the parametric model on-line using performance error information.

Adaptive controllers are controllers with adjustable parameters and a mechanism for adjusting them [7]. This renders the overall controller non-linear so it opposes constant-gain feedback. An adaptive controller consists of two loops:

- Inner feedback loop that constitutes of the process and the low-level controller

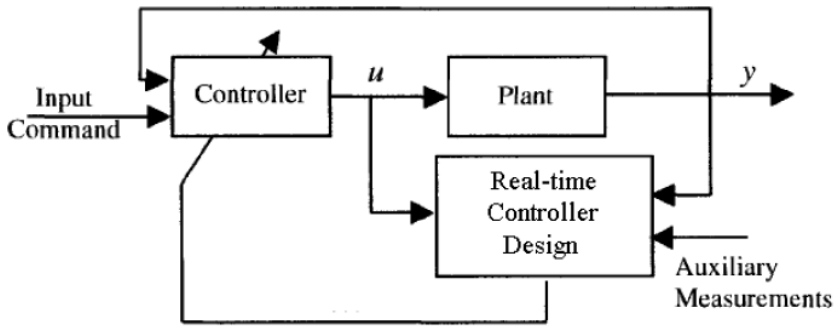


**Figure 4-9:** A general adaptive control scheme, from [6].

- Outer loop for parameter adjustment and set-point generation

The first loop contains the previously described low-level controller that stabilises the system, given a required set-point. The outer loop often has slower dynamics and is accountable for providing the low-level controller with the parameters and the set-points. A general scheme of an adaptive controller can be found in Figure 4-9. The inner loop consists of the controller, the plant and the upper line that represents the feedback. The outer loop consists of the Real-time Controller Design block together with the adaptable controller. Several types of adaptive control schemes can be distinguished:

- Gain Scheduling
- Model Reference Adaptive Control (MRAC)

The general working principle and the possible application in this project will be described below.

**Gain Scheduling**
The block diagram of a gain scheduling controller can be found in Figure 4-10. The main principle of this scheme is that the controller parameters are adapted according to an operating condition. This can be a performance function indicating the performance of the controller or just a state of the system, for example the temperature. Based on this measurement a predefined set of controller parameters is selected. This can be based on a function but also on a look-up table. This controller, in principle, is able to deal with all operating points (i.e. all kinds of different products), however, only if the tuning parameters for all those points are predetermined. This is impractical because the variety of items in a warehouse is large and varying over time. So, because it is able to deal with a wide variety of items but not with an unknown variety of items, it scores low at the selection criterion: 2.

**Model Reference Adaptive Control**
A block diagram of a MRAC can be found in Figure 4-11. The controller parameter adjustment is based on the error between the output of the system and output of a desired reference model. In this case the controller parameters are directly set by the adjustment mechanism: this is direct MRAC. Indirect MRAC, on the contrary, first estimates the model parameters

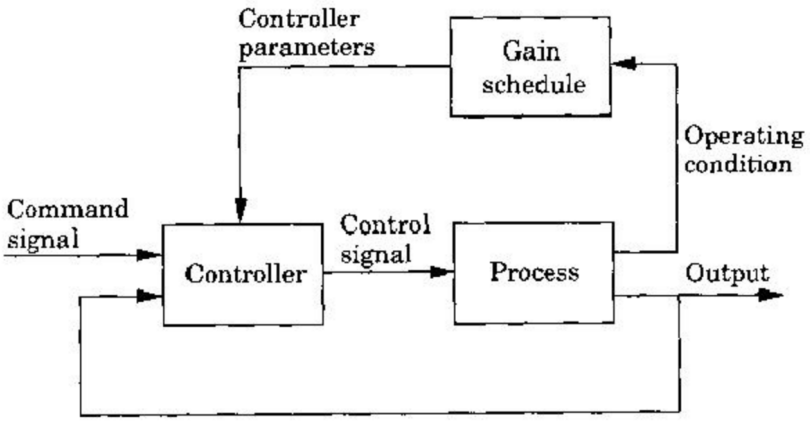


**Figure 4-10:** A block diagram for a system with gain scheduling, from [7].

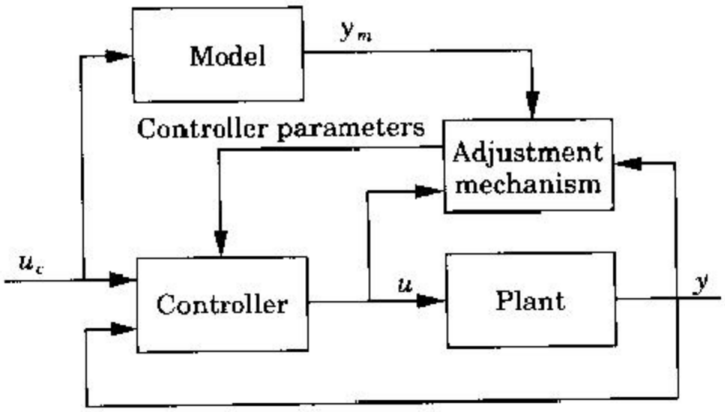


**Figure 4-11:** A block diagram for a MRAC system, from [7].

based on which the controller is tuned. The certainty equivalence principle has to be used here: the controller is tuned as if the estimated parameters are the true parameters [7].

Adaptive controllers can be based on a gradient method or Lyapunov stability theory. The adjustment rules that are obtained via both methods are similar. The only difference is that the rules in the latter case are not normalized and that arbitrary high adaptation gains can be used while the error is still guaranteed to go to zero. In both approaches, the parameters are not ensured to go to the true parameters. The direct MRAC based on a gradient method is discussed next, together with an example.

A general direct MRAC control scheme can be found in Figure 4-11. The controller is adapted based on the measurement of the input and the output of the the plant and possibly some other measurements. An important part of the adaptive controller is the on-line parameter estimation or adaptive law, which generates estimates of the unknown parameters to be used for calculating or updating the controller parameters in real-time [75].

In order to estimate the system dynamics, the unknown parameters have to be separated

from the known parameters. Generally the following form is used for that:

$$\zeta = \theta^T \phi, \tag{4-28}$$

where $\zeta$ is called the observation, $\theta$ the regressand containing the unknown parameters and $\phi$ the regressor. The observation and the regressor can be measured, while the regressand is unknown and is to be estimated. An example is found in the standard mass-spring-damper system generally formulated as follows:

$$M\ddot{x} + b\dot{x} + kx = F. \tag{4-29}$$

For simplicity it is assumed that the acceleration ($\ddot{x}$), speed ($\dot{x}$) and position ($x$) can directly be measured. The mass, damping coefficient and spring constant need to be estimated so the regressand is as follows:

$$\theta = \begin{bmatrix} M \\ b \\ k \end{bmatrix}. \tag{4-30}$$

The measurements linked to these parameters end up in the regressor:

$$\phi = \begin{bmatrix} \ddot{x} \\ \dot{x} \\ x \end{bmatrix}. \tag{4-31}$$

Finally by putting the external force $F$ in the observation the system dynamics can be written as:

$$\zeta = \theta^T \phi = \begin{bmatrix} M \\ b \\ k \end{bmatrix}^T \begin{bmatrix} \ddot{x} \\ \dot{x} \\ x \end{bmatrix} = M\ddot{x} + b\dot{x} + kx = F. \tag{4-32}$$

Because the dynamics of the model are unknown, the parameters need to be estimated. This can be done, among others, using a gradient-based algorithm. Based on the estimated parameters in the regressand, an estimate of the observation can be made, which is indicated using a hat:

$$\hat{\zeta} = \hat{\theta}^T \phi. \tag{4-33}$$

This estimate can be compared with the real observation resulting in an error signal:

$$\epsilon = \zeta - \hat{\zeta} = \zeta - \hat{\theta}^T \phi. \tag{4-34}$$

A logical cost function to minimise this error is the following:

$$J(\hat{\theta}) = \frac{1}{2}\epsilon^2 = \frac{\left(\zeta - \hat{\theta}^T \phi\right)^2}{2}. \tag{4-35}$$

This is minimised using the gradient method:

$$\dot{\theta} = -a \nabla J(\hat{\theta}) = -a \left(-(\zeta - \hat{\theta}^T \phi)\phi\right) = a\epsilon\phi, \tag{4-36}$$

where $a$ is a gain indicating the speed of adaptation. This is also called the MIT rule for adaptive control [7]. Other minimisation algorithms are also possible. Because of the fact

that $J(\hat{\theta})$ is convex, the gradient method is expected to converge to a global minimum if the system is persistently excited [75]. At that point the estimated parameter vector is equal to the real parameter vector.

$$\hat{\theta} \to \theta. \tag{4-37}$$

The control action of the low-level controller is based on the parametric model and once this model converges to the real model, the performance of the system increases. This approach relies on a reference model but with an unknown variety of items this is not possible. If it would be a known wide variety of items it would be possible to create a reference model for each product but with an unknown variety of items this is not possible. So it can be concluded that the same objections hold with MRAC as with Gain Scheduling. One more objection is that the states of the reference model should be measured which is also not possible because of deformability and variability of the items. Therefore it scores lower compared to gain scheduling on the criterion: 1.

### Extremum Seeking Control

ESC is an approach for processes of which the reference value is not easy to determine. The goal of this approach is to find an optimal operating point and track it. In this approach there are also two feedback loops: one regulator loop that regulates the system to the set-point generated by the second loop, which determines this set-point based on the result of the evaluation of a performance function. It is assumed that the low-level controller is a stabilising controller on the given trajectory. The estimation of the parameters in an adaptive control scheme is based on the knowledge of the structure of the model, while in ESC the estimation of parameters and generation of reference values is model free. Therefore this approach is also called model free adaptive control [76]. A division can be made between analogue optimisation based ESC and numerical optimisation based ESC. The general working principle and the possible application in this project will be described below.

**Analog Optimisation based Extremum Seeking Control**
Assume a system given as follows:

$$\dot{x} = f(x, u), \tag{4-38}$$
$$u = \alpha(x, \theta), \tag{4-39}$$
$$y = J(x), \tag{4-40}$$

representing a non-linear system for which a controller exist that is parametrised by $\theta$. The performance function $y$ is not an output of the system but just a performance measure based on the states. The closed loop system is:

$$\dot{x} = f(x, \alpha(x, \theta)). \tag{4-41}$$

This is the system that closes the inner loop i.e. the low-level controller. ESC is a high-level controller that closes the outer loop.

A general scheme for analogue optimisation based ESC can be found in Figure 4-12. Here one can see the previously described non-linear closed-loop system separated from the performance

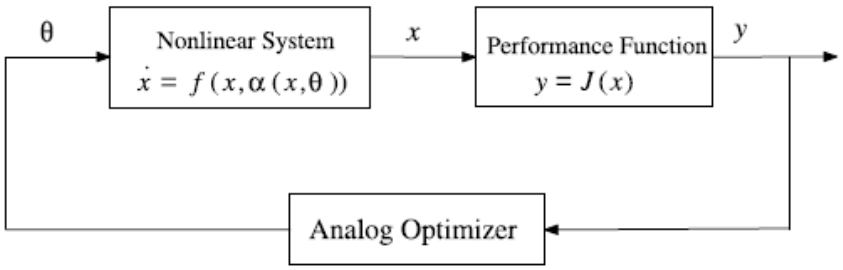


**Figure 4-12:** A general scheme for Analogue Optimisation based ESC, from [8].

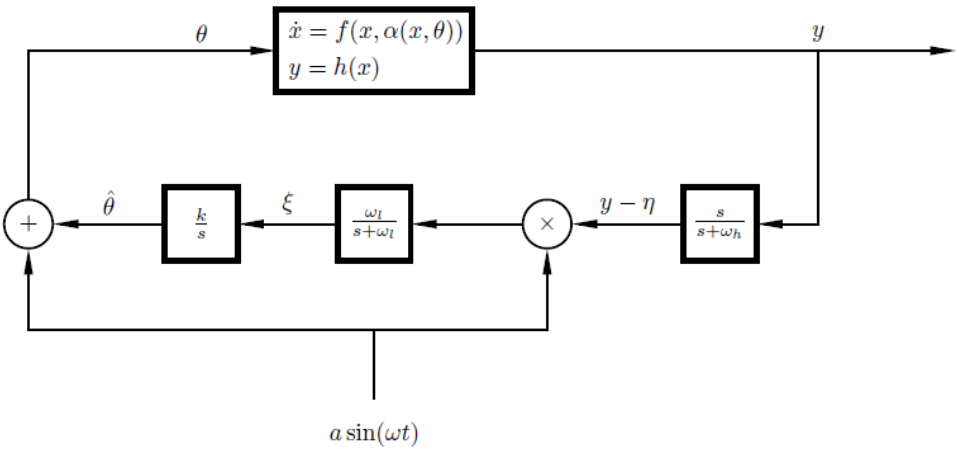


**Figure 4-13:** The scheme for excitation based ESC, from [9].

function. A gradient based optimisation based approach adapts the parameter vector $\theta$ as follows [8]:

$$\dot{\theta} = k\frac{dJ}{d\theta}, \quad k > 0. \tag{4-42}$$

It can be proven that this law converges towards the true parameter vector by using Lyapunov theory. The underlying principle in this approach is that the derivative of the performance function is assumed to be known. This approach relies on the analytical description of the gradient, however, this is not available in case of unknown items. The limited knowledge on the gradient can be solved by the excitation based optimisation method, which is an extension to this approach.

The scheme for excitation based analogue optimisation based ESC can be found in Figure 4-13. The sinusoidal excitation signal excites the system to get an idea of the gradient of the performance function. If the system is operating in a local minimum, the excitation signal can help in getting out of this local minimum to end up at the global minimum. The separation of the time scales of the dynamics of the system is the key element in this scheme. The plant with the stabilising controller has the fastest time scale, this is the low-level controller. The excitation signal has a medium time scale and the setpoint adaptation law, the high-level

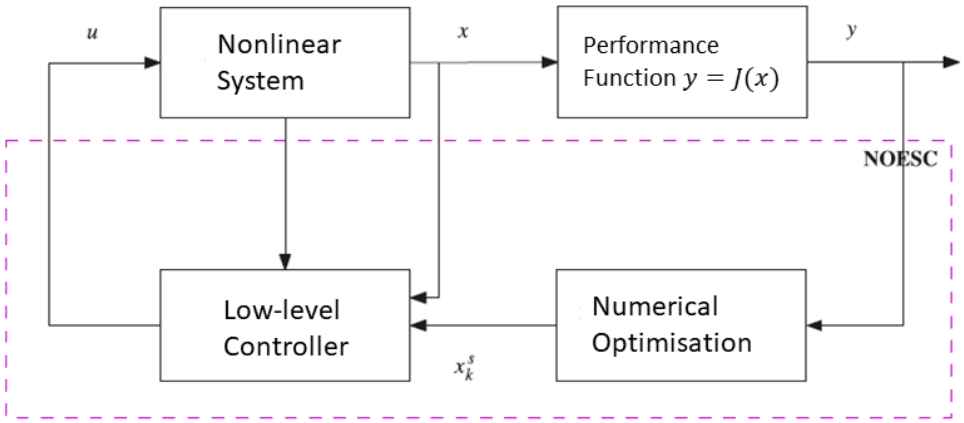


**Figure 4-14:** A general scheme for Numerical Optimisation based ESC, adapted from [8].

controller, has the lowest. This allows the optimiser to see the process with the low-level controller as a static map of which the optimum performance can be found based on the performance function.

Because of the fact that this approach does not require knowledge of tuning parameters or models, as within Adaptive Control, this approach scores high on the criterion. Besides that the gradient adaptation law and the excitation to obtain knowledge on the system dynamics are appealing advantages of ESC. However, this approach is not suited to tune the setpoints of the low-level controller. This inability makes this approach score 4 on the criterion. A way to extend the analog optimisation based ESC such that it can generate setpoints is explained next.

**Numerical Optimisation based Extremum Seeking Control**

A general scheme for Numerical Optimisation based ESC can be found in Figure 4-14. This approach is also called Learning-based Adaptive Control [76] because it makes use of a model as much as possible, complemented with a model free learning approach. ESC is now seen from the perspective of optimisation. In this approach the optimizer determines the setpoint for the low-level controller to follow. It is also possible to determine controller parameters of the state regulator in the optimisation algorithm. It is formulated as follows:

$$\begin{aligned} &\min\ J(x), \\ &\text{s.t. } \dot{x} = f(x,u), \end{aligned} \tag{4-43}$$

with $u$ the input of the nonlinear system. The state regulator of Figure 4-14 can be seen as the low-level controller. This loop works on the fastest time scale. On a much slower time scale, the performance function is evaluated. Based on this evaluation the setpoint for the low-level controller is updated.

This approach has the same advantages as analog optimisation based ESC, but without the disadvantage. So, it is model free, has the ability to generate setpoints, uses the gradient law and has the possibility of excitation. Therefore it scores 5 on the criterion and this approach is selected for this project. The details with respect to the application in this project are given in the next section.

### 4-3-2 Numerical Optimisation based Extremum Seeking Control Details

This section describes how the chosen high-level controller can be applied within this project. The high-level controller has to determine the reference gripping force based on measurements. The available measurements are the angles and velocities of the finger joints, the force on the fingers and the COP on the fingers. These measurements are captured in the vector $z$, which is a vector containing the states and the measurements. The non-linear system consists of the combined dynamics of the system, this is shown in the upper left box in Figure 4-15. These dynamic equations and $z$ are used by the low-level computed torque controller. To create a slip-based high-level controller, the COP of both fingers have to be in the measurement function. This is the function on which the adaptation of the reference is based.

$$J(z) = \begin{bmatrix} COP_1 \\ COP_2 \end{bmatrix}. \tag{4-44}$$

To determine the setpoint on the reference gripping force, the gradient adaptation law is used. The absolute value of the derivative of the measurement function is taken because any displacement, i.e. both positive and negative, has to be prevented, resulting in the following gradient based adaptation law:

$$\dot{f_n} = \begin{bmatrix} \gamma & \gamma \end{bmatrix} \left| \frac{\partial J}{\partial t} \right|. \tag{4-45}$$

Note that the derivative of this specific measurement function is a measure of the slip $\eta$ of both fingers. This is logical because if the object is moving with respect to one of the fingers, there is slip. The gradient based adaptation law becomes;

$$\dot{f_n} = \gamma(|\eta_1| + |\eta_2|), \tag{4-46}$$

which is also intuitive to understand because if a slip is detected, the gripping force is not high enough so it has to be increased in order to hold the object. The output of the adaptation law is the reference gripping force, which is used by the low-level Computed Torque Controller to calculated the torques in the joints of the fingers. This completes the loop in scheme of Figure 4-15.

The model-free adaptation of setpoints by making use of the gradient law is discussed, what is left unmentioned is the excitation. Excitation in the view of this project means shaking the gripper while it is holding the object. In this way the slips that are required to let the high-level controller adapt are induced before the actual trajectory is started. In this way the optimal reference gripping force is found and there is no need to adapt this while executing the movement. The shaking motion will be in the direction of the highest acceleration of the trajectory in order to adapt to the worst case scenario. This ends the discussion on how this controller approach will be applied on this project. This high-level controller will be implemented in Chapter 6.

## 4-4 Conclusion

The control goal is to grasp and hold deformable items with minimal gripping force and maximal *grasp quality*. *Grasp quality* is a measure defining the relation between forces and

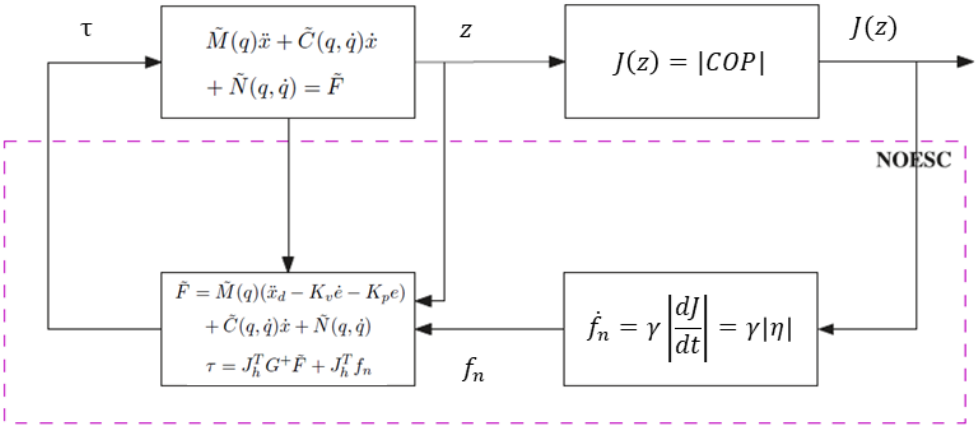


**Figure 4-15:** The scheme for Numerical Optimisation based ESC applied on this project, adapted from [8].

moments on the object that can be withstood by the gripper. The excess in gripping force is defined by looking at human factors research and uses a safety factor of 50%. The control goal is divided in a low-level and a high-level control goal. The low-level controller is selected to be a Computed Torque Controller because it has good tracking performance, stability and robustness. The high-level controller will make use of Numerical Optimisation based Extremum Seeking Control (ESC) because it performs best on the criterion that is defined. This control strategy, containing the low-level and high-level controller, will be used in a test environment in Chapter 6. The test environment that will be used is the topic of the next chapter, Chapter 5.

# Chapter 5

# Simulation Environment

In order to be able to judge the performance of the control strategy and optimise the controller parameters, a test environment needs to be defined. This is the topic of this chapter.

## 5-1 Test Environment

The test environment can either be a real test set-up or a simulation environment. It is chosen to test the controllers in a virtual environment because:

- It enables quick implementation of controller principles
- It omits practical issues that arise when creating a real test set-up such as real-time controllers, discontinuous systems and sensor delays that are not considered
- It is safe because failing controllers will not result in equipment being damaged or humans getting injured
- It is cheap because no time and money have to be invested in order to produce the hardware of the test set-up

The simulation environment hence acts as a rapid prototyping environment with the advantages mentioned above.

The choice of testing in a virtual environment also enables the possibility to simplify the problem further because it allows to consider the planar case only. This means that the gripper is only acting in the plane. This also holds for the objects and the motion of the gripper on the trajectory. The motivation for this is that the pick-and-place task mainly works in the plane because the path that is followed by the robot is a 2D path. Also the swaying of the items occurs in one direction because the path is in 2D. Besides the fact that it is realistic to look at the 2D situation, there is also a practical reason behind it because the simulation time increases when going from 2D to 3D. A small test is performed in Simulink

**Table 5-1:** Comparison of simulation time with one ball on table.

| | Simulation time [s] | Standard deviation [s] |
|---|---|---|
| 2D | 2.49 | 1.24 |
| 3D | 2.83 | 1.15 |

**Table 5-2:** Comparison of simulation time with two balls on table.

| | Simulation time [s] | Standard deviation [s] |
|---|---|---|
| 2D | 3.99 | 0.99 |
| 3D | 5.01 | 1.50 |

to show this effect. First one ball is dropped on a table. The interaction between the ball and the table in 2D is described by the interaction between a circle and a line. In 3D this is a sphere with a plane. 10 runs were performed and the mean simulation time and standard deviation are shown in Table 5-1. The mean simulation time increased with 13.6%. Secondly, two balls on top of each other are dropped on a table. In 2D the interaction between the two balls is a circle on a circle. The interaction of the balls with the table is again a circle on a line. In 3D the interaction between the balls is a sphere on a sphere. The interaction of the balls with the table is again a sphere on a plane. Also here 10 runs were performed and the mean simulation time and the standard deviation are shown in Table 5-2. There is an increase in mean simulation time of 25.6%. So, by adding one more ball, the increase in simulation time from 2D to 3D almost doubled. In case of more complex items and contact surfaces, this increase will grow and become unacceptable to work with. This test is relevant for this project because the products that will be used will also be represented by balls, as will be explained in Section 5-7. This finalises the argumentation to only look at 2D for now.

## 5-2 Software Environment

A software environment needs to be selected to perform the simulations. The environment needs to be able to deal with contacts between the gripper and objects. Five of such environments were often encountered in literature on grasping. They are described next.

- GraspIt! focusses on grasp planning by quickly testing thousands of different grasp poses and analyse the performance of each. This only holds in 3D because in a 2D case without wrist rotation there is only one grasp pose. GraspIt! is less suited to model contact interactions, execute movements and implement controllers.
- Mujoco focusses on speed and accuracy in simulation of interactions between bodies. It is possible to execute trajectories but implementing controllers is less convenient.
- NVidea PhysX SDK is developed to quickly calculate the motion of particles that interact with each other in preprogrammed scenes. It is hard to create custom scenes and to put controllers in the loop.
- Unity 3D is a physics engine created for the gaming industry. The focus is on realistic visualisations. Also here it is hard to put controllers in the loop.

**Table 5-3:** Software environments weighted against the criteria.

| | 1. Speed | 2. Flexibility | 3. Interactivity | 4. Proficiency | Score |
|---|---|---|---|---|---|
| GraspIt! | 2 | 1 | 1 | 1 | 8 |
| Mujoco | 3 | 2 | 1 | 1 | 11 |
| NVidea PhysX SDK | 3 | 1 | 1 | 1 | 9 |
| Unity 3D | 2 | 2 | 1 | 1 | 10 |
| Matlab/Simulink | 1 | 2 | 3 | 3 | 17 |
| Weighting | 1 | 2 | 2 | 2 | |

- Matlab/Simulink is a common software environment in research. Within Simulink there is a package, Simscape Multibody, to model contacts and execute movements, however objects and contacts need to be defined separately which is cumbersome. Reading out sensor values and directly acting on that by means of a controller is possible. Because this is a very multifunctional program, the focus is not on speed.

It can be concluded that there is no dedicated simulation environment that is directly suited for the problem described in this thesis so independent of the simulation environment, a lot of custom development needs to be performed. In order to select the software environment that will be used in this thesis, criteria will be set up to judge the different options.

1. The first criterion is the speed of the program: it is beneficial if tests can be performed quickly.
2. Secondly, flexibility in the program is desired. Because of the experimental character of this research, a wide variety of scenarios need to be tested. Scenarios can, for example, differ in executed trajectory, product that is being gripped and changing control strategy. It is desirable if the program allows for this flexibility.
3. Next, it needs to be possible to implement controllers in the loop, i.e. it needs to be possible to interact with the system based on sensory information in real-time. This is required to implement en test the controllers.
4. Finally, it is desirable if there is no need to learn new programs, because it saves time and it allows to quickly get to results. Therefore, proficiency with the program is the fourth criterion.

Because some criteria are more important than others, a weighting is introduced. The experimental setting and the limited development time result in the fact that flexibility, interactivity and proficiency are more important than speed in this research. Therefore, the weighting of the latter is lower, as shown in Table 5-3.

The different software environments are judged on the criteria on a scale from 1 to 3, where 1 is a low score and 3 a high score. The result is shown in Table 5-3. GraspIt! is relatively fast, but less suited to model contact interactions, execute movements and implement controllers. Therefore, it scores 2 on speed, and 1 on flexibility and interactivity. Mujoco focusses on speed, so it scores 3 on the first criterion. Changing the scenario is possible to some extend,

therefore, it scores 2 on the flexibility criterion. Implementing controllers is less convenient, therefore it scores 1 on the interactivity criterion. NVidea PhysX SDK also scores high on speed. The scene are preprogrammed and it is hard to implement controllers in the loop, therefore, it scores 1 on flexibility and interactivity. Unity scores average on speed. Changing the scenes is possible to some extend, therefore it scores 2 on the second criterion. It is hard to put controllers in the loop so it scores low on interactivity. Matlab/Simulink does not focus on speed because the program is very multifunctional. It is relatively cumbersome to define the scenarios but it scores high on interactivity, 2 and 3 respectively. Because of proficiency with Matlab/Simulink, it score high on the last criterion while the other programs score low because of inexperience. It can be concluded that Matlab/Simulink will be used. The coming sections will elaborate more on the implementation in this program.

## 5-3 Gripper

Within Simulink there is a possibility to simulate multibody environments in Simscape Multibody. Bodies are imported as 3D CAD files and the interconnection between different bodies can be described by joints that constrain the motion in specified directions. The dimensions and a 3D model of the Schunk SDH gripper are obtained via the manufacturer. The dimensions are shown in Figure 5-1. The 3D model of the gripper in the simulation environment is shown in Figure 5-2. The 3D model is implemented with an eye on future work but the model will only be used in 2D in this thesis. The joint that is used to connect the fingers is the revolute joint that allows rotation around only one axis.

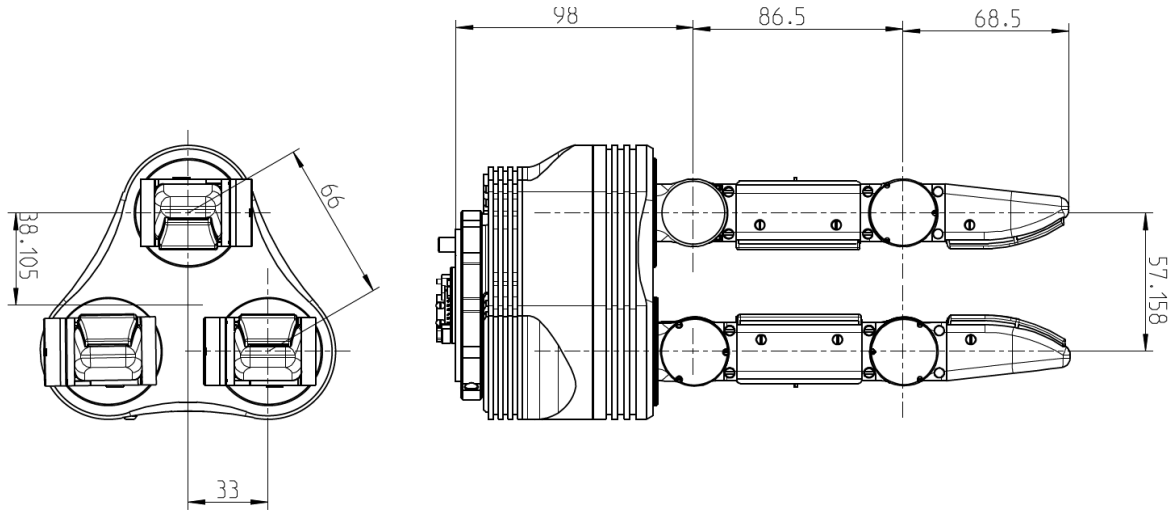


**Figure 5-1:** The dimensions of the Schunk SDH gripper.

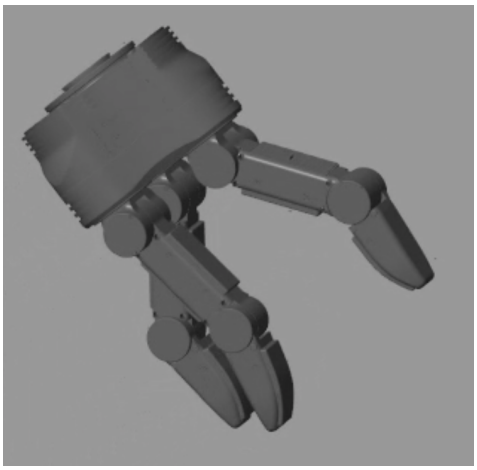

**Figure 5-2:** The 3D model of the Schunk SDH gripper that is used in simulations.

## 5-4 Contacts

Within Simscape Multibody, contacts between bodies can be described by making use of the Simscape Multibody Contact Force Library. The principles behind this library are explained next.

A contact is a binary condition: either there is no contact or there is contact with its incorporated dynamics. The contacts between the gripper phalanges and the items are modelled as binary mass-spring-damper systems. This means that the mass-spring-damper system is only active if there is contact. This results in a repelling force until the items in contact are separated again. The value of the stiffness and damping is dependent on the type of product that is being gripped, this will be explained in Section 5-7. Figure 5-3 shows the definition of the penetration direction in which the following normal force acts:

$$F_n = \begin{cases} kx_{pen} + b\dot{x}_{pen} & \text{for } x_{pen} > 0,\ \dot{x}_{pen} > 0 \\ kx_{pen} & \text{for } x_{pen} > 0,\ \dot{x}_{pen} < 0 \\ 0 & \text{for } x_{pen} \leq 0 \end{cases} . \tag{5-1}$$

Hence, a linear spring-damper resist penetration when penetration is increasing. During outward motion only the spring is active to quickly bring penetration to zero. If there is no contact, there is also no force acting between the bodies. The approach of using springs and dampers to model contacts with deformable items have widely and effectively been used for modelling deformable objects [77]. The specific form used here, with a spring and damper in parallel, is the Kelvin-Voigt model [20]. This model is used to model deformable materials like rubber and polymers [78]. This makes this model perfectly suited to model the deformable materials of the items considered in this project.

Besides the normal forces that are separating the parts from each other, there are also tangential forces modelled that represents the friction between particles. The normal force induces a tangential force because of friction, see Figure 5-4. The Coulomb friction law is used for this [79]. This incorporates a static and a kinematic friction coefficient. The value of the friction coefficient is determined based on the value of the velocity between the parts, this is shown in Figure 5-5. The contact speed is defined in the opposite direction of the friction

force $F_f$ in Figure 5-4. With zero speed the static friction coefficient will be used. In case of small positive velocity, a negative tangential force will be applied, and vice versa. Given this friction coefficient $\mu$ as function of contact velocity, the following friction law can be defined:

$$F_f = \mu(v_c)F_n. \tag{5-2}$$

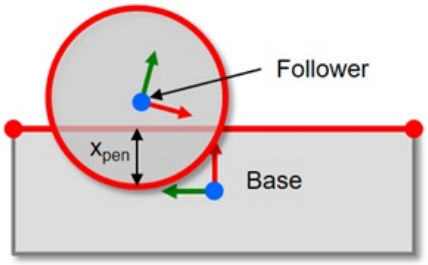


**Figure 5-3:** The direction of penetration used in the contact model.

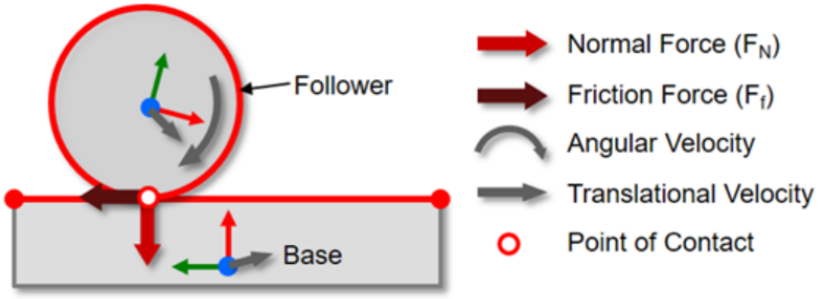


**Figure 5-4:** The normal force and friction force used in the contact model.

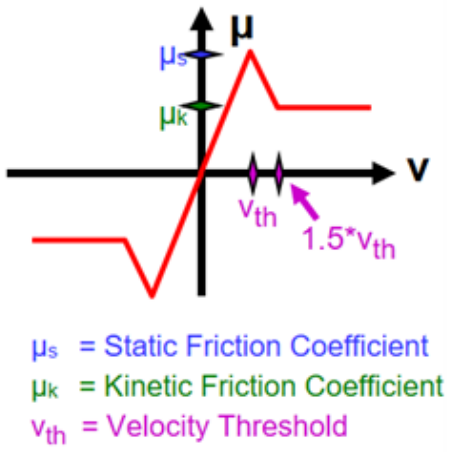


**Figure 5-5:** The contact velocity dependent friction coefficient used in the contact model.

## 5-5 Pick-and-place Environment

The pick-and-place environment consists of a Transport Storage Unit (TSU) at the pick location and a TSU at the place location. The size of a TSU is 600 $mm \times 400$ $mm \times 300$ $mm$. In a 2D situation, only the section of the TSU is taken into account so the resulting dimension is $600 \times 300$ $mm$. The distance between the centres of both TSUs is 0.96 $m$. The contact between the products and the floor of the TSU is modelled as described in the previous section.

## 5-6 Trajectory

The fixed and given trajectory of the pick-and-place robot makes use of trapezoidal trajectories. The maximum acceleration of the gripper is 3 $m/s^2$, the maximum speed is 1.5 $m/s$. The robot makes a horizontal movement of 0.96 $m$, the distance between the two TSUs in x-direction. The height of the path is 0.66 $m$ in y-direction. For the first part of the move this means that the total distance is:

$$\sqrt{0.96^2 + 0.66^2} = 0.82 \ m. \tag{5-3}$$

The maximum acceleration and velocity in the two directions are now calculated as:

$$a_{x,max} = \frac{0.96}{0.82} \cdot 3 = 1.76 \ m/s^2, \tag{5-4}$$

$$v_{x,max} = \frac{0.96}{0.82} \cdot 1.5 = 0.88 \ m/s, \tag{5-5}$$

$$a_{y,max} = \frac{0.66}{0.82} \cdot 3 = 2.43 \ m/s^2, \tag{5-6}$$

$$v_{y,max} = \frac{0.66}{0.82} \cdot 1.5 = 1.21 \ m/s^2. \tag{5-7}$$

The time required to get to the maximum speed with the given maximum accelerations in every direction is now calculated as:

$$t_{acc} = \frac{v_{x,max}}{a_{x,max}} = \frac{v_{y,max}}{a_{y,max}} = 0.5 \ s. \tag{5-8}$$

The cruising time is the time between acceleration and deceleration, the velocity is then equal to the maximum velocity and the acceleration is zero. This time is calculated by calculating the travelled distance for one of the directions and setting this equal to the required distance in the given time.

$$\frac{0.96}{2} = \frac{1}{2} a_{x,max} t_{acc} + v_{x,max} t_{cruise}. \tag{5-9}$$

This can be solved to calculate $t_{cruise}$, which is 0.0451 $s$. The parameters corresponding to the second part of the movement can be calculated in a similar way. The resulting acceleration, velocity and position profiles for both direction are shown in Figure 5-6. It can be seen that the maximum values are equal to the calculated ones. The path that the gripper is following, given these trajectories, is shown in Figure 5-7. It can be seen that the travelled distances are as required.

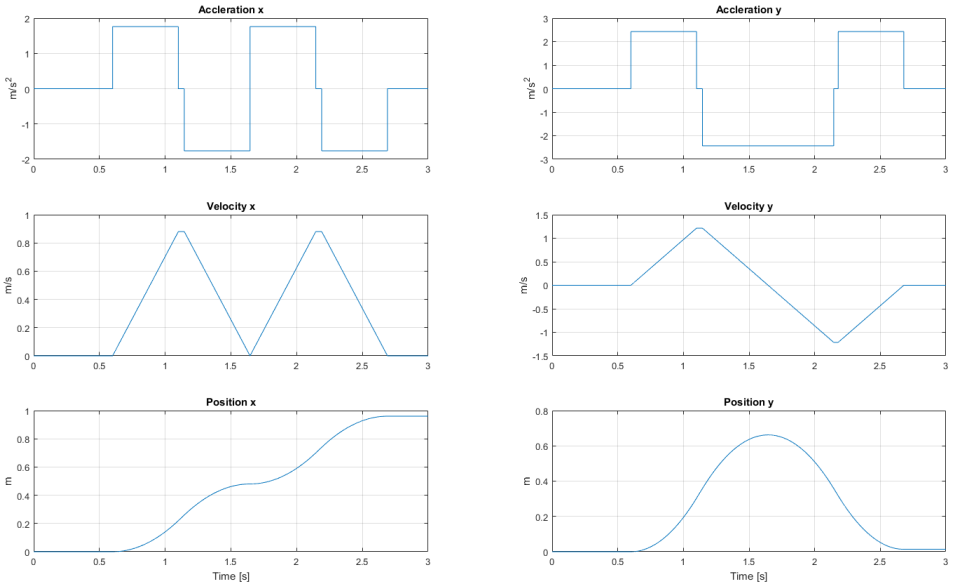


**Figure 5-6:** The acceleration, velocity and position profiles in x and y direction.

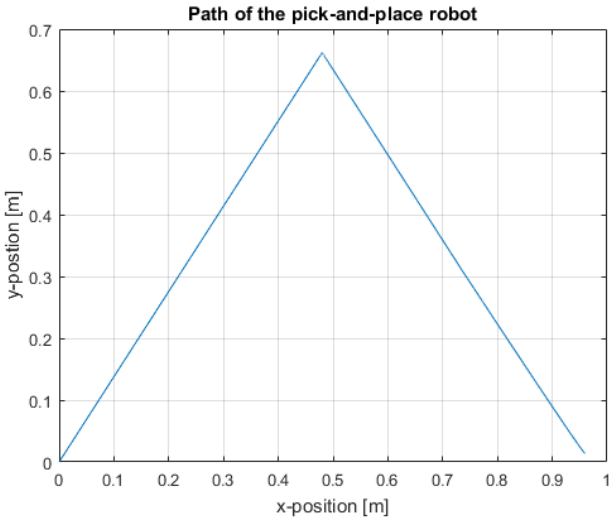


**Figure 5-7:** The path that the gripper follows in the pick-and-place environment.

## 5-7 Virtual Product Inventory

This research focusses on deformable products because these are challenging items for a robotic gripping system. Deformability here means that the object changes volume and shape once an external force is applied [20]. In order to be able to test the controller in the simulation environment, a set of test products need to be defined. The non-packed deformable items are represented by a ball. The feature that the controller has to be able to cope with, the low stiffness deformability, is independent on the shape of the object in this case.

Items from the other deformable categories are the nets and bags. The physical principle that makes this a challenging category to pick up are the forces that result from the fact that the item is not picked up at once and from the swaying motion during movement. The simplest object that captures this phenomenon is a pendulum because the product is not completely lifted once one of the elements is picked and a swaying motion during movement can occur. The pendulum needs to consist of a shape that has to be grasped by the gripper and a weight that has to be able to rotate at a distance from the first element. The first element is the ball that was used to represent the non-packed deformable items, a second ball is used to represent the displaced weight. The distance between the balls is chosen such that the gripper finger is able to fit between the balls. This abstraction of nets and bags makes it possible to quickly test the working principle of the controller.

The pendulum is not a real product in the inventory of a warehouse. An item that is present in the category list in Appendix A is a net with oranges. This is an item from the net category. At a higher level of abstraction it also represents the bag category, if only a small amount of items in the bag are actually in contact with the gripper. The shape and the dynamics of the items are then more or less the same. Therefore, as an example of a real product, the net with oranges is used to represent the category of deformable items that deals with variability in Center of Mass (CM), hence the nets and bags.

Table 5-4 shows the list of test products that will be used, together with the properties. The stiffness and damping correspond to the material model as described in Section 5-4. A nominal ball-shaped product is defined with a radius of 50 $mm$, the size of the softball. The mass is chosen to be 0.250 $kg$. The final properties required to define the object are the stiffness and the damping. The material of the ball is polyurethane foam with a stiffness of 6800 $N/m$ and a damping of 68 $Ns/m$ [80]. This ball, together with the gripper in 2D and the pick-and-place environment is shown in Figure 5-8. The items have a large variability in mass: this can be between 0.050 $kg$ and 1 $kg$. Therefore, balls with a mass of 0.050 $kg$, 0.125 $kg$, 0.500 $kg$ and 1 $kg$ are defined. Within the non-packed deformable items, also a teddy bear can be found. This teddy bear is modelled as a ball with a radius of 60 $mm$, the maximum size of the objects considered. Finally, a smaller item is added to the virtual product inventory: an orange with a radius of 38 $mm$. In [80] it can be seen that there can be quite some variation in the stiffness and damping of the foam, mainly depending on the compression level during the tests. One of the lowest stiffness measurements was 3200 $N/m$ and one of the highest was 12600 $N/m$. Regarding the damping, more or less the same variety was observed. Therefore, a product with a damping of 34 $Ns/m$ and a damping of 136 $Ns/m$ are added to the virtual product inventory.

The pendulum can now be defined a set of two connected nominal balls with each ball having half of the weight of the nominal ball. This is done in order to let the total mass be equal to

**Table 5-4:** The items in the virtual product inventory with corresponding item properties.

| Product | Mass [kg] | Radius [mm] | Stiffness [N/m] | Damping [Ns/m] |
|---|---|---|---|---|
| Nominal ball | 0.250 | 50 | 6874 | 67.8 |
| Lightest ball | 0.050 | 50 | 6874 | 67.8 |
| Light ball | 0.125 | 50 | 6874 | 67.8 |
| Heavy ball | 0.500 | 50 | 6874 | 67.8 |
| Heaviest ball | 1.000 | 50 | 6874 | 67.8 |
| Orange | 0.250 | 38 | 6874 | 67.8 |
| Teddy bear | 0.250 | 60 | 6874 | 67.8 |
| Low-stiffness ball | 0.250 | 50 | 3200 | 67.8 |
| High-stiffness ball | 0.250 | 50 | 12600 | 67.8 |
| Low-damping ball | 0.250 | 50 | 6874 | 34.0 |
| High-damping ball | 0.250 | 50 | 6874 | 136.0 |
| Pendulum | $2 \times 0.125$ | 50 | 6874 | 67.8 |
| Net with oranges | Contents: 0.225 | 38 | 6874 | 67.8 |
| | Package: 0.025 | 10 | 6874 | 67.8 |
| | Total: 0.250 | | | |

the case with the single ball. Besides that the radius, stiffness and damping of the ball that is gripped is taken equal to the nominal ball. The pendulum as described, together with the gripper in 2D and the pick-and-place environment can be seen in Figure 5-9. The connection between the balls is added to this picture for clarity.

The net with oranges contains 11 oranges with the same diameter as the orange used before. It is assumed that the gripper picks the upper orange and uses the grip on that orange and the net to lift the other 11 oranges. The net is represented by a series of small masses with a radius of 10 $mm$, connected by a stiff spring in order to represent the net. These masses are connected at a distance such that the oranges cannot go through, 48 $mm$. In order to be able to compare the performance of the controller in this case to the previous items, the total mass is again set to 0.250 $kg$ (package 0.050 $kg$ and contents 0.225 $kg$).

The items as described here need to interact with the gripper and the environment according to the contact laws from Section 5-4. The stiffness and damping are dependent on the item and given in Table 5-4. The contact law also requires a friction coefficient to determine the friction forces. In all cases, the friction between the gripper and the object is set to $(\mu_{stat}; \mu_{kin}) = (1.0; 0.8)$, based on friction coefficient of rubber [81]. In the net with oranges there is also friction between the oranges. The friction between the oranges in the net is set to $(\mu_{stat}; \mu_{kin}) = (0.30; 0.33)$, based on [82]. The net with oranges, together with the gripper in 2D and the pick-and-place environment is shown in Figure 5-10. The springs that are present between the particles representing the net, are indicated by lines.

**Figure 5-8:** The virtual ball and the gripper in 2D in the pick-and-place environment.

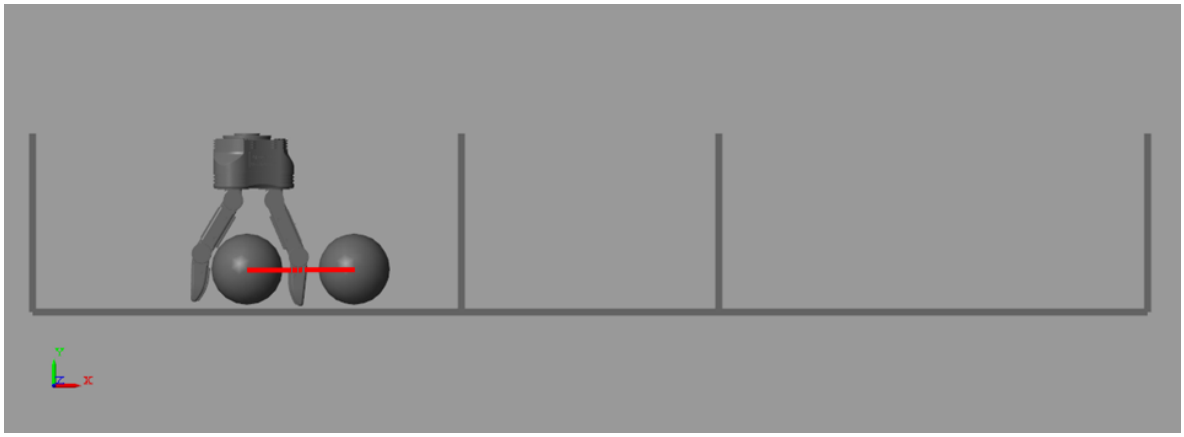

**Figure 5-9:** The virtual pendulum and the gripper in 2D in the pick-and-place environment. The connection between the balls is indicated in red for clarity, but not present in the real simulation.

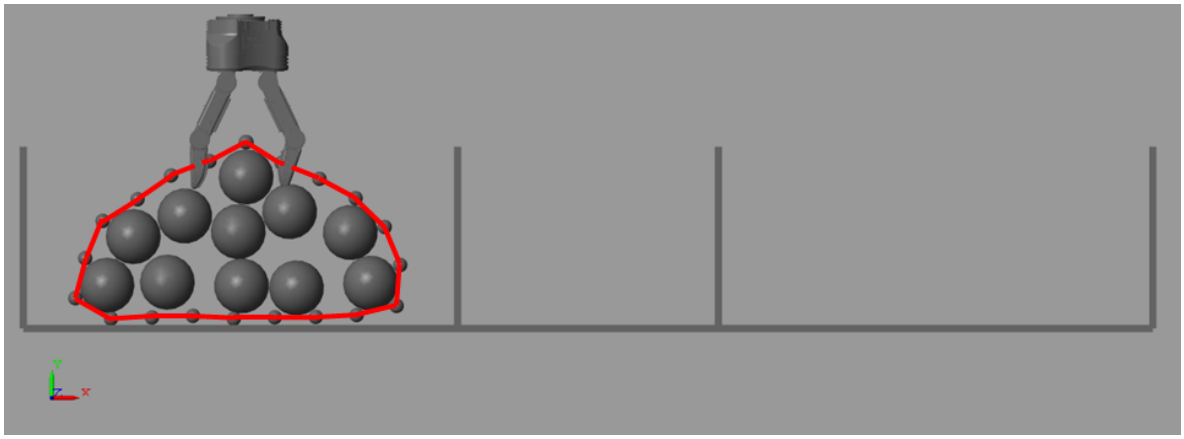

**Figure 5-10:** The virtual net with oranges and the gripper in 2D in the pick-and-place environment. The connections between the particles of the net are indicated in red for clarity, but not present in the real simulation.

## 5-8 Implementation in Simscape Multibody

Now that the gripper, contacts, pick-and-place environment, trajectory of the gripper and virtual product inventory are defined, they can be formalised in Simscape Multibody. This section shows how these concepts are implemented. First it is shown how the gripper is modelled. This is shown in Figure 5-11. The 3D CAD models of both the proximal and distal phalanges of the finger are loaded into the program. They need to be connected and besides that, it needs to be possible to apply a torque on the joint between them. Because of the fact that the origin and the rotation in the CAD files is not at the point of rotation, some Rigid Transform blocks are required. Once the bodies are transformed such that the origin of the CAD file is at the point of rotation, a revolute joint can be added. This joint has a torque as input and outputs the position and velocity of the joint which is used by the controller. After performing the inverse transformations, the distal finger can be connected. This shows how one of the fingers is modelled in Simscape Multibody.

Next is is shown how the pendulum is implemented. This is shown in Figure 5-12. The pendulum consists of two balls connected by a rod. This rod is modelled as a revolute joint connected to the first ball in order to be able to rotate and a prismatic joint connected to this revolute joint in order to create an offset between the balls. The rigid transform that is in between these two joints is required to align the axis of actuation of the specific joint types. The pendulum is located at the floor of the TSU. This means that there is a contact between the pendulum and the TSU. Because the pendulum balls are circles in a 2D environment and the TSU floor is a line, this contact can be described by a circle to line contact. This is done by the contact block coming from the Contact Force Library in Simscape Multibody. This contact block contains the contact models as described in Section 5-4. The pendulum does not only interact with the floor, but also with the gripper fingers. Only the first ball of the pendulum is gripped, so contacts with the fingers only need to be implemented on this ball. For simplicity, the contact in Figure 5-12 is only shown for one of the fingers. The proximal finger consists of a surface, this is a line in 2D. Therefore, the contact between the first ball of the pendulum and the proximal finger is described by the circle to line block (34 in Figure 5-12). The dotted line is connected to the proximal joint because the surface rotates as the finger rotates. The distal finger is composed of a surface which is a line in 2D. Besides that it has a camber at the end of the finger. From the CAD files it turned out that this camber is composed of two circles with different radii and centres. Therefore, the contact between the pendulum ball and the end of the finger is described by two circle to circle contacts. The overall contact between the first pendulum ball and the distal finger hence is described by one circle to line contact (31) and two circle to circle contacts (297 and 296). The dotted lines coming from these blocks are all connected to the distal joint.

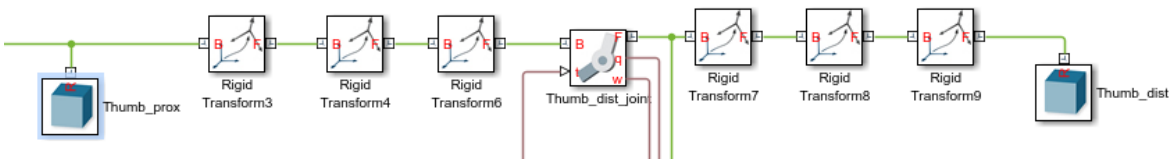


**Figure 5-11:** The implementation of a finger in Simscape Multibody.

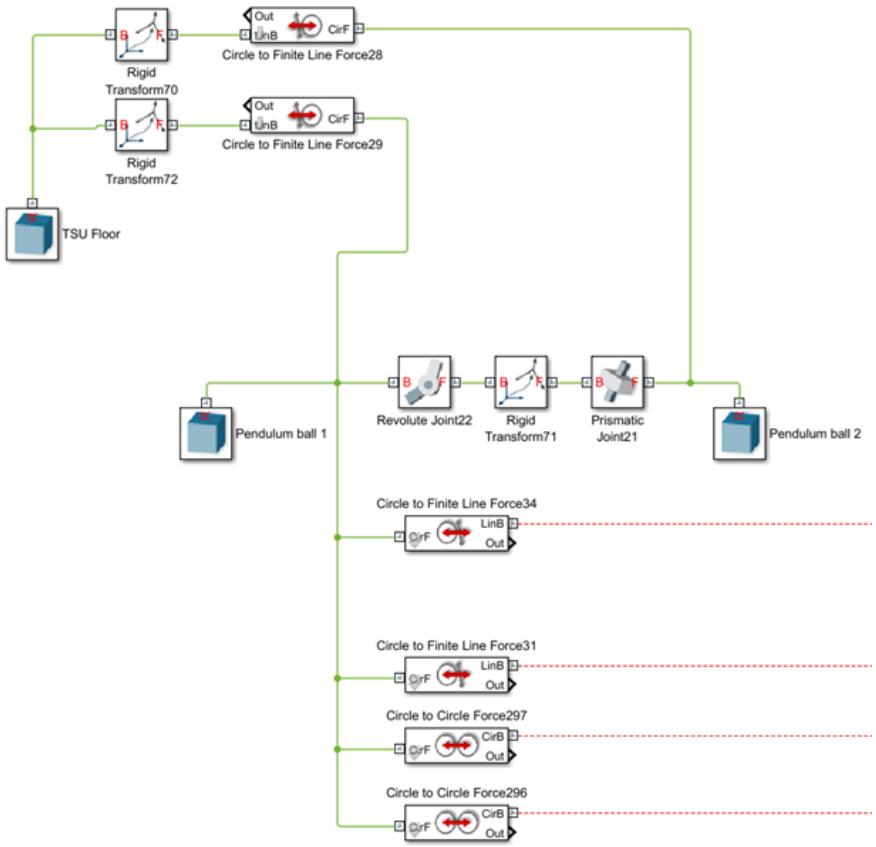


**Figure 5-12:** The implementation of the pendulum in Simscape Multibody, interacting with the TSU floor and one of the gripper fingers.

## 5-9 Conclusion

A simulation environment will be used as a test environment because it is cheap, safe, more convenient compared to a real test set-up and allows for quick implementation of controller principles. Matlab/Simulink is selected to be used as a simulation environment because of proficiency with the program, the interactive nature of the environment and the flexibility. A pick-and-place environment is defined, together with the gripper, the trajectory and the contacts. Besides that, a virtual product inventory is created in order to test the performance of the system on the deformable items from the considered product categories. The chapter ended by showing how these concepts are implemented in the simulation environment.

# Chapter 6

# Simulation Results

Now that the controller approach and simulation environment are known, the controller can be tuned by making use of simulations. The decoupling between the low-level and high-level controller allows for individual optimisation of the two controller levels. Therefore, this chapter first selects the optimal parameters for the low-level controller. After that, the high-level controller can be tuned. It is also discussed how the measurement of the slip signal is used by the high-level controller. In the last part of this chapter excitation is applied on the gripper to quickly converge to the gripping force that is required.

## 6-1 Low-level Controller

The low-level controller is implemented in the simulation environment. In order to optimise the low-level controller parameters, the friction coefficient and reference gripping force are set to a higher value such that no slip occurs while tuning the low-level controller. Only the static friction coefficient needs to be defined because no slip occurs during the run: $\mu_{stat} = 2.0$. Next to a higher friction coefficient, the reference gripping force is set to a higher value, which is required to deal with the inertial effects while not having the possibility to adapt the gripping force because there is no high-level controller that takes this into account yet. The reference gripping force based on a friction coefficient of $\mu = 0.5$ is used:

$$f_{n,ref} = \frac{m_{nom} g}{\mu} = \frac{0.250 \cdot 9.81}{0.5} = 4.91 \ N. \tag{6-1}$$

The nominal ball from the virtual product inventory is used to tune the low-level controller. The parameters of the Computed Torque Controller are set to $K_p = I$ and $K_d = 100I$ for the first run. The Grasp Quality Measure (GQM) over the run completed with these parameters is shown in Figure 6-1 [1] [2]. The mean GQM over the run is 0.0373. The controller was switched

[1] The corresponding video can be found at https://youtu.be/J2cHIk801fg or on the USB-stick that is included with this thesis (Video2). Note that the playback speed of the video is reduced by a factor 4.

[2] The corresponding video can be found at https://youtu.be/iAI9lgLgjDU or on the USB-stick that is included with this thesis (Video3). Note that the playback speed of the video is reduced by a factor 4.

on at 0.25 $s$. The vertical lines in the plots correspond to the steps in the acceleration profile from Figure 5-6. It can be seen that the acceleration influences the GQM. At around 1.2 $s$ the gripper is moving upwards and it is decelerating because it almost reaches the top of the triangular path (see Figure 5-7). At that moment the ball is moving upwards with respect to the gripper resulting in high quality. The same happens when the gripper is accelerating downwards, this can be seen from 1.2 $s$ on. If the gripper is moving downwards to the end of the triangular path and it is decelerating, the ball comes closer to a release resulting in a lower grasp quality. In the lower plot one can see changes in the gripping force resulting from changing accelerations. The fact that the gripping force is not always the same as the reference gripping force comes from the fact that the torques consist of two components: one from the Fundamental Grasping Constraint (FGC) and one from the reference gripping force, as discussed in Section 4-2-2. The latter torques result in the required gripping force while the first part of the torque calculation maintains the FGC. A close-up of the gripper at the start of the run is shown in the left picture of Figure 6-2. The gripper pose at the maximum GQM, at 1.35 $s$, is shown in the middle picture. The right picture shows the gripper pose at the end of the run. The gripping forces are indicated, as well as the direction of movement of the ball with respect to the gripper.

### 6-1-1 Optimisation of controller parameters on the nominal ball

The scenario as described is now tested for a set of 195 different controller parameter pairs. The controller parameters that are tested are:

$$K_p \in \{0.01, 0.1, 0.5, 1, 5, 10, 50, 100, 250, 500, 750, 1000, 2500, 5000, 10000\}\,, \tag{6-2}$$

$$K_d \in \{0.1, 0.5, 1, 5, 10, 50, 100, 250, 500, 750, 1000, 5000, 10000\}\,. \tag{6-3}$$

These are selected based on small tests that investigated the range of feasible controller parameter pairs. The average GQM in each run is computed in order to compare the performance among the different controller parameter pairs. The low-level control goal is to maximise the *grasp quality*, indicated by the GQM, while having the constant reference gripping force from (6-1). The average GQM of all runs is shown in Figure 6-3. It becomes clear that the controller fails for low values of both parameters and high values of both parameters. There exists a value for $K_p$ that gives good performance, almost independent of the value of $K_d$. The same holds for a range of values of $K_d$. It would be obvious that the optimal parameters of the controller are at the intersection of these two regions. In order to support this, a second measure based on the GQM is evaluated next to further differentiate between controller parameter pairs.

The maximum GQM over all runs is found to be 0.0512. For comparison of the controller parameters, the GQM is normalised with respect to this maximum value. This is called the GQM%. Besides having a high mean GQM, it is also desirable to have a high value of the GQM for a large amount of time. Therefore, the second measure looks at the percentage of the time that the GQM% is above 95%. This threshold is chosen empirically, the recommendations will further elaborate on this. This measure is called $t\%(GQM\% > 95\%)$ and is plotted in Figure 6-4. The shape of the surface is more or less the same as with the first measure that was plotted, however in this case a clear optimum arose.

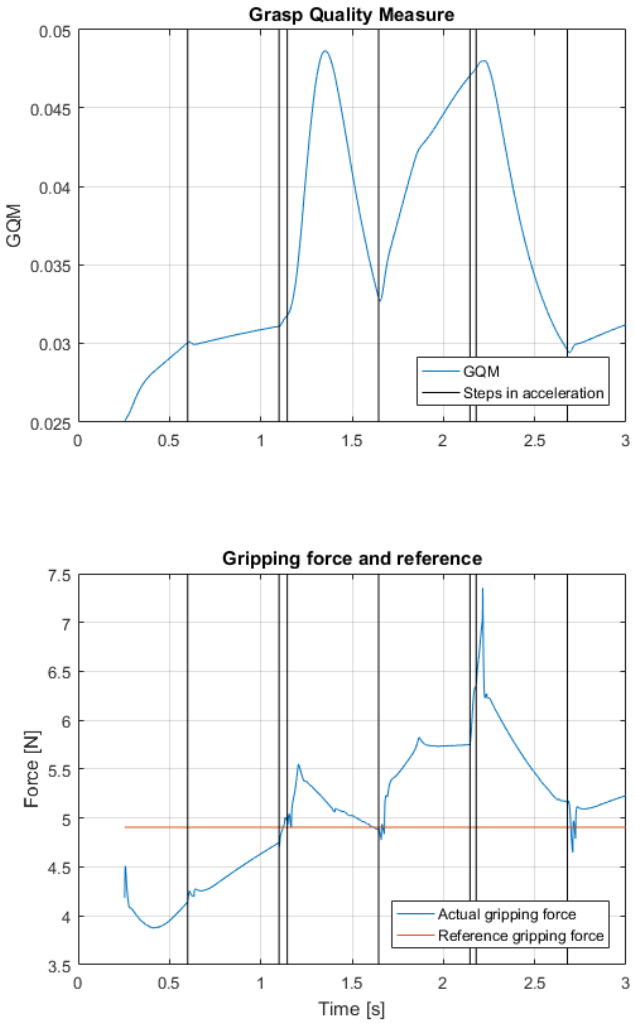


**Figure 6-1:** GQM and gripping force from the simulation with $K_p = I$ and $K_d = 100I$.

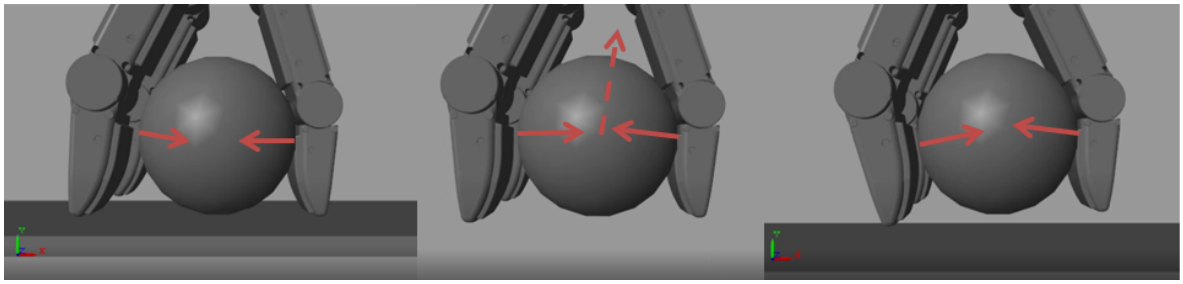

**Figure 6-2:** The gripper pose at the start, at $1.35\ s$ and at the end of the simulation with $K_p = I$ and $K_d = 100I$. The arrows indicate the gripping forces of the fingers on the object. The dotted arrow indicates the direction of movement of the ball relative to the gripper.

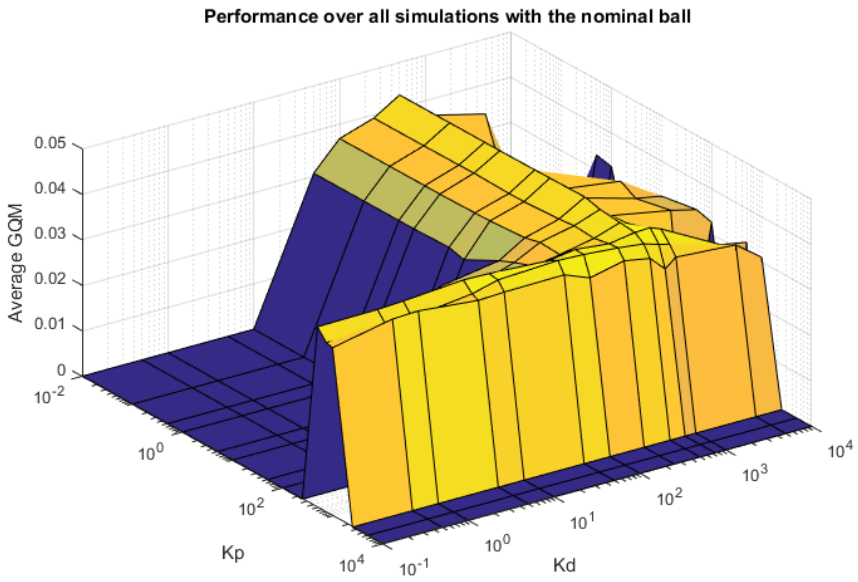


**Figure 6-3:** Average GQM plotted against the tested controller parameter pairs in the simulation with the nominal ball.

In order to see in one plot what the performance of the different controller parameter pairs is, the two measures are combined. Because of the fact that both are represented by a percentage, they can be averaged. The combined performance measure hence is defined as:

$$GQM\%_{comb} = \frac{1}{2}\left(GQM\% + t\%(GQM\% > 95\%)\right). \tag{6-4}$$

The combined performance measure and the found optimum are plotted in Figure 6-5. The optimal low-level controller parameters for the nominal ball are $K_p = K_d = 500I$.

### 6-1-2 Optimisation of controller parameters on the other virtual products

Because of the fact that the friction coefficient and the reference gripping force are set to high values compared to the properties of the items that are picked, no slip occurs. Because the size of the part of the pendulum and the net with oranges that is gripped by the gripper are the same as one of the ball-shaped items, the result of the optimisation is the same. From simulations it became clear that the inertial effects do not have influence on the performance because of the high gripping force. In the next section, the values for the friction coefficient and reference gripping force are set to the realistic values from Chapter 5 in order to tune the high-level controller. For now the optimisation is only performed on the other ball-shaped items from the virtual product inventory.

The controller needs to be able to pick up and hold the ball-shaped items from the virtual product inventory. It does not make sense to look at the controller pairs that were not able to do this, therefore, only a subset of the controller parameters pairs is looked at now. This subset consists of the region around the optimal controller parameters found on the nominal

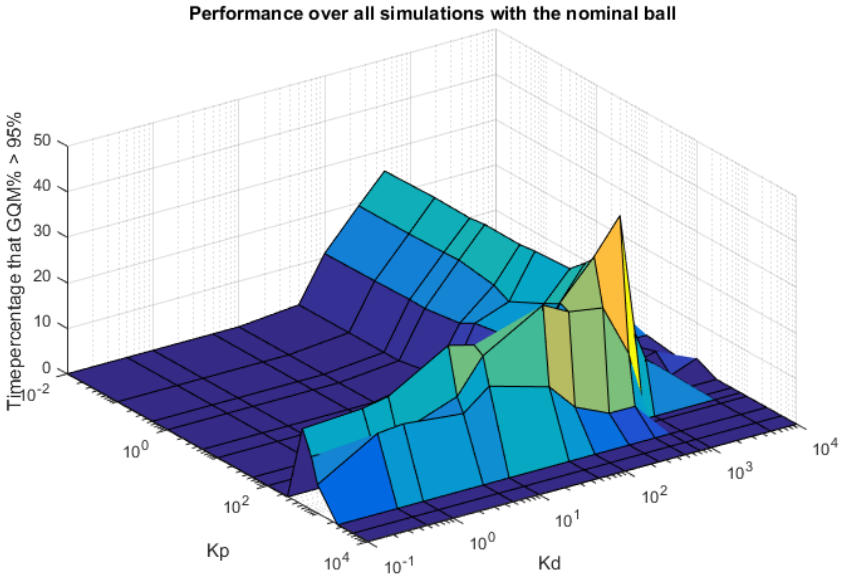


**Figure 6-4:** Percentage of the time that GQM$\%$ is above $95\%$ plotted against the tested controller parameter pairs in the simulation with the nominal ball.

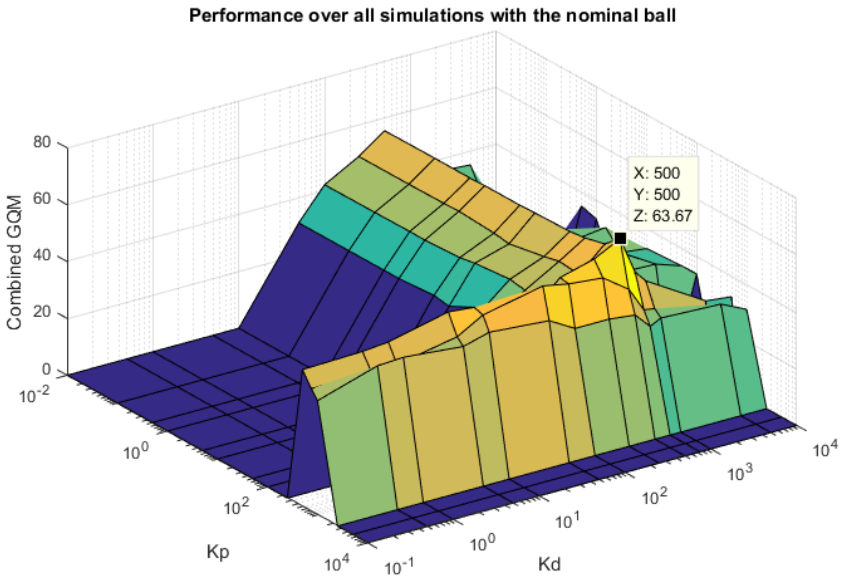


**Figure 6-5:** Combined performance measure plotted against the tested controller parameter pairs in the simulation with the nominal ball. The maximum value is indicated by the black square.

ball, namely:

$$K_p \in \{50, 100, 500, 1000, 5000\}, \tag{6-5}$$

$$K_d \in \{50, 100, 500, 1000, 5000\}. \tag{6-6}$$

First the optimisation performed on the virtual products that vary in mass is analysed. These are the lightest, light, heavy and heaviest ball. The combined performance measure $GQM\%_{comb}$ is again used to evaluate the performance of the different controller pairs. The result for the four products, together with the optima that were found, are plotted in Figure 6-6. The value of the optimal parameters and the combined performance measure is shown in Table 6-1. In case of the light ball, it can be seen that the optimum is still at $K_p = 500$ and $K_d = 500$, however slightly higher values result in bad performance. With the nominal ball, this drop in performance occurs at much higher values of the controller parameters. This suggests bad performance for even lighter object with the same controller parameters. It can be seen in the plot of the optimisation of the lightest ball, that this is indeed the case. The original controller parameters result in a failing grasp, as indicated by 0.00 in Table 6-1. Selecting the controller parameters to be $K_p = 100$ and $K_d = 500$ gives better performance for light items. For higher masses the opposite effect can be seen: the area of controller parameters on which the controller performs without failing is increasing. The difference between the value of the combined measure of the different controller pairs is decreasing. This means that good parameters for heavy objects are still $K_p = 500$ and $K_d = 500$, but by choosing the optimum parameter the performance can slightly be increased. It is expected that the observed effect comes from the fact that the controller actions are too aggressive in case of light objects. Only small torques are required to displace a light object. This is also supported by the fact that the value of $K_p$ has to be decreased for lower masses because that parameter influences the speed of the movement as seen in Section 4-2-2; the value of the damping term $K_d$ is not of influence here.

Secondly, the results with the virtual products that vary in size are analysed. These are the orange and the teddy bear. The plots of the $GQM\%_{comb}$ with the optima are shown in Figure 6-7. In case of the orange, the performance is more or less the same compared to the nominal ball. However, slightly better performance is achieved when selecting $K_p = 500$ and $K_d = 50$. Selecting $K_p = 500$ and $K_d = 500$ still gives more or less the same performance. The same holds for the bigger object, the teddy bear.

Next, the results with the virtual products that vary in stiffness are analysed. The plots of the $GQM\%_{comb}$ with the optima are shown in Figure 6-8. In case of lower stiffness of the object, the optimal controller parameters are stiffer, i.e. a higher value of $K_p$. This also holds vice versa: a higher stiffness of the object results in a less stiff optimum controller. The damping term of the controller, $K_d$, is not of influence in case of changing stiffness of the object. Despite the fact that slight improvements in performance can be made, still $K_p = 500$ and $K_d = 500$ give good performance in case of changing stiffness of the object.

Finally, the results with the virtual products that vary in damping are analysed. The plots of the $GQM\%_{comb}$ with the optima are shown in Figure 6-9. The optimal values of controller parameters are not influenced here. Note that a slightly higher damping term of the controller may cause problems in case of low-damping items.

All in all it can be stated that the found optimal controller parameters on the nominal ball do transfer to the other products in the virtual product inventory. The lightest ball is an

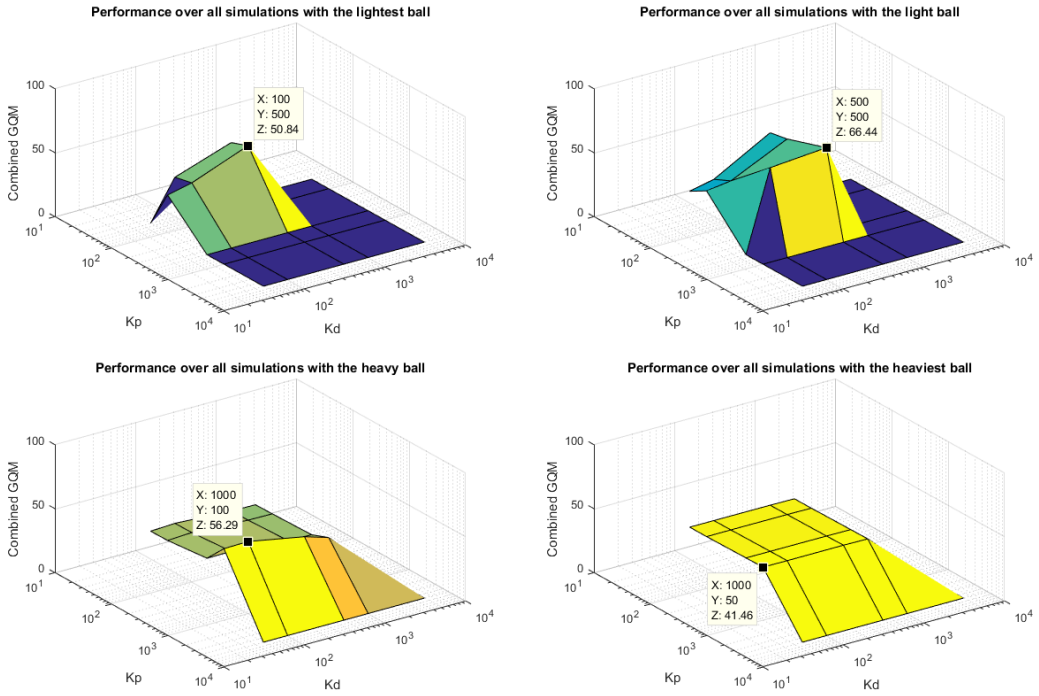


**Figure 6-6:** Performance over all simulations for the virtual products that vary in mass.

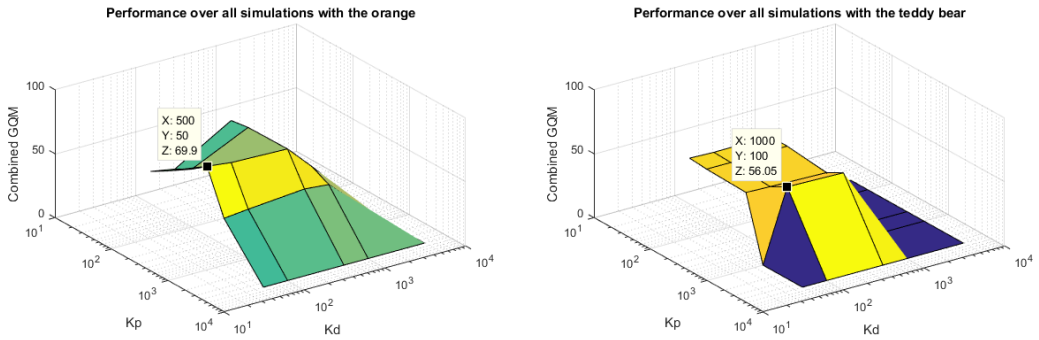


**Figure 6-7:** Performance over all simulations for the virtual products that vary in size.

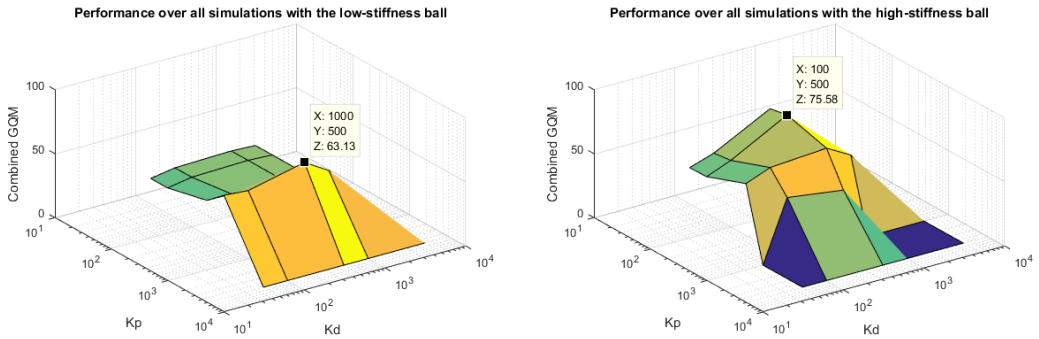


**Figure 6-8:** Performance over all simulations for the virtual products that vary in stiffness.

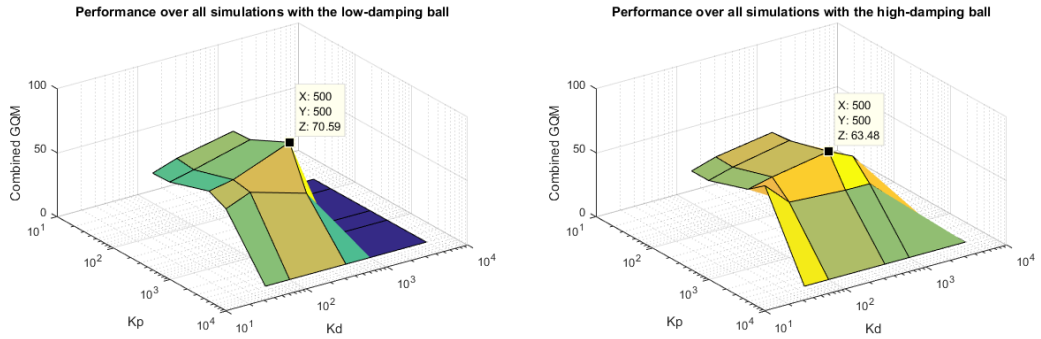


**Figure 6-9:** Performance over all simulations for the virtual products that vary in damping.

**Table 6-1:** The combined performance with the optimal low-level controller parameters for the ball-shaped items in the virtual product inventory, compared with the combined performance of two other controller parameter pairs.

| Product | $K_{p,opt}$ | $K_{d,opt}$ | $GQM\%_{comb}$ at optimum | $GQM\%_{comb}$ with $K_p = 500$ and $K_d = 500$ | $GQM\%_{comb}$ with $K_p = 100$ and $K_d = 500$ |
|---|---|---|---|---|---|
| Nominal ball | 500 | 500 | 63.67 | 63.67 | 57.08 |
| Lightest ball | 100 | 500 | 50.84 | 0.00 | 50.84 |
| Light ball | 500 | 500 | 66.44 | 66.44 | 56.03 |
| Heavy ball | 1000 | 100 | 56.29 | 37.75 | 36.38 |
| Heaviest ball | 1000 | 50 | 41.46 | 41.13 | 40.74 |
| Orange | 500 | 50 | 69.90 | 66.23 | 65.84 |
| Teddy bear | 1000 | 100 | 56.05 | 47.71 | 51.22 |
| Low-stiffness ball | 1000 | 500 | 63.13 | 39.87 | 40.14 |
| High-stiffness ball | 100 | 500 | 75.58 | 66.78 | 75.58 |
| Low-damping ball | 500 | 500 | 70.59 | 70.59 | 55.48 |
| High-damping ball | 500 | 500 | 63.48 | 63.48 | 54.82 |

exception to this: $K_p = 500$ and $K_d = 500$ result in a failing grasp with this product. $K_p = 100$ and $K_d = 500$ are optimal for this product and give good performance for the other products in the virtual product inventory, as shown in the last column of Table 6-1. Higher performance is possible for the specific products but generally speaking $K_p = 100$ and $K_d = 500$ give good performance over a wide range of items. Therefore, these parameters of the low-level Computed Torque controller will be used in the sequel of this report.

## 6-2 Slip Measurement

The scenario of picking up the nominal ball is now adapted to a realistic situation. This means that the friction coefficient is now set to the real value of $(\mu_{stat}; \mu_{kin}) = (1.0; 0.8)$, as discussed in section Section 5-7. Besides that, the reference normal force is calculated based on this value of the friction coefficient instead of a lower one that ensured a fixed grasp:

$$f_{n,min,static} = \frac{m_{nom}g}{\mu_{stat}} = \frac{0.250 \cdot 9.81}{1} = 2.45\ N. \tag{6-7}$$

No high-level controller is implemented yet. This results in the fact that the ball is lost [3]. This is because the reference gripping force does not take into account accelerations and kinetic friction. In a later phase the high-level controller will take this into account. In order for the high-level to be able to do this, the slip measurement is used because this value indicates that the reference gripping force is too low and adaptation is based on that. The raw slip signal that is measured in the realistic scenario is shown in Figure 6-10. It can be seen that quite some high-frequency components are present in the slip signal. Because the reference gripping force is determined based on slip measurements, high-frequency components will also be present in the reference gripping force. As can be seen in Section 4-2-2, the Computed Torque Controller requires some time to converge to the reference states. If the reference gripping force is changing at high frequency, over-adaptation can be the result because then the adaptation is faster than the Computed Torque Controller. Therefore, it is proposed to apply a first order low-pass filter on the signal. In order to select the cut-off frequency of this filter, the power spectral density of the measured slip signal is analysed. Figure 6-11 shows the full range of frequencies on the left and a close up on the right. The cut-off frequency of the the low-pass filter is set to 250 $Hz$ because most of the signal content is present before that frequency. Setting is to 10 $Hz$ will not get all important characteristics of the signal, whereas setting it to 1000 $Hz$ will not add extra information as compared to 250 $Hz$. The result of applying the filter is shown in Figure 6-12. It can be seen that the trend is well followed, as well as that the high-frequency peaks are filtered out. This signal can now be used as a basis for the adaptation of the reference gripping force.

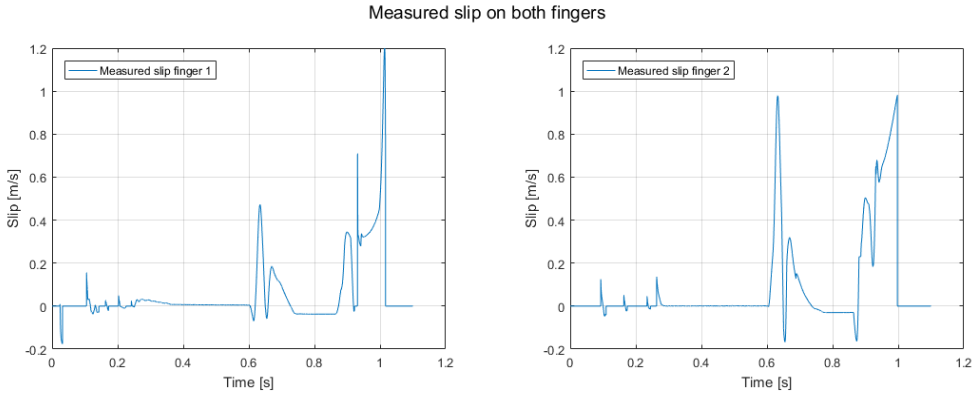


**Figure 6-10:** The slip measurement on finger 1 (left) and finger 2 (right) without filter.

[3]The corresponding video can be found at https://youtu.be/MG20c_liLLg or on the USB-stick that is included with this thesis (Video4). Note that the playback speed of the video is reduced by a factor 4.

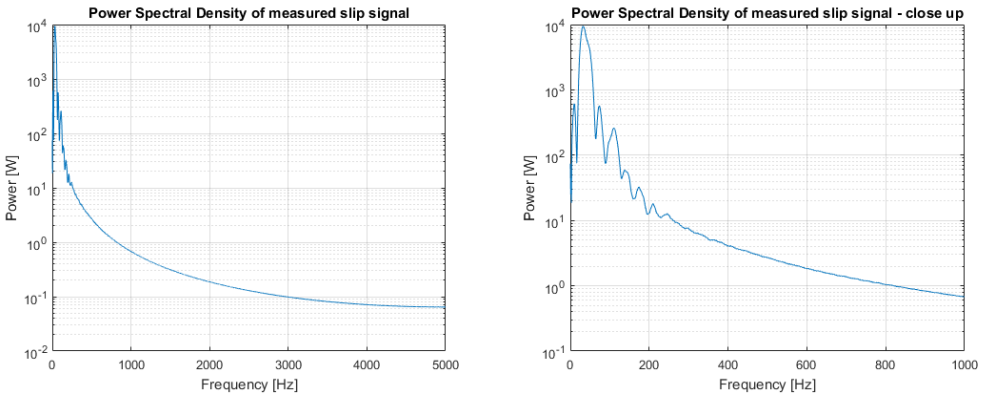


**Figure 6-11:** The spectral analysis of the measured slip signal of finger 1 (left), and a close-up (right).

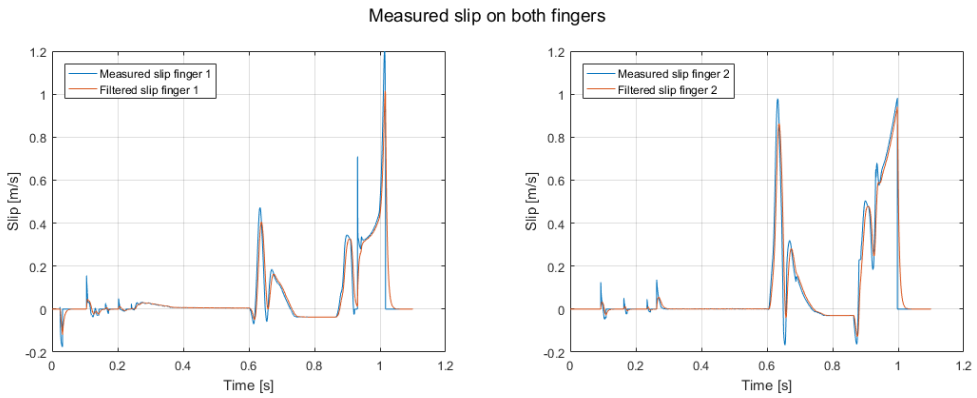


**Figure 6-12:** The slip measurement filtered at $250\ Hz$ on finger 1 (left) and finger 2 (right).

## 6-3 High-level Controller

In order to be able to judge the relative performance between different high-level controllers, a baseline run is performed in which the controller knows all the properties of the item. This hypothetical case is used as a baseline to compare the performance of the controllers that do not know this. As in the previous section, Section 6-2, the nominal ball is considered. The minimum required static gripping force is not enough to hold the ball, as was shown. This comes from the fact that slip and accelerations occur. Therefore, the minimum required dynamic gripping force can be calculated as follows:

$$f_{n,min,dynamic} = \frac{m_{nom}(g + a_{y,max})}{\mu_{kin}} = \frac{0.250 \cdot 9.81}{0.8} = 3.82\ N. \tag{6-8}$$

Due to the lack of inertial effects resulting from swaying in case of the ball, this is enough to hold the object. A run with a constant reference (no adaptation) is performed to show this. The resulting grasp quality and gripping force reference is shown in Figure 6-13. For completeness, the actual gripping force is also visualised. It can be seen that this is not equal to the reference gripping force. This comes from the fact that the torque computation consists of two parts, as explained in Section 4-2-2. The reference gripping force is equal to the minimum required dynamic gripping force and is therefore overlapping in the figure. The grasp quality of this run is used as a baseline to compare the performance of the high-level controller at different controller gains. This is done next.

As discussed in Section 4-3-2, the high-level adaptive law that will be used is:

$$\dot{f_n} = \gamma(|\eta_1| + |\eta_2|). \tag{6-9}$$

Only now the filtered version of the slip measurement will be used:

$$\dot{f_n} = \gamma(|\eta_{1,f}| + |\eta_{2,f}|). \tag{6-10}$$

A first version of the controller uses $\gamma = 30$. The initial value of the reference gripping force is set to a lower value than the dynamic minimum gripping force to see the high-level controller working, it is chosen to set it to the static minimum gripping force. It has to be noted that the scenario is the same as the scenario from Section 6-2, except for the fact that the high-level controller is now implemented: the result is that the ball is not lost any more, because of the adaptation of the reference gripping force. The resulting grasp quality, together with the baseline from the run performed with minimal dynamic gripping force is shown in the upper plot of Figure 6-14 [4]. It can be seen that the grasp quality of the run with high-level controller is higher for a large part of the run as compared to the run performed with minimal dynamic gripping force. The lower plot of Figure 6-14 shows that the final reference value of the gripping force is higher than the dynamic minimum gripping force. This comes from the fact that slip occurs at the beginning of the run. Slip means displacement so the contact location is different compared to the first run. Because of this initial displacement, more adaptation is required in a later phase. In the next section this excess in gripping force is related to the control goal and the optimisation is performed with respect to the adaptation gain $\gamma$.

[4]The corresponding video can be found at https://youtu.be/x0Y7AXNVvgg or on the USB-stick that is included with this thesis (Video5). Note that the playback speed of the video is reduced by a factor 4.

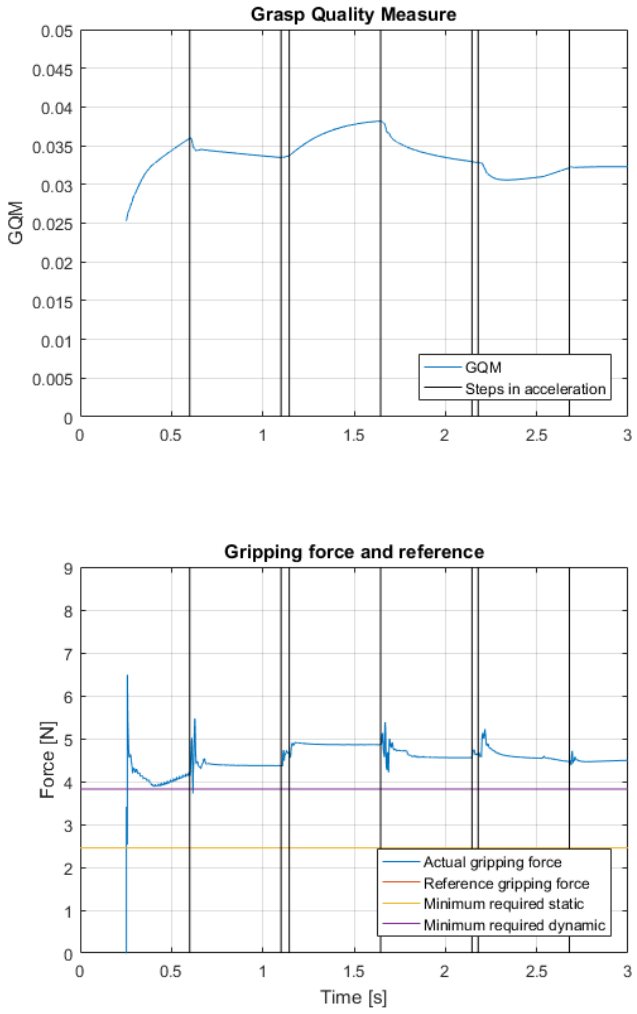


**Figure 6-13:** The grasp quality and gripping forces on the run without adaptation. Because the reference gripping force is equal to the minimum required dynamic gripping force, they are overlapping in the plot.

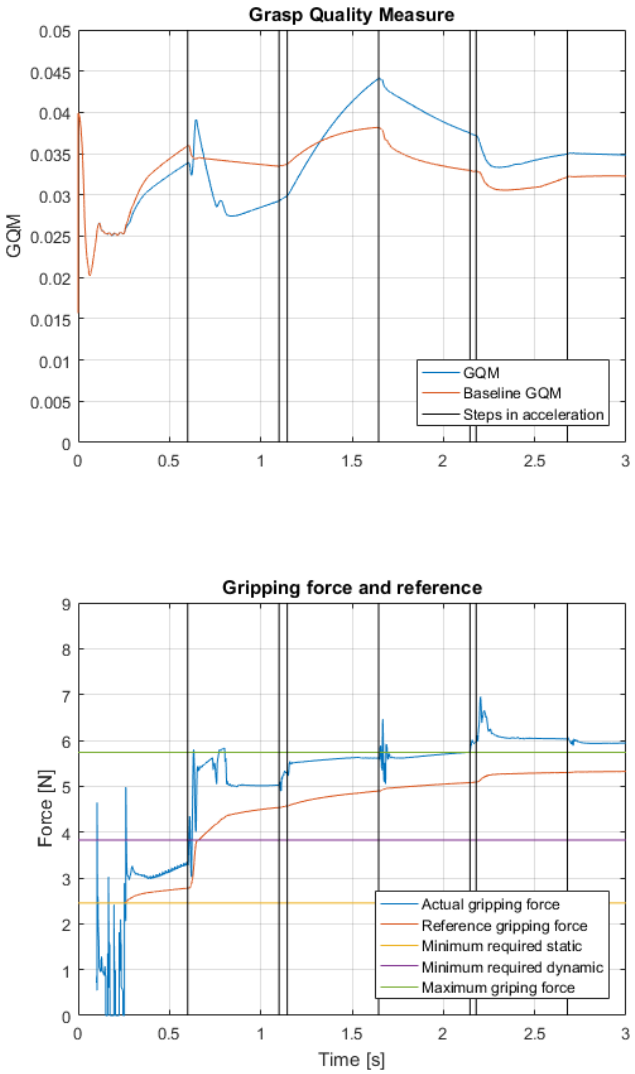


**Figure 6-14:** The grasp quality and gripping forces with $\gamma = 30$.

### 6-3-1 Optimisation of controller parameters on the nominal ball

The parameters of the adaptation gain $\gamma$ that are tested are:

$$\gamma \in \{10, 30, 50, 70, 90\}\,. \tag{6-11}$$

The results are plotted in Figure 6-15 to Figure 6-17. The run with $\gamma = 10$ fails because the adaptation is too low. This can also be seen in the grasp quality which is lower compared to the baseline for a large part of the run. For higher adaptation gains, the reference gripping force becomes higher. It can be seen that, generally, higher reference gripping forces lead to higher grasp quality. This is logical because more forces and moments can be withstood if higher gripping forces are applied. So, in order to maximise the grasp quality, the adaptation gain should be very high. However, the high level control goal also contains a maximum on the reference gripping force in order to not damage the products. It is based on the minimum required dynamic gripping force and the safety factor humans apply, as explained in Section 4-1-2:

$$f_{n,max} = 1.5\frac{m_{nom}(g + a_{y,max})}{\mu_{kin}} = 5.74\ N. \tag{6-12}$$

This maximum gripping force is also plotted in Figure 6-15 to Figure 6-17. It can be seen that the reference gripping force does not exceed this value while it increases the grasp quality with respect to the baseline, when applying the controller with $\gamma = 30$. The controller with $\gamma = 50$ just does not pass the maximum reference gripping force while the grasp quality is higher for a larger part of the run, as compared to the controller with $\gamma = 30$. The controller with $\gamma = 70$ just exceeds the set maximum reference gripping force, besides that there is almost no improvement in the part of the run that the grasp quality is higher than the baseline with respect to the controller with $\gamma = 50$. An even higher gain, $\gamma = 90$, results in a large exceedance of the reference gripping force. The grasp quality is relatively high, as compared with the controller with $\gamma = 70$, in the latter case. Higher adaptation gains will lead to even higher values of the grasp quality but in respect to the high-level control goal, a gain of $\gamma = 50$ maximises the grasp quality while not exceeding the maximum reference gripping force. This hence is the optimal value of the adaptation gain in the high-level controller for the nominal ball.

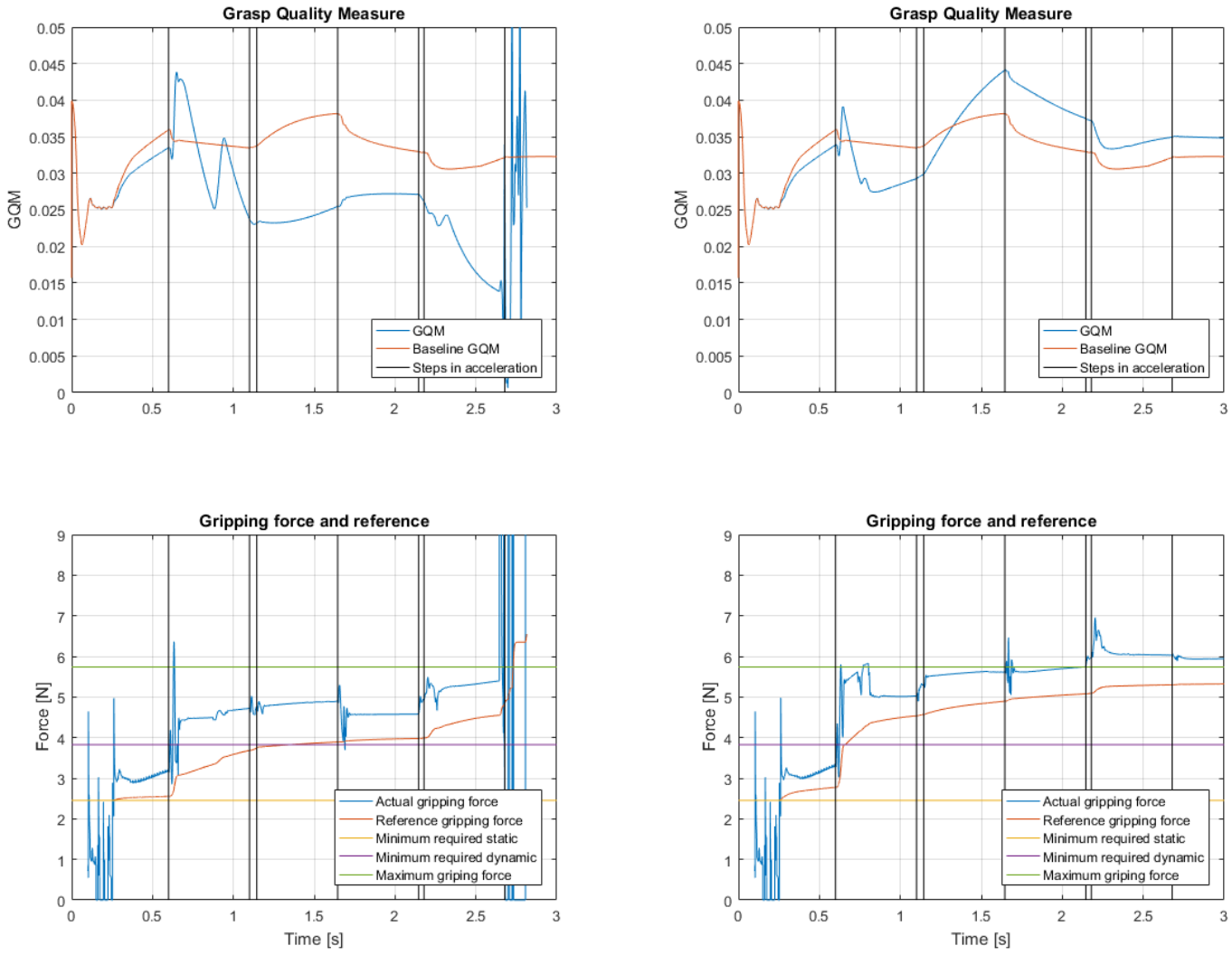


**(a)** $\gamma = 10$. **(b)** $\gamma = 30$.

**Figure 6-15:** Results of the runs with $\gamma = 10$ and $\gamma = 30$.

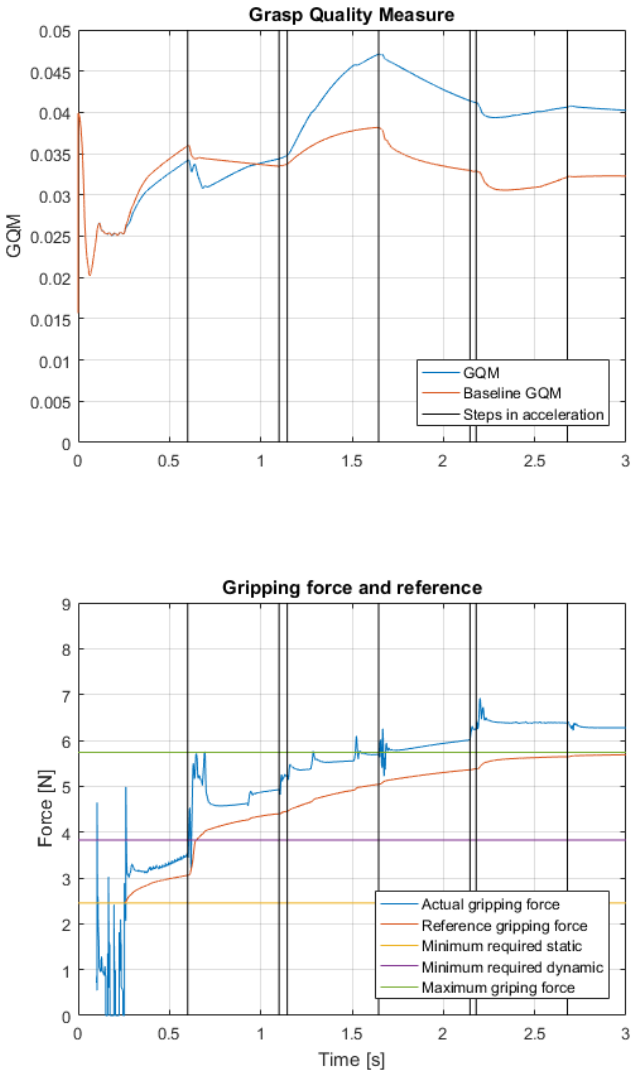


**Figure 6-16:** Results of the run with $\gamma = 50$.

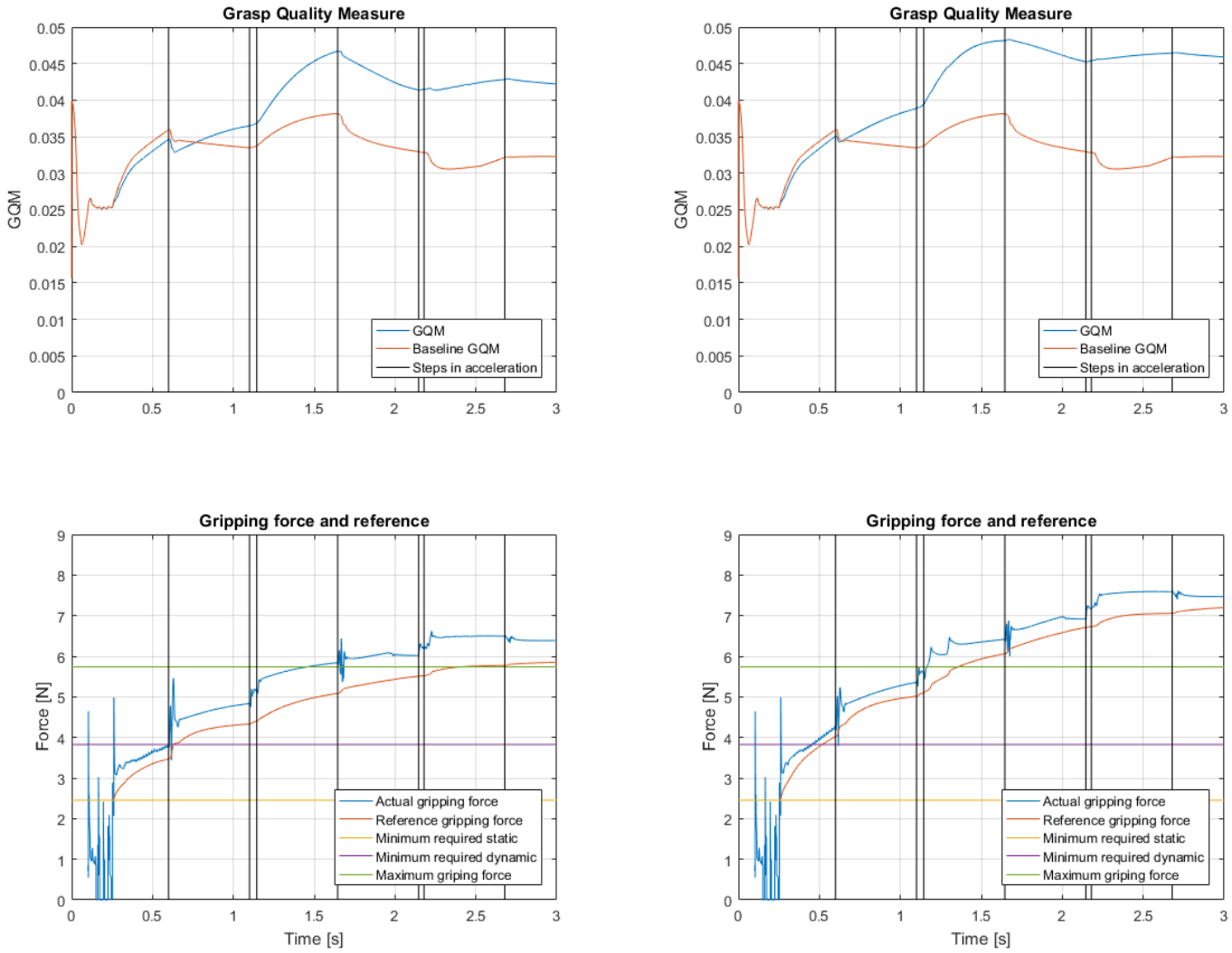


**(a)** $\gamma = 70$. **(b)** $\gamma = 90$.

**Figure 6-17:** Results of the runs with $\gamma = 70$ and $\gamma = 90$.

### 6-3-2 Application on other virtual products

During the optimisation of the low-level controller the other ball-shaped objects in the virtual product inventory were taken into account. This was because the low-level controller has to work for a variety of items in terms of mass, radius, stiffness and damping. The high-level controller is now optimised with respect to the ability to adapt to inertial effects and deformability. Therefore, it is not required to look at the other ball-shaped objects for the optimisation of the high-level controller. Because of this, the high-level controller as it is tuned now, will be applied on the pendulum and the net with oranges.

#### Pendulum

The weight of the pendulum is equal to the weight of the nominal ball. Therefore, the minimum required static gripping force and the minimum required dynamic gripping force are the same as with the ball. If the constant minimum static gripping force is applied, the controller is not able to hold the pendulum, as with the nominal ball. The minimum required dynamic gripping force is based on acceleration and slip on the ball, therefore a controller that applies this force on the ball is able to hold it. In case of the pendulum, additional inertial effects from swaying occur. The minimum required dynamic gripping force does not take this into account and therefore this force will also not be able to hold the pendulum [5]. This means that the adaptive controller needs to take this into account. Using the adaptive gain of $\gamma = 50$ results in the pendulum being held. The results can be seen in Figure 6-18 [6]. The baseline grasp quality from the baseline run on the nominal ball is also plotted for comparison. It can be seen that the grasp quality oscillates around the baseline grasp quality. Note that the oscillation in the grasp quality comes from the swaying motion of the pendulum. There is a large adaptation in the reference gripping force at the moment the second ball is lifted. It can also be seen that the gripping force is much higher compared to the gripping forces on the ball. This comes from the fact that the pendulum is an extreme version of a deformable product. The inertial effects during lifting are not distributed among multiple balls. Besides that, the inertial effects from swaying are higher in case of a single ball attached to the pendulum. Therefore, it is expected that a controller with these settings will be able to pick up the net with oranges, as will be demonstrated next.

#### Net with Oranges

The inertial effects from swaying and lifting are less in case of the net because the inertial forces are distributed over all the balls in the net instead of only one ball in case of the pendulum. This means that the controller has more small slip measurements based on which it can adapt the reference gripping force. This is demonstrated by means of a simplified version of the net with oranges because of long simulation times with the original net with oranges. The interaction between the particles of the net, between the oranges and between the particles of the net and the oranges causes the simulation to fail or to last very long

[5] The corresponding video can be found at https://youtu.be/0KDHzPYoGTU or on the USB-stick that is included with this thesis (Video6). Note that the playback speed of the video is reduced by a factor 4.

[6] The corresponding video can be found at https://youtu.be/huPyo2fLGkA or on the USB-stick that is included with this thesis (Video7). Note that the playback speed of the video is reduced by a factor 4.

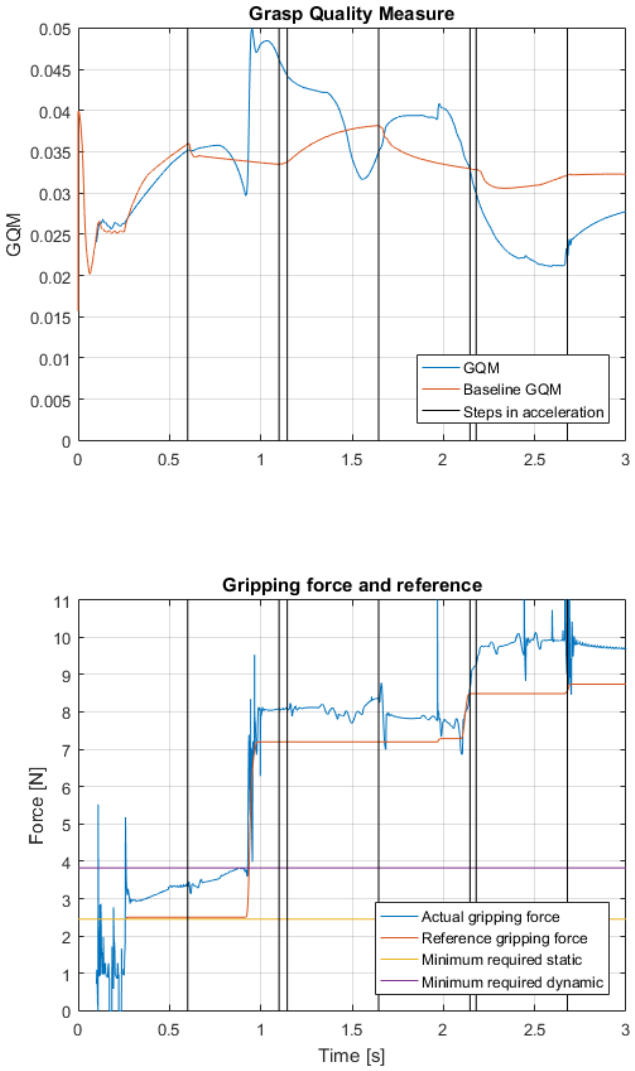


**Figure 6-18:** Results of the run with $\gamma = 50$ on the pendulum.

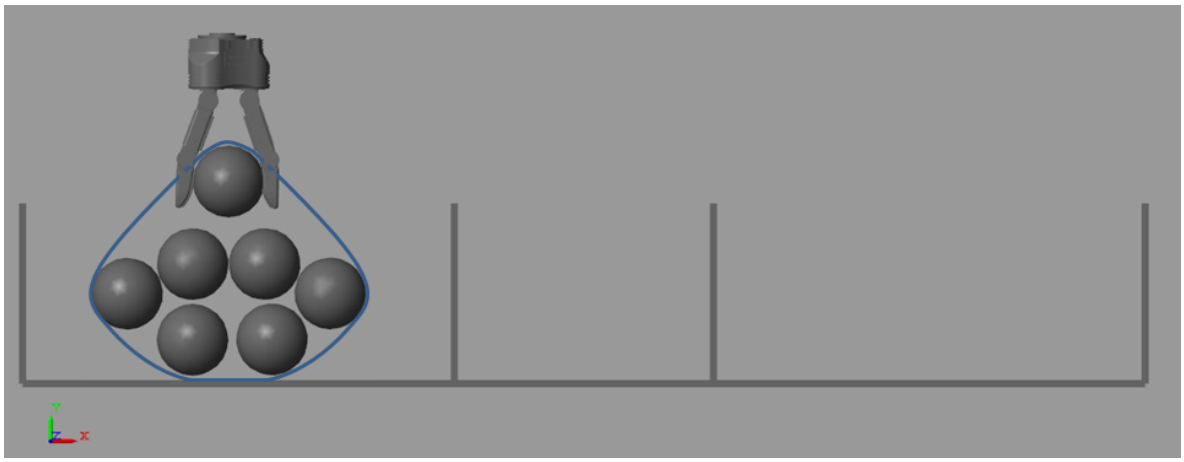

**Figure 6-19:** The simplified version of the virtual net with oranges and the gripper in 2D in the pick-and-place environment. The virtual net is indicated in blue for clarity, but not present in the real simulation.

(in the order of days). Therefore, the net is approximated by a set of single and double pendulums. This simplified version of the net, together with the gripper in 2D and the pick-and-place environment is shown in Figure 6-19. A run with the same adaptive gain of $\gamma = 50$ is performed on this simplified net with oranges. The results can be seen in Figure 6-20 [7]. The result can be compared with Figure 6-18, because the same adaptation gain was used. The only difference now is that the weight of the second ball of the pendulum is distributed over six balls, representing the oranges. It can be seen that the initial slip that occurs is less, resulting in less adaptation. This results in a lower reference gripping force. Note that the grasp quality is lower compared to the run with the pendulum. This comes from the fact that the reference gripping force is lower. A higher adaptation gain can be used to respond more to the small slips in order to increase the reference gripping force and hence increase the grasp quality.

[7]The corresponding video can be found at https://youtu.be/xAiVoM74oAk or on the USB-stick that is included with this thesis (Video8). Note that the playback speed of the video is reduced by a factor 4.

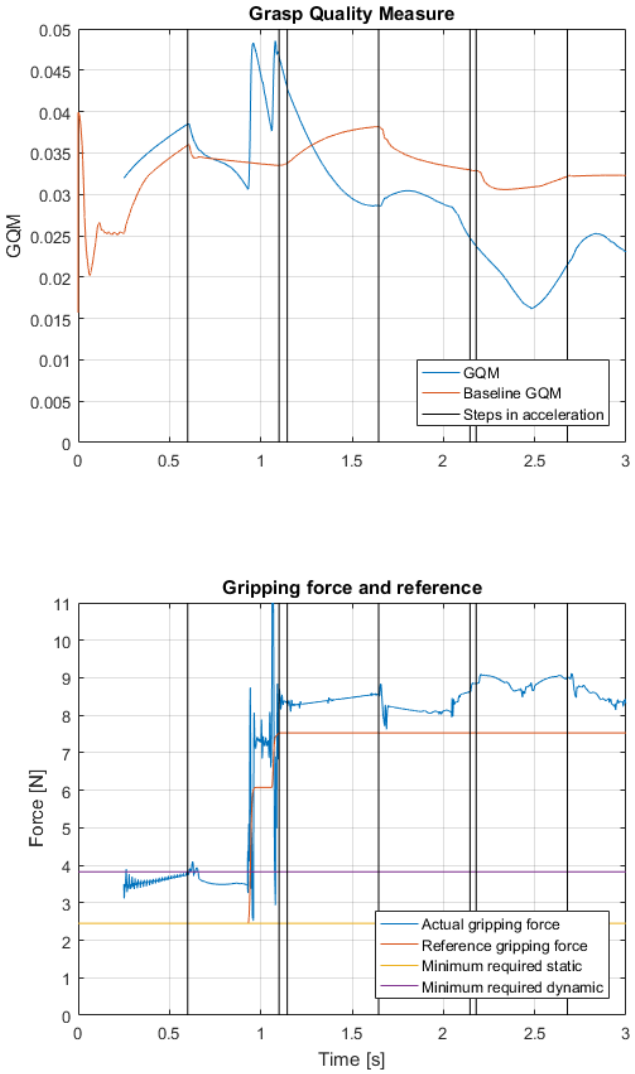


**Figure 6-20:** Results of the run with $\gamma = 50$ on the simplified net with oranges.

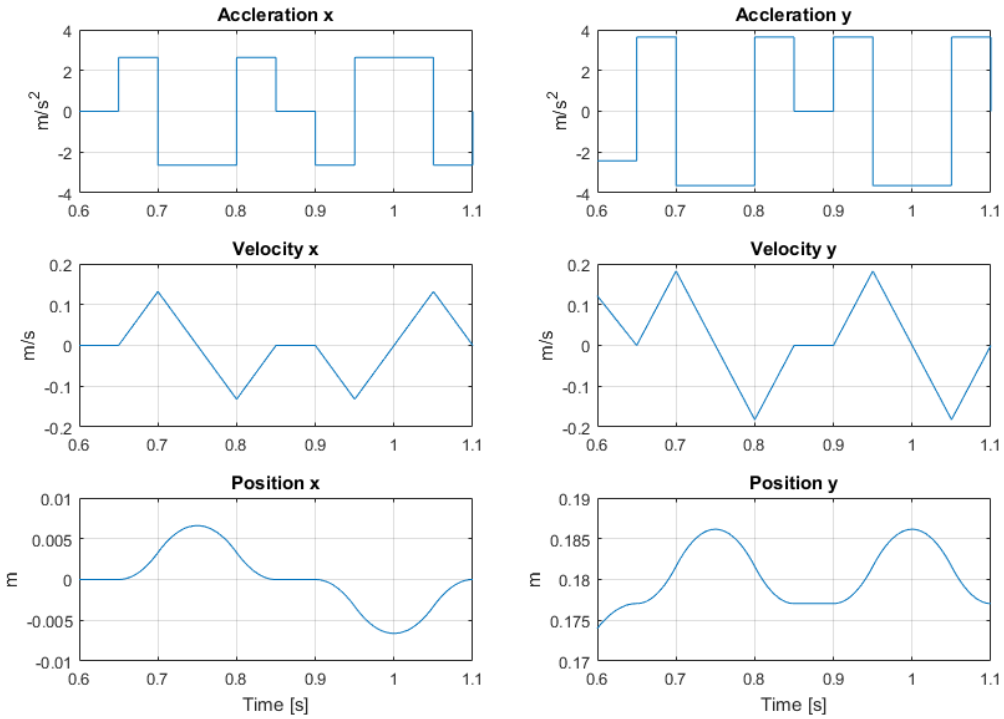


**Figure 6-21:** Acceleration profile used during excitation.

## 6-4 Excitation

Excitation based Extremum Seeking Control (ESC) uses small excitations to quickly find to optimum operating point. In the application described in this thesis, this means that the object will be shaken above the picking location to adapt the reference gripping force before the trajectory starts. In this way there will be less adaptation during the transportation and hence, at the start of the trajectory it is known that it will finish it without the product being lost. Excitation will be applied on the pendulum because then the advantage of this method becomes clear. The acceleration profile that is used during excitation is shown in Figure 6-21. The resulting velocity and displacement profiles are also shown. This excitation is applied in the direction of the maximum acceleration on the trajectory. The value of this acceleration is equal to the maximum acceleration on the trajectory.

The result of applying this profile on the run with the pendulum is shown in Figure 6-22 [8]. This result can be compared with the results from Figure 6-18 because the same adaptation gain was used. It can be seen that adaptation of the reference gripping force occurs earlier in time, this comes from the excitation at that moment. Because the reference gripping force is adapted before the actual trajectory is started, there is less adaptation at the start of the movement because the gripping force is already higher which prevents the occurrence of slip. This results is less adaptation that is based on slip measurement at the start of the

[8]The corresponding video can be found at https://youtu.be/sWpQHTLFSWY or on the USB-stick that is included with this thesis (Video9). Note that the playback speed of the video is reduced by a factor 4.

movement and therefore, the overall gripping force during the run is lower. It has to be noted that the grasp quality is lower during the run, as compared with the run without excitation, which comes from the fact that the gripping force is lower. A higher adaptation gain could result in more adaptation with higher grasp quality as a result. At the end of the run the gripper is moving downwards and decelerating, while at the same moment the pendulum exerts maximum inertial effect on the gripper. This results in slip and induces an increase in the reference gripping force. This shows that the excitation at the start of the run cannot take into account all scenarios that can occur during movement so it is not guaranteed that there is no adaptation any more during movement. It is shown that excitation is an approach to converge to the required gripping force faster and decrease the dependence on the occurrence of the initial slips. This is beneficial because those initial slips result in large displacements that result in a grasp that is closer to a loss. By reducing the displacement during the start of the movement, by using small excitation before the start of the movement, the risk of loosing the item is decreased.

## 6-5 Summary and Discussion

While tuning the low-level controller, it became clear that it is hard to create a measure of the performance on which the controller can be judged. The complete profile of the grasp quality over all runs cannot be compared, so it has to be captured in one single measure in order to compare the performance because it is not feasible to compare all runs by visual inspection of the grasp quality profile. The mean grasp quality does not differentiate enough between the low-level controller parameters. In order to further differentiate between different controller parameters, the second performance measure was introduced. This took into account the percentage of the time that the grasp quality was relatively high: above a certain threshold (95%). The value of this threshold is arbitrary and the result might be different if the threshold is chosen differently. The equally weighted linear combination of these two measures led to the combined performance measure based on which the optimal parameter for the low-level controller was selected. The weighting within this linear combination also effects the outcome of this optimisation. The combined measure is created based on an intuitive feeling of a 'good' grasp based on the plots of the grasp quality over time in combination with the videos from simulations. Future research should focus on creating a measure that is comparable among all future research on the topic of grasping with fingered grippers. This benchmark is required to judge the performance of all future work on this topic.

While tuning the low-level controller on the other ball-shaped products in the virtual product inventory, it became clear that different masses result in different optima. For higher masses the performance differences decreased. For lower masses, the controller with the optimal parameters found with the nominal ball was too aggressive. This comes from the fact that the response of the system is faster if the mass is lower, when applying the same torques.
While varying the stiffness of the object in the runs with the low-level controller, it became clear that higher stiffness of the object induced lower stiffness of the controller, and vice versa. This results in an overall stiffness of the gripper/object combination to be more or less constant. It turned out that this stiffness is optimal with respect to the selected performance measures.
The variation in performance shows that the performance is dependent on the mass, size,

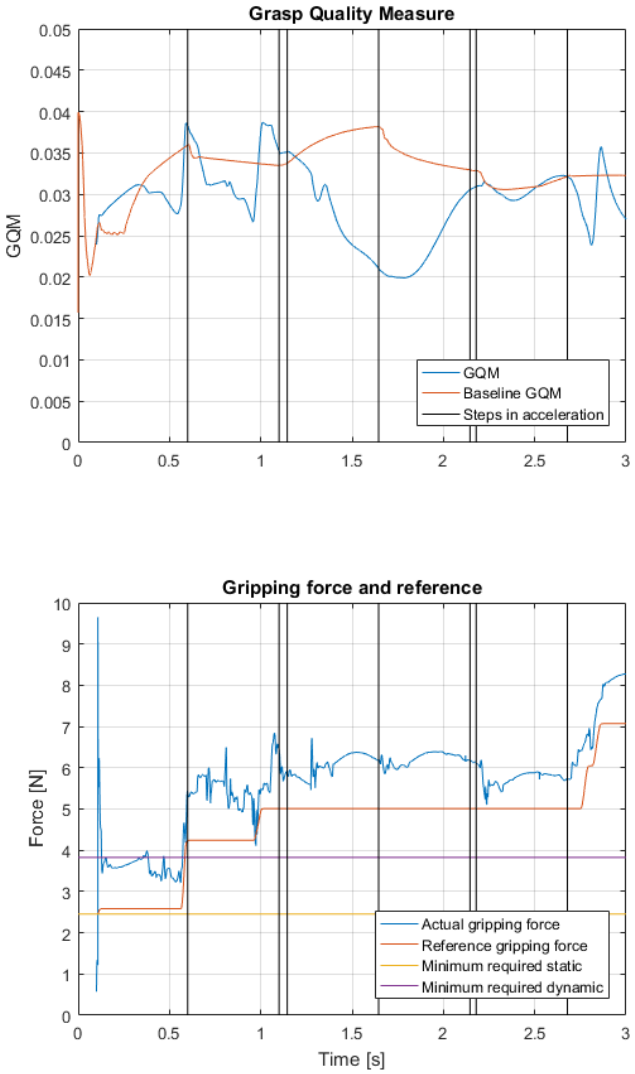


**Figure 6-22:** Results of the run with excitation with $\gamma = 50$ on the pendulum.

stiffness and damping of the item that is being grasped. A suggestion is to use mass, size, stiffness and damping dependent low-level controller parameters. The mass can for example be measured by a force/torque sensor in the wrist of the gripper. The initial size of the object can be measured by using inverse kinematics of the gripper fingers. Stiffness and damping can be estimated by some small squeezing tests at the start of the run. The controller parameters are then selected based on these measurements. This can be a self-learning approach or a look-up-table that differentiates between different regions of these parameters. This approach extends the functionality of the high-level controller because, next to passing the reference gripping force, it also passes the low-level controller parameters based on these measurements.

It was expected that the slip signal coming from the simulation would be a smooth signal because the simulation environment does not take into account sensor noise and delays. However, it turned out the the measured slip signal contained high-frequency components. High-frequency components in the slip signal induce high-frequency adaptations of the reference gripping force. Because this results over-adaptation, a first order low-pass filter is implemented to filter out these components. The tuning of the filter is based on the analysis of the power spectral density of the measured slip signal. The order of magnitude of the cut-off frequency of the filter became clear from this analysis. Small deviations from the selected cut-off frequency may change the performance of the system but it is not expected that these changes are significant. Big deviations from 250 $Hz$ will result in degrading performance because the trend is not followed in case of a low value and high-frequency components are not filtered out in case of a high value.

While tuning the high-level controller it became clear that the grasp quality can be increased if the adaptive gain on the reference gripping force is high. The limitation in the adaptation gain came from the fact that the object is not allowed to get damaged, so by applying a maximal reference gripping force. If the limit on this maximum reference gripping force is different, the result would also be different. A different approach would be to adjust the maximum reference gripping force based on a deformability measurement performed in real-time on the object. This results in a limit on deformation instead of a limit in gripping force. This increases the performance in case of low-deformable items because then higher forces are allowed.

It was seen that, in case of ball-shaped items, the controller was able to deal with accelerations and slip when using a constant reference gripping force. The adaptation law in the high-level controller ensured that the grasp quality was increased if a slip was measured.

It turned out that the controller that was tuned on the ball-shaped items, was transferable to other items as well. The minimum dynamic gripping force is not sufficient to cope with the inertial effects from swaying, because this minimum dynamic gripping force is only based on accelerations and slip. The high-level controller is able to cope with the inertial effects coming from swaying because it increases the gripping force once slip is measured.

In case of the pendulum, it is expected that the slip is high at the moment the second ball is lifted. This turned out to be the case: the reference gripping force was increased by the high-level controller at that moment. Besides that, the swaying motion of the pendulum is visible in the profile of the grasp quality. At the moment that the second ball is exactly below the gripper during a swaying motion, the vertical force is maximal. This results in a lower vertical force on the object that can be withstood by the gripper, which induces a lower grasp quality. This is exactly what is seen in the plots of the run with the pendulum.

The pendulum can be seen as a worst case scenario for the net with marbles because the inertial effect during lifting is created by one heavy ball instead of several light balls. Because of the fact that the tuned controller is able to deal with the pendulum, it is also able to deal with the simplified net with oranges, as expected. The weight of pendulum and the simplified net with oranges is the same, but the final reference gripping force is lower because the slips resulting from inertial effects during lifting are less. If the weight is distributed over multiple balls, there is more time to gradually adapt the slip, resulting in a lower reference gripping force. The grasp quality is lower in this case. Higher adaptation gains would result in more adaptation of the reference gripping force, which increases the grasp quality.

Excitation results in the adaptation of the reference gripping force before the actual movement starts. The dependence on the measurement of slip at the start of the movement reduces. Because there is less slip at the start of the movement, there is less adaptation of the reference gripping force. This results in a lower reference gripping force during the run. It was shown that the grasp quality reduced because of the lower reference gripping force. The grasp quality can be increased by increasing the adaptation gain. This ensures that the reference gripping force increases more during excitation. The grasp quality then increases while not exceeding the maximum gripping force.

The adaptive gain can also be made dependent on the contact location. If the contact location on the fingers indicates that the object is close to a loss, it can be imagined that more adaptation of the reference gripping force is allowed to hold the object. If the distance from the contact point to the end of the finger is bigger, the urgency to save the object from being lost is less, so less adaptation is needed.

The tuning of the parameters of the individual controller levels is decoupled. This resulted in relatively fast optimisations because the amount of tunable parameters was low. On the contrary, the optimisation could look at all controller parameters simultaneously. This would require high computational power, more time and more parameter combinations to evaluate. It is not expected that the result would be significantly better because the architecture allows for this decoupling because of the separation of time scales. The optimisation of the high-level controller is independent of the performance of the low-level controller, as long as the latter is maintaining the grasp.

# Chapter 7

# Conclusions and Recommendations

## 7-1 Conclusions

The research objective addressed in this thesis is:

*Design a control strategy for a fingered robotic gripper to grasp and hold deformable items with minimal gripping force and maximal grasp quality while moving over a desired trajectory using active feedback*

Inspired by how humans approach the problem of grasping items, a multi-level control architecture is devised. The human controller consists of a low-level part that includes reflexes and model-based feedforward actions, complemented with tactile feedback signals that are used for low-level control. Next to that humans have the Central Nervous System (CNS) that is able to use sensory information from the human skin to update the model parameters of the models used by the low-level controller and determine the setpoints that need to be followed in order to achieve the high-level control goals. A high-level control goal is for example the transportation of an item from A to B, whereas a low-level control goal is to have a secure grasp on the object.

The system devised in this thesis uses a computed torque low-level control approach that is based on a kinematic and dynamic model created with screw theory. The Computed Torque Controller is used because it has good tracking performance, is stabilising and is robust. The controller parameters are optimised with respect to the grasp quality while having a constant gripping force, this is the low-level control goal.

The setpoint of the low-level controller is the gripping force of the gripper on the object. This setpoint can be calculated if the item properties are known. In case of unknown items, an intelligent control system has to be able to determine this setpoint. This is possible by making use of measurement signals coming from the hardware. A high-level controller that is based on the Numerical Optimisation version of Extremum Seeking Control (ESC) is used for this purpose because it is able to deal with a wide variety of unknown items. Here a measurement

function based on contact location is used in an adaptive law that is based on the gradient method to update the setpoint for the low-level controller. The controller is optimised with respect to the grasp quality while having a limited gripping force on a ball that is adaptable based on the measurement of the slip.

The control strategy is tested and optimised on a wide variety of deformable items in a simulation environment because this enables quick and safe testing. A virtual product inventory is created for this purpose. The gripper, that executes the desired trajectory, interacts with these products via the defined contact properties.

Finally, excitation based ESC is used to converge to the required gripping force before the actual movement from warehouse Transport Storage Unit (TSU) to order TSU started. In this way, there is less adaptation of the gripping force during movement which increases the reliability of the smart gripping system because the risk of loosing an item during the run is reduced.

This thesis showed the advantage of using a control architecture based on the human control system in item picking. The control architecture consists of a low-level controller that is able to follow a desired gripping force setpoint and a high-level controller that determines the gripping force setpoint based on sensory information from the fingers. The decoupling between low-level quality control and high-level setpoint control is beneficial for optimisation of controller parameters. It is shown that this control strategy is perfectly suited to be used on a fingered robotic gripper to grasp and hold deformable items with minimal gripping force and maximal *grasp quality* while moving over a desired trajectory using active feedback.

## 7-2 Recommendations

Below recommendations are given for the different topics that were investigated during this thesis.

**Pick-and-place environment**
Because of simplification and because of the fact that the trajectory in item picking is in 2D, only 2D was considered in this thesis. Besides that a wrist joint (which would be planar in 2D) is not taken into account. Future research can make use of a wrist joint. This allows for a 3D application. This wrist joint can then also be used to pick items out of the corner of the box at the pick location. This adds extra functionality to the system because the assumption that the items are at the center of the TSU is not needed then.

Another advantage of working in 3D by using a wrist joint is that the direction in which maximal force can be withstood can be aligned with the direction of maximum acceleration on the trajectory. This direction follows from the singular value decomposition when computing the grasp quality. In this way the grasp quality can be higher when applying the same gripping force. This requires that the trajectory needs to be adapted, which was not considered in this thesis but could be considered in future research. Note that the trajectory that is followed by the wrist is fixed in this research. If a wrist joint is implemented, the trajectory of the gripper is different because of the rotation of this wrist joint.

Besides that, the gripper is able to form around the object in the third dimension by rotating the fingers. This increases the contact area, resulting in a higher grasp quality.

**Controller selection**
The controllers that are used in the multi-level controller are selected based on the score on different criteria. The scores on the criteria are determined based on literature rather than a real implementation. In future research all controller approaches could be implemented on a small test set-up in order to validate the scores on the criteria based on actual simulations instead of theoretical performance.

**Simulation environment and Experiments**
When going to 3D, a different simulation environment can best be used because the simulation times in Matlab/Simulink are already high in case of 2D. This was the reason to switch to a simplified version of the net with oranges when applying the control strategy on this product. Switching to another simulation environment goes at the expense of the possibility to easily extract information and implement a controller in the loop in a convenient way. The investment in time that is required to get these overhead functionalities working, will pay off when doing the simulations and tuning relatively fast. Future research has to investigate this and once a solution has been found, the proposed control strategy should be tested on the original version of the net with oranges. It is expected that the performance will not deviate much from the performance as seen with the simplified version, because the characteristics of the objects are similar (i.e. distributed mass, swaying behaviour, connections between masses).

Parallel to the development of a simulation environment, research has to focus on implementation of the smart gripping system on a real test set-up. Next to the fact that practical issues will arise, it will uncover the potential of the control strategy designed in this thesis.

**Pick-and-place Application**
Minimal a-priori knowledge is used by the controller here. This is to be able to pick up an object the first time it is encountered. It is beneficial if the parameters of the product are saved so the controller can use them the second time it encounters the same object. This could for example be the final reference on the gripping force. This force could be applied at the start of the task so there is no need to build up the force based on slip measurements during shaking and moving. This could increase the performance in case of slowly varying item inventories.

It is expected that the performance will increase if a feedforward action is added to the controller. The correction based on slip measurement can be seen as a reactive measure to prevent the item being lost. The path is known, so it is also known when the accelerations are coming. The value of the maximum acceleration is already used in the calculation of the minimum required gripping force. If it is also known when these accelerations are coming, the reference gripping force can be increased before they actually occur. The disadvantage of this approach is that there is no guarantee the the gripping force is minimal for the specific object because it is possible that there does not occur any slip. Another possibility is to combine this feature with the learning capabilities of the system. If it is known when the reference gripping force was increased in a previous run, it could be used to increase the reference force slightly before this time to prevent the occurrence of slip. If the value of the reference force is equal to the reference value of the reference force at the end of the first run, it is known that this is the minimum required gripping force.

Now that is is possible to pick up and hold deformable items by using the control strategy conceived in this thesis, a suggestion for further research is to investigate the possibility to

pick up the non-deformable items from Figure 1-3, that are not considered in this thesis. It is expected that the developed smart gripping system provides a unified solution for all medium sized items from all product categories of GS1. Research should focus on this by implementing the control strategy on a real set-up.

This thesis focusses on medium sized items and presents a control strategy to pick and place these items. Large items are not covered because of the limitations on the workspace of the gripper. In future research, the design methodology used in this thesis can be used to design a smart gripping for the items that are not covered in this thesis. This entails the investigation of the possibility to increase the gripper size, or to apply other gripper modalities. This introduces a need for different gripper modalities and/or sizes in order to be able to pick up the full range of item sizes in a warehouse. Next, different suggestions for integration of such a system, next to the system developed here, are discussed. A first suggestion is to investigate the development of a gripper with multiple gripper modalities to be able to switch during pick-up from collaboration between the modalities to single-modal use, once the gripper detects that the first applied gripping modality does not work. For this it is required that the gripper first senses that it is not possible to do this. The performance of the system can further be increased if there is knowledge of item properties based on previous pick-and-place actions. If the dedicated gripper already knows from the previous pick that it has to use the fingered gripper instead of the suction cup, for example, it is not required to sense this any more. This saves time because the trial and error phase is skipped. This would be the most convenient solution because still one single picking station is satisfactory and there is no need for tool exchange. Tool exchange is the second option to integrate a multi-modal gripping system. A disadvantage compared to the first suggestion is that this leads to waiting times during switching. Besides that, upstream knowledge needs to be provides or generated in order to let the system pick the right gripping modality. A third option is to introduce parallel picking stations with different gripper modalities. This eliminates waiting times during tool exchange, at the expense of having multiple picking stations. Also in this case separation of products needs to be performed upstream.

Placement is not considered, however, the integrated sensors are perfectly suited to support the process of placing items. The height of the item that is being picked is not known in advance, if the item is not known in advance. Therefore, current solutions often make use of a vision system in between the pick and place location in order to estimate the height of the object that is being gripped relative to the gripper. This requires the robot to stop its motion, which reduces the cycle time. The slip measurements that are used in this thesis provide the solution for this. The sensors are able to detect a touch down of that item at the bottom of the TSU. This means that the robot can move down until the sensors detect a touch down. At that moment the robot can stop moving and the gripper can be opened in order to release the item without dropping it or crushing it.

**Other Applications**

Beyond pick-and-place applications, this approach can be used in domestic and extra-terrestrial environments. These applications namely also deal with an unlimited set of items that possibly have to be displaced. The former application deals with high variability and unpredictability of items, both in form and location, whereas the latter deals with completely unknown, unexplored items that can have unprecedented form, density and/or surface properties. Teaching (i.e. creating a database with item properties beforehand) is impossible in these applications and the approach presented in this thesis also does not require teaching.

The learning capability (i.e. saving results form previous experiences) can be used but is also not required. This makes it useful for more generic applications as described above.

A specific application in a domestic environment is the application in elderly care. Also this sector deals with personnel shortages. An example of a task that nurses have to perform is to manually reposition the elderly in their beds in order to prevent pressure ulcers. This is a physically intensive task that can also be performed by a robot. The problem shows some similarities with the topic of this thesis because it also deals with deformable objects that vary in size, weight and position. The approach that was used in this thesis to design a control strategy for a pick-and-place task can also be applied on this problem. The learning capability of the system can then be used to save individual preferences of the patients with respect to gripper pose, moving speed and clamping force.

Another application that can benefit from the results of this thesis is teleoperation. Teleoperation can be applied in the previously discussed extra-terrestrial environements, but also in surgery and during maintenance and diagnosing in hazardous environments. If the operator at the master side has to pick and place and object with a gripper on the slave side, often there is only force feedback or no feedback at all. Force feedback can be used to transfer the forces that are encountered by the slave to the master side. Slips measured at the slave side are more complicated to transfer. Tactile sensors can be used but it is hard to transfer the sensation of the slip that is present at the slave side to the master [83]. The controller devised in this thesis is perfectly suited to solve this locally, so at the slave side without transfer to the master side. This omits the problem of creating a sensation of slip at the master side from measurements at the slave side. The advantage of applying the smart gripping system in this case is that the operator at the master side can focus on other tasks while the gripping force adaptation and application is accounted for locally, at the slave side.

# Appendix A

# GS1-GPC Standards

## GS1-GPC STANDARDS

23 categories

| Name | Example | GDSN code | Description |
|---|---|---|---|
| Ampoule |  | AM | A relatively small packaging, consisting of a glass or plastic tube, from which the end (after fillage) is pulled to a stipe and closed molted. The bottom of an ampoule can be opened by breaking the stipe. |
| Tray |  | CT | Box with lid, from which at least 3 sides are loose (not attached) to the rest of the box. |
| Cup, bowl |   | CU | A packaging with a flat bottom side with an undefined shape, whether or not closed using a lid. These packages are mostly made from paper, plastic or other materials and are usually (but not always) used for food products (e.g. rice, butter, yoghurt, sour cream, candy, etc.) |
| Container |   | CY | A non-flexible, cylindrical packaging with straight sides and circular ends of the same size. |
| Blister packaging |   | BPG | A type of packaging where the article is packed between a preshaped 'bubble' (usually transparent plastic) and a carton carrier. |
| Box |   | BX | A non-specific term that refers to a non-flexible, three-dimensional packaging with closed sides which encompass the content and which can be made from every material. Although some boxes are suitable to be re-sealed or to be used more than once, they can also be meant for one time usage. |

| Name | Example | GDSN code | Description |
|---|---|---|---|
| Bottle |  | BO | A packaging with a round neck of which the diameter is smaller than the belly, with an opening that can be sealed using a cap. More specific: a packaging with a narrow neck in comparison to a jar or packaging with a wide opening. The section of the bottle can be round, oval, squared, rectangular or a combination of these. Bottles are often made of glass or plastic, but also from pottery or metal. Bottles can be recyclable, returnable, re-usable or intended to be used one time only. |
| Case |  | CS | A non-specific term for packaging that is meant to contain content, encompass, and/or protect during distribution, storage and presentation. Cases are often meant to contain products and keep them in good condition during their entire life cycle. Examples are CD-sleeves. |
| Sleeve |  | SY | A flexible packaging with open sides, mostly from paper, carton or plastic, which are put over the product for protection or presentation. |
| Card |  | CM | A flat packaging on which the product hangs or is mounted for presentation. |
| Shrink wrapping |  | SW | A packaging consisting of plastic foil around an article or group of articles, which is heated so it shrinks and keeps everything together. Crimp foil is used to wrap packages or units for further processing or sending, so it is bounded, protected and immobilized. |
| Basket |  | BK | A semi star packaging, often open on the top side, it is traditionally used for the collection, transport, and selling of agricultural products. |

| Name | Example | GDSN code | Description |
|---|---|---|---|
| Multi-Pack |   | MPG | A bundle of products that are hold together using the packaging, to provide carrying comfort to the consumer. A multi-pack is always a consumer unit. With exception of the products hold together using a packing band. |
| Net |  | NT | A packaging with an open structure of wires or strokes, woven in a regular pattern with opens between the wires. The packaging is meant to hold and carry products. |
| Pack |  | BRI | A rectangular, stackable packaging, which is mainly used for liquids such as milk or juices. |
| Pack with point | 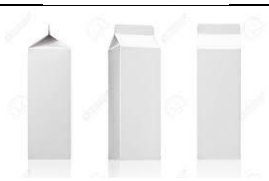 | GTG | A rectangular, non-stackable packaging, which is mainly used for liquids such as milk or juices. |
| Jar |  | JR | A non-flexible packaging with a large opening, made of glass, stone, pottery, plastics or any other suitable material, which is used to store products (e.g. jam, cosmetics, crème, pickles). |
| Tube |   | TU | A cylindrical packaging which is sealed on one side and the other side is closed using a cap or dosing device. |

| Name | Example | GDSN code | Description |
|---|---|---|---|
| Bag |   | BG | A preformed, flexible packaging, often open at one side, of which the opening can be sealed after filling. |
| Box Blister Open |   | BBO | A mostly rectangular packaging, often from carton, of which on ore more sides are open so that the product is better visible. |
| Box Plastic one side |   | BXP1 | A rectangular packaging (BX) but with a plastic transparent hole at one side, such that the product is better visible. |
| Box plastic two sides |  | BXP2 | A rectangular packaging (BX) but with a larger plastic see through hole at two or more sides, but not fully from plastic, so that the product is better visible. |
| Not packed |   | NE | The article or product is not packed. |

# Appendix B

# Kinematics of Finger 2

The rotational axis of both joints is pointing into the paper such that positive rotation results in a closing action, as with the first finger. The rotational axis hence is:

$$\omega_2 = \begin{bmatrix} 0 \\ 0 \\ -1 \end{bmatrix} \tag{B-1}$$

The value of rotation is defined by $\theta_{21}$ for the proximal joint and $\theta_{22}$ for the distal joint. The axis point of the proximal joint with respect to the spatial frame in reference configuration is:

$$q_{21} = \begin{bmatrix} a \\ -b \\ 0 \end{bmatrix} \tag{B-2}$$

These are the ingredients required to calculate the twist corresponding to the proximal joint of finger 2 in reference configuration. It is defined and calculated as follows:

$$\zeta_{21} = \begin{bmatrix} -\omega_2 \times q_{21} \\ \omega_2 \end{bmatrix} = \begin{bmatrix} -b \\ -a \\ 0 \\ 0 \\ 0 \\ 1 \end{bmatrix} \tag{B-3}$$

This can be interpreted as the movement of a point attached to the proximal joint, moving through origin $s$ with a unit rotation, expressed in origin frame $s$. This is also the way to read the common notation for this twist: $\zeta^s_{s,21}$.

For the distal joint, the contact point in reference configuration is:

$$q_{22} = \begin{bmatrix} a \\ -b - c \\ 0 \end{bmatrix} \tag{B-4}$$

The twist now is:

$$\zeta_{22} = \zeta^s_{s,22} = \begin{bmatrix} -\omega_2 \times q_{22} \\ \omega_2 \end{bmatrix} = \begin{bmatrix} -b-c \\ -a \\ 0 \\ 0 \\ 0 \\ 1 \end{bmatrix} \tag{B-5}$$

The homogeneous matrix from spatial frame $s$ to distal joint in zero configuration needs to be determined. The reference position is chosen such that this is convenient. There is no rotation between the frames and therefore the displacement is logical to set up, resulting in the following matrix:

$$H^s_2(0) = \begin{bmatrix} 1 & 0 & 0 & a \\ 0 & 1 & 0 & -b-c \\ 0 & 0 & 1 & 0 \\ 0 & 0 & 0 & 1 \end{bmatrix} \tag{B-6}$$

The transformation between spatial and distal frame can now be calculated by filling in the correct values for the twists. The homogeneous matrix of the distal joint with respect to the spatial frame is now defined as the multiplication of the individual matrix exponentials times the initial homogeneous matrix as follows:

$$H^s_2(\theta_{21}, \theta_{22}) = e^{\tilde{\zeta}_{21}\theta_{21}} e^{\tilde{\zeta}_{22}\theta_{22}} H^s_2(0) \tag{B-7}$$

In reference configuration, the line of contact location $F$ can be described in the local frame of the distal joint as follows:

$$q^2_F = \begin{bmatrix} 0 \\ -d \\ 0 \end{bmatrix} \tag{B-8}$$

This position can be expressed in the spatial frame, as a function of the angles of the joints, as follows:

$$q^s_F = H^s_2(\theta_{21}, \theta_{22}) q^2_F \tag{B-9}$$

The derived twists can be used to easily create the Jacobian (for the second finger) because twists already describe the motion with respect to the spatial frame.

$$J_2 = \begin{bmatrix} \zeta_{21} & \zeta_{22}(\theta_{21}) \end{bmatrix} \tag{B-10}$$

The speed of the contact point is:

$$\dot{q}^s_F = \left( J_2 \tilde{\dot{\theta}}_2 \right) q^s_F \tag{B-11}$$

with

$$\dot{\theta_2} = \begin{bmatrix} \dot{\theta}_{21} \\ \dot{\theta}_{22} \end{bmatrix} \tag{B-12}$$

# Appendix C

# M-file for gripper dynamics

```
%% Dynamics of gripper
clear all
close all
clc

%% Model parameters
base_width = 57.158e-3;      %[m] width of base
base_height = 98e-3;         %[m] height of base

leng_prox_fing = 86.5e-3;    %[m] lenght of proximal finger
leng_dist_fing = 68.5e-3;    %[m] lenght of distal finger (to fingertip)

%% Dynamics of finger
syms g L1 L2 m1 m2              real  % model parameters:
syms u                          real  % absolute displacements: u = [u11;
    u21; u12; u22]
syms theta theta1 theta2        real  % degrees of freedom (dof): theta =
    [ theta1; theta2 ]
syms t                          real  % time
syms T1 T2                      real  % torques
syms ud                         real  % absolute velocities
syms thetad theta1d theta2d     real  % time derivitaves of dofs
syms thetadd theta1dd theta2dd real  % second time derivatives of dofs

theta   = [theta1   ; theta2   ];
thetad  = [theta1d  ; theta2d  ];
thetadd = [theta1dd; theta2dd];

% positions expressed as a function of the generalised coordinates. This
% directly follows from the kinematic equations
u  = [ -base_width/2;
       -base_height;
       -base_width/2 + 0.5*L1*sin(theta1);
```

```
32          -base_height - 0.5*L1*cos(theta1);
33          -base_width/2 + L1*sin(theta1) + 0.5*L2*sin(theta1+theta2)
34          -base_height - L1*cos(theta1) - 0.5*L2*cos(theta1+theta2)];
35
36  ud = jacobian(u,theta)*thetad ;
37
38  % compute energies according to their definitions
39
40  T =  1/2*(m1*(ud(3:4)'*ud(3:4))+m2*(ud(5:6)'*ud(5:6)));
41  T = simplify(T);
42
43  V =  m1*g*u(4) + m2*g*u(6) ;
44
45  % - compute dT/dqd
46  dT_dqd     = simplify(jacobian(T,thetad))';
47
48  % - compute D(dT/dqd)/Dt
49  % --> total D/Dt of dT/dqd =  partial d(dT/dqd)/dt
50  %                           + d(dT/dqd)/dq*qd
51  %                           + d(dT/dqd)/dqd*qdd
52  DdT_Dtdqd =  simplify(jacobian(dT_dqd,t)) ...
53              + simplify(jacobian(dT_dqd,theta))  * thetad ...
54              + simplify(jacobian(dT_dqd,thetad)) * thetadd;
55
56  % - compute dT/dq
57  dT_dq      = simplify(jacobian(T,theta))' ;
58
59  % - compute dV/dq
60  dV_dq      = simplify(jacobian(V,theta ))' ;
61
62  % - torques in the joints
63  tau = [T1;T2];
64
65  %- Set up equations
66
67  Equations = DdT_Dtdqd - dT_dq + dV_dq - tau ; %=0
68
69  %%%%%%%%%%%%%%%%%%%%%%%%%%%%%%%%%%%%%%%%%%%%%%%%%%%%%%%%%%%%
70  T
71  V
72  Equations
73
74  % write in common form
75  M = simplify(jacobian(Equations,thetadd));
76  C = 0.5*simplify(jacobian(Equations,thetad));
77  N = [0.5*g*m1*L1*sin(theta1) + g*m2*L1*sin(theta1) + 0.5*g*m2*L2*sin(
        theta1+theta2);
78       0.5*g*m2*L2*sin(theta1+theta2)];
79  Equations2 = M*thetadd + C*thetad + N - tau;
80
81  simplify(det(M))
82  M_dot = [jacobian(M(1,1),theta2)*theta2d jacobian(M(1,2),theta2)*theta2d;
```

```
83          jacobian(M(2,1),theta2)*theta2d jacobian(M(2,2),theta2)*theta2d
                ];
84  skew = simplify(M_dot-2*C);
85  if (skew(1,1)==0)&&(skew(2,2)==0)&&(skew(2,1)==-skew(1,2))
86      disp('Second property holds')
87  end
88
89  %% Dynamics of thumb
90  syms g L1 L2 m1 m2                          real  % model parameters:
91  syms u_th                                   real  % absolute displacements: u
        = [u11; u21; u12; u22]
92  syms theta_th theta1_th theta2_th           real  % degrees of freedom (dof):
        theta = [ theta1; theta2 ]
93  syms t                                      real  % time
94  syms T1_th T2_th                            real  % torques
95  syms ud_th                                  real  % absolute velocities
96  syms thetad_th theta1d_th theta2d_th        real  % time derivitaves of dofs
97  syms thetadd_th theta1dd_th theta2dd_th real  % second time derivatives
       of dofs
98
99  theta_th   = [theta1_th  ; theta2_th  ];
100 thetad_th  = [theta1d_th ; theta2d_th ];
101 thetadd_th = [theta1dd_th; theta2dd_th];
102
103 % positions expressed as a function of the generalised coordinates. This
104 % directly follows from the kinematic equations
105 u_th  = [ +base_width/2;
106        -base_height;
107        +base_width/2 - 0.5*L1*sin(theta1_th);
108        -base_height - 0.5*L1*cos(theta1_th);
109        +base_width/2 - L1*sin(theta1_th) - 0.5*L2*sin(theta1_th+theta2_th
               )
110        -base_height - L1*cos(theta1_th) - 0.5*L2*cos(theta1_th+theta2_th)
               ];
111
112 ud_th = jacobian(u_th,theta_th)*thetad_th ;
113
114 % compute energies according to their definitions
115 T_th =  1/2*(m1*(ud_th(3:4)'*ud_th(3:4))+m2*(ud_th(5:6)'*ud_th(5:6)));
116 T_th = simplify(T_th);
117
118 V_th =  m1*g*u_th(4) + m2*g*u_th(6) ;
119
120 % - compute dT/dqd
121 dT_dqd     = simplify(jacobian(T_th,thetad_th))';   % simple->to simplify
        as much as possible the expression
122                                                 % note: transposed used to
                                                        adjust dimension
123 % - compute D(dT/dqd)/Dt
124 % --> total D/Dt of dT/dqd =  partial d(dT/dqd)/dt
125 %                           + d(dT/dqd)/dq*qd
126 %                           + d(dT/dqd)/dqd*qdd
127 DdT_Dtdqd =  simplify(jacobian(dT_dqd,t)) ...
```

```
128             + simplify(jacobian(dT_dqd,theta_th))  * thetad_th ...
129             + simplify(jacobian(dT_dqd,thetad_th)) * thetadd_th;
130
131 % - compute dT/dq
132 dT_dq      = simplify(jacobian(T_th,theta_th))' ;
133
134 % - compute dV/dq
135 dV_dq      = simplify(jacobian(V_th,theta_th))' ;
136
137 % - torques in the joints
138 tau_th = [T1_th;T2_th];
139
140 %- Set up equations
141
142 Equations_th = DdT_Dtdqd - dT_dq + dV_dq - tau_th ; %=0
143
144 %%%%%%%%%%%%%%%%%%%%%%%%%%%%%%%%%%%%%%%%%%%%%%%%%%%%%%%%%%%%%%%%%%%%%%%
145 T_th
146 V_th
147 Equations_th
148
149 % write in common form
150 M_th = simplify(jacobian(Equations_th,thetadd_th));
151 C_th = 0.5*simplify(jacobian(Equations_th,thetad_th));
152 N_th = [0.5*g*m1*L1*sin(theta1_th) + g*m2*L1*sin(theta1_th) + 0.5*g*m2*L2
        *sin(theta1_th+theta2_th);
153      0.5*g*m2*L2*sin(theta1_th+theta2_th)];           %N = Equations-M*
            thetadd-C*thetad
154 Equations2_th = M_th*thetadd_th + C_th*thetad_th + N_th - tau_th
155
156 %% Gripper Dynamics
157 M_g = eval(blkdiag(M,M_th));
158
159 C_g = eval(blkdiag(C,C_th));
160
161 N_g = eval([N;N_th]);
162
163 tau_g = [tau;tau_th];
```

# Appendix D

# Hand Jacobian and Grasp Matrix for gripper pose and object from Section 4-2-2

$$J_h = \begin{bmatrix} 0.0874 & 0.0263 & 0 & 0 \\ -0.0483 & 0.0128 & 0 & 0 \\ 0 & 0 & 0 & 0 \\ 0 & 0 & 0.0874 & 0.0263 \\ 0 & 0 & 0.0483 & -0.0128 \\ 0 & 0 & 0 & 0 \end{bmatrix} \tag{D-1}$$

$$G = \begin{bmatrix} 1 & 0 & 0 & -1 & 0 & 0 \\ 0 & 1 & 0 & 0 & -1 & 0 \\ 0 & 0 & 1 & 0 & 0 & 1 \\ 0 & 0 & 0 & 0 & 0 & 0 \\ 0 & 0 & 0.0769 & 0 & 0 & -0.0769 \\ 0 & -0.0769 & 0 & 0 & -0.0769 & 0 \end{bmatrix} \tag{D-2}$$

# Appendix E

# M-file for integration of Computed Torque controller

```
%% Computed Torque controller integration
clear all
%close all
clc

% declaration of global variables
global G_eval
global mu m_block g

%% Constants
base_width = 57.158e-3;      %[m] width of base
base_height = 98e-3;         %[m] height of base

leng_prox_fing = 86.5e-3;    %[m] lenght of proximal finger
leng_dist_fing = 68.5e-3;    %[m] lenght of distal finger (to fingertip)

g = 9.81;                    %[m/s^2] the gravitational constant

m_block = 0.25; %[kg]
obj_width = 2*0.0769;        %[m] corresponds to a theta of 45 degrees
obj_height = 0.025;          %[m] does not matter, just for visual

mu = 2;                      %[-] This is the static friction coefficient

%% Contact kinematics object
% the grasp matrix G for the block is derived
syms r real

g_c1 = [eye(3) [-r;0;0] ; 0 0 0 1];
B_1 = [eye(3);zeros(3)];     %point contact with friction
G_1 = Adjoint(inverseH(g_c1))'*B_1;
```

```
32
33 g_c2 = [[-1 0 0;0 -1 0;0 0 1] [r;0;0] ; 0 0 0 1];
34 B_2 = B_1;
35 G_2 = Adjoint(inverseH(g_c2))'*B_2;
36
37 G = [G_1 G_2];          %the grasp matrix
38
39 r = 0.5*obj_width;      %because the object is known, r is known
40 G_eval = eval(G);
41
42 %% Integration of controller and animation
43 figure(7); clf; hold on
44 clear movie
45
46 clc
47 theta1 = deg2rad(-45); %this are the angles that match with the width of
       the known object
48 theta2 = -theta1;
49 theta1_th = theta1;
50 theta2_th = -theta1_th;
51
52 y_obj = -0.1854; %this follows from the constraint at theta1 = -45 and
       speeds zero
53 y_objd = 0;
54
55 thetadot_p = 0;  %start with zero speeds
56 thetadot_d = 0;
57
58 theta1d = thetadot_p;
59 theta2d = thetadot_d;
60 theta1d_th = thetadot_p;
61 theta2d_th = thetadot_d;
62
63 y_init = zeros(20,1);
64 y_init(1) = 0;       %xd_init
65 y_init(2) = y_objd; %yd_init
66 y_init(3) = 0;       %zd_init
67 y_init(4) = 0;       %alphad_init
68 y_init(5) = 0;       %betad_init
69 y_init(6) = 0;       %gammad_init
70
71 y_init(7) = 0;       %x_init
72 y_init(8) = y_obj;  %y_init
73 y_init(9) = 0;       %z_init
74 y_init(10) = 0;      %alpha_init
75 y_init(11) = 0;      %beta_init
76 y_init(12) = 0;      %gamma_init
77
78 y_init(13) = theta1;
79 y_init(14) = theta2;
80 y_init(15) = theta1_th;
81 y_init(16) = theta2_th;
82
```

```
83  %additional inputs for the constraint
84  y_init(17) = theta1d;
85  y_init(18) = theta2d;
86  y_init(19) = theta1d_th;
87  y_init(20) = theta2d_th;
88
89  dydt = func_ov(0,y_init)
90
91  h = 1e-2;      %[s] stepsize
92  t_end = 0.5;           %final time
93  tvec = 0:h:t_end;
94  y_sol = zeros(20,length(tvec));
95  y_sol(:,1) = y_init;
96  Torques = zeros(4,length(tvec)-1);
97  Torques_FC = zeros(4,length(tvec)-1);  %from f_n
98  Torques_FGC = zeros(4,length(tvec)-1); %form constraint
99  constraint = zeros(6,length(tvec)-1);
100 GQM = zeros(1,length(tvec)-1);
101
102 % EULER
103 for k = 1:length(tvec)-1
104
105 [dy , Torques(:,k) , Torques_FC(:,k) , Torques_FGC(:,k) , constraint(:,k)
    ] = func_ov(0,y_sol(:,k));  %not dependent on time sol fill in 0
106
107 y_sol(1:16,k+1) = y_sol(1:16,k) + h*dy(1:16); %do an integration for the
    states
108 y_sol(17:20,k+1) = dy(17:20); %save the joint speeds for the next
    evaluation
109
110 H = pinv(G_eval)'*J_hand_func(y_sol(13,k),y_sol(14,k),y_sol(15,k),y_sol
    (16,k));
111 svd_H = svd(H);
112 H_new = H([1:2,6],:); %because of 2D rows 3:5 always 0 (that is the Fz,
    Rx and Ry)
113 svd_H_new = svd(H_new);
114 GQM(k) = svd_H_new(end)/svd_H_new(1);
115
116 % animation
117 cla
118
119 x_objd = y_sol(1,k);
120 y_objd = y_sol(2,k);
121 z_objd = y_sol(3,k);
122 alpha_objd = y_sol(4,k);
123 beta_objd = y_sol(5,k);
124 gamma_objd = y_sol(6,k);
125 x_obj = y_sol(7,k);
126 y_obj = y_sol(8,k);
127 z_obj = y_sol(9,k);
128 alpha_obj = y_sol(10,k);
129 beta_obj = y_sol(11,k);
130 gamma_obj = y_sol(12,k);
```

```
131 theta1 = y_sol(13,k);
132 theta2 = y_sol(14,k);
133 theta1_th = y_sol(15,k);
134 theta2_th = y_sol(16,k);
135 %extra inputs
136 theta1d = y_sol(17,k);
137 theta2d = y_sol(18,k);
138 theta1d_th = y_sol(19,k);
139 theta2d_th = y_sol(20,k);
140
141 %finger
142 q_prox_finger = [-base_width/2 ; -base_height ; 0]; %axis point of
    proximal joint in zero configuration
143 q_dist_finger = [-base_width/2 + leng_prox_fing*sin(theta1) ; -
    base_height-leng_prox_fing*cos(theta1) ; 0]; %axis point of distal
    joint in arbitrary configuration
144 q_ee_finger = [-base_width/2 + leng_prox_fing*sin(theta1) +
    leng_dist_fing*sin(theta1+theta2); -base_height - leng_prox_fing*cos(
    theta1) - leng_dist_fing*cos(theta1+theta2) ; 0]; %axis point of
    fingertip in arbitrary configuration
145 q_cp_finger = [-base_width/2 + leng_prox_fing*sin(theta1) + 0.02628*sin(
    theta1+theta2) + 0.01283*cos(theta1+theta2); -base_height -
    leng_prox_fing*cos(theta1) - 0.02628*cos(theta1+theta2) + 0.01283*sin(
    theta1+theta2); 0]; %axis point of contact point in arbitrary
    configuration
146
147 plot([0 q_prox_finger(1)],[0 q_prox_finger(2)],'b','LineWidth',1)
148 plot([q_prox_finger(1) q_dist_finger(1)],[q_prox_finger(2) q_dist_finger
    (2)],'b','LineWidth',2)
149 plot([q_dist_finger(1) q_ee_finger(1)],[q_dist_finger(2) q_ee_finger(2)],
    'b','LineWidth',2)
150 plot([q_dist_finger(1) q_cp_finger(1)],[q_dist_finger(2) q_cp_finger(2)],
    'b','LineWidth',2)
151 plot([q_ee_finger(1) q_cp_finger(1)],[q_ee_finger(2) q_cp_finger(2)],'b',
    'LineWidth',2)
152 plot(q_prox_finger(1),q_prox_finger(2),'r*')
153 plot(q_dist_finger(1),q_dist_finger(2),'r*')
154 plot(q_ee_finger(1),q_ee_finger(2),'r*')
155 plot(q_cp_finger(1),q_cp_finger(2),'r*')
156 axis equal
157 axis([-0.15 0.15 -0.3 0])
158 grid on
159
160 %thumb
161 q_prox_thumb = [base_width/2 ; -base_height ; 0]; %axis point of proximal
     joint in zero configuration
162 q_dist_thumb = [base_width/2 - leng_prox_fing*sin(theta1_th) ; -
    base_height-leng_prox_fing*cos(theta1_th) ; 0]; %axis point of distal
    joint in arbitrary configuration
163 q_ee_thumb = [base_width/2 - leng_prox_fing*sin(theta1_th) -
    leng_dist_fing*sin(theta1_th+theta2_th); -base_height - leng_prox_fing
    *cos(theta1_th) - leng_dist_fing*cos(theta1_th+theta2_th) ; 0]; %axis
    point of fingertip in arbitrary configuration
```

```
164 q_cp_thumb = [base_width/2 - leng_prox_fing*sin(theta1_th) - 0.02628*sin(
    theta1_th+theta2_th) - 0.01283*cos(theta1_th+theta2_th); -base_height
    - leng_prox_fing*cos(theta1_th) - 0.02628*cos(theta1_th+theta2_th) +
    0.01283*sin(theta1_th+theta2_th); 0]; %axis point of contact point in
    arbitrary configuration
165
166 plot([0 q_prox_thumb(1)],[0 q_prox_thumb(2)],'b','LineWidth',1)
167 plot([q_prox_finger(1) q_prox_thumb(1)],[q_prox_finger(2) q_prox_thumb(2)
    ],'b','LineWidth',1)
168 plot([q_prox_thumb(1) q_dist_thumb(1)],[q_prox_thumb(2) q_dist_thumb(2)],
    'b','LineWidth',2)
169 plot([q_dist_thumb(1) q_ee_thumb(1)],[q_dist_thumb(2) q_ee_thumb(2)],'b',
    'LineWidth',2)
170 plot([q_dist_thumb(1) q_cp_thumb(1)],[q_dist_thumb(2) q_cp_thumb(2)],'b',
    'LineWidth',2)
171 plot([q_ee_thumb(1) q_cp_thumb(1)],[q_ee_thumb(2) q_cp_thumb(2)],'b','
    LineWidth',2)
172 plot(q_prox_thumb(1),q_prox_thumb(2),'r*')
173 plot(q_dist_thumb(1),q_dist_thumb(2),'r*')
174 plot(q_ee_thumb(1),q_ee_thumb(2),'r*')
175 plot(q_cp_thumb(1),q_cp_thumb(2),'r*')
176
177 %speeds at contact point
178 cp_speeds = J_hand_func(theta1,theta2,theta1_th,theta2_th)*[theta1d;
    theta2d;theta1d_th;theta2d_th];
179 quiver(q_cp_finger(1),q_cp_finger(2),cp_speeds(1),cp_speeds(2),0.2)
180 quiver(q_cp_thumb(1),q_cp_thumb(2),-cp_speeds(4),-cp_speeds(5),0.2)
181
182 %object center and contact points
183 plot(x_obj,y_obj,'.g','MarkerSize',20); % the object center
184 plot(x_obj-obj_width*cos(gamma_obj),y_obj-obj_width*sin(gamma_obj),'.g','
    MarkerSize',20)
185 plot(x_obj+obj_width*cos(gamma_obj),y_obj+obj_width*sin(gamma_obj),'.g','
    MarkerSize',20)
186
187 %speed of box
188 quiver(x_obj,y_obj,x_objd,y_objd,0.2)
189
190 %plot the box
191 plot([x_obj+0.5*obj_width*cos(gamma_obj)-0.5*obj_height*sin(gamma_obj)
    x_obj+0.5*obj_width*cos(gamma_obj)+0.5*obj_height*sin(gamma_obj)],[
    y_obj+0.5*obj_width*sin(gamma_obj)+0.5*obj_height*cos(gamma_obj) y_obj
    +0.5*obj_width*sin(gamma_obj)-0.5*obj_height*cos(gamma_obj)],'g','
    LineWidth',1)
192 plot([x_obj-0.5*obj_width*cos(gamma_obj)-0.5*obj_height*sin(gamma_obj)
    x_obj-0.5*obj_width*cos(gamma_obj)+0.5*obj_height*sin(gamma_obj)],[
    y_obj-0.5*obj_width*sin(gamma_obj)+0.5*obj_height*cos(gamma_obj) y_obj
    -0.5*obj_width*sin(gamma_obj)-0.5*obj_height*cos(gamma_obj)],'g','
    LineWidth',1)
193 plot([x_obj-0.5*obj_width*cos(gamma_obj)+0.5*obj_height*sin(gamma_obj)
    x_obj+0.5*obj_width*cos(gamma_obj)+0.5*obj_height*sin(gamma_obj)],[
    y_obj-0.5*obj_width*sin(gamma_obj)-0.5*obj_height*cos(gamma_obj) y_obj
```

```
    +0.5*obj_width*sin(gamma_obj)-0.5*obj_height*cos(gamma_obj)],'g','
    LineWidth',1)
194 plot([x_obj+0.5*obj_width*cos(gamma_obj)-0.5*obj_height*sin(gamma_obj)
    x_obj-0.5*obj_width*cos(gamma_obj)-0.5*obj_height*sin(gamma_obj)],[
    y_obj+0.5*obj_width*sin(gamma_obj)+0.5*obj_height*cos(gamma_obj) y_obj
    -0.5*obj_width*sin(gamma_obj)+0.5*obj_height*cos(gamma_obj)],'g','
    LineWidth',1)
195
196 %plot the normal forces on the box
197 fc_real = pinv(J_hand_func(y_sol(13,k),y_sol(14,k),y_sol(15,k),y_sol(16,k
    )))'*Torques(:,k);
198 quiver(x_obj-0.5*obj_width*cos(gamma_obj),y_obj-0.5*obj_width*sin(
    gamma_obj),fc_real(1),0,0.03)
199 quiver(x_obj-0.5*obj_width*cos(gamma_obj),y_obj-0.5*obj_width*sin(
    gamma_obj),0,fc_real(2),0.03)
200 quiver(x_obj+0.5*obj_width*cos(gamma_obj),y_obj+0.5*obj_width*sin(
    gamma_obj),-fc_real(4),0,0.03)
201 quiver(x_obj+0.5*obj_width*cos(gamma_obj),y_obj+0.5*obj_width*sin(
    gamma_obj),0,-fc_real(5),0.03)
202
203 drawnow
204 movie(k) = getframe;
205 disp(['Progress: ',num2str(k),'/',num2str(length(tvec)-1)])
206 end
207
208 v = VideoWriter('VIDEO5_V.mp4','MPEG-4');
209 open(v);
210 writeVideo(v,movie([1 1:end]));
211 close(v);
212
213 %plot grasp quality
214 figure(8); clf
215 plot(tvec(2:end),GQM)
216 grid on
217 xlabel('Time [s]')
218 ylabel('Grasp Isotropy Index')
219 title('Grasp Quality Measure')
220 % NOTE: the grasp matrix G is assumed to be constante here, in reality
    this
221 % matrix changes as a result of changing contact points and orientations.
222
223 % plot states
224 figure(9); clf
225 subplot(2,3,1)
226 plot(tvec,y_sol(8,:))
227 grid on
228 xlabel('Time [s]')
229 ylabel('Y-position [m]')
230
231 subplot(2,3,2)
232 plot(tvec,rad2deg(y_sol(13,:)))
233 grid on
234 xlabel('Time [s]')
```

```
235 ylabel('\theta_1_f [deg]')
236
237 subplot(2,3,3)
238 plot(tvec,rad2deg(y_sol(15,:)))
239 grid on
240 xlabel('Time [s]')
241 ylabel('\theta_1_t_h [deg]')
242
243 subplot(2,3,4)
244 plot(tvec(1:end-1),constraint)
245 grid on
246 xlabel('Time [s]')
247 ylabel('Elements of constraint vector')
248
249 subplot(2,3,5)
250 plot(tvec,rad2deg(y_sol(13,:)))
251 grid on
252 xlabel('Time [s]')
253 ylabel('\theta_2_f [deg]')
254
255 subplot(2,3,6)
256 plot(tvec,rad2deg(y_sol(16,:)))
257 grid on
258 xlabel('Time [s]')
259 ylabel('\theta_2_t_h [deg]')
260
261 % plot torques
262 figure(10); clf
263 subplot(2,2,1)
264 plot(tvec(1:end-1),Torques(1,:))
265 hold on
266 plot(tvec(1:end-1),Torques_FC(1,:))
267 plot(tvec(1:end-1),Torques_FGC(1,:))
268 legend('Total','From FC','From FGC')
269 grid on
270 xlabel('Time [s]')
271 ylabel('T_1_f')
272
273 subplot(2,2,2)
274 plot(tvec(1:end-1),Torques(3,:))
275 hold on
276 plot(tvec(1:end-1),Torques_FC(3,:))
277 plot(tvec(1:end-1),Torques_FGC(3,:))
278 grid on
279 xlabel('Time [s]')
280 ylabel('T_1_t_h')
281
282 subplot(2,2,3)
283 plot(tvec(1:end-1),Torques(2,:))
284 hold on
285 plot(tvec(1:end-1),Torques_FC(2,:))
286 plot(tvec(1:end-1),Torques_FGC(2,:))
287 grid on
```

```
288 xlabel('Time [s]')
289 ylabel('T_2_f')
290
291 subplot(2,2,4)
292 plot(tvec(1:end-1),Torques(4,:))
293 hold on
294 plot(tvec(1:end-1),Torques_FC(4,:))
295 plot(tvec(1:end-1),Torques_FGC(4,:))
296 grid on
297 xlabel('Time [s]')
298 ylabel('T_2_t_h')
299
300 suptitle('Torques in the joints of the gripper')
301 %positive torques give gripping action
```

# Appendix F

# Function for integration of Computed Torque controller

```
function [ dydt , Torques , Torques_FC , Torques_FGC , constraint ] = f(t
    , y)

global G_eval
global mu m_block g

%renaming for in EoM
x_obj = y(7);
y_obj = y(8);
z_obj = y(9);
alpha_obj = y(10);
beta_obj = y(11);
gamma_obj = y(12);
x_objd = y(1);
y_objd = y(2);
z_objd = y(3);
alpha_objd = y(4);
beta_objd = y(5);
gamma_objd = y(6);
theta1 = y(13);
theta2 = y(14);
theta1_th = y(15);
theta2_th = y(16);
%extra inputs
theta1d = y(17);
theta2d = y(18);
theta1d_th = y(19);
theta2d_th = y(20);

%inputs, the required gripping force to lift the object
f_c1_1 = (1/mu)*0.5*m_block*g;
```

```
31 f_c1_2 = 0; %no force in y direction
32 f_c1_3 = 0; %no force in z direction
33 f_c2_1 = (1/mu)*0.5*m_block*g;
34 f_c2_2 = 0; %no force in y direction
35 f_c2_3 = 0; %no force in z direction
36 f_c = [f_c1_1;f_c1_2;f_c1_3;f_c2_1;f_c2_2;f_c2_3];
37
38 % CT controller
39 dots_des = zeros(16,1); %zero desired acceleration and speeds
40 s_des = [zeros(6,1) ; 0.0 ; -0.1854+0.01 ; 0 ; 0 ; 0 ; 0 ; deg2rad(-45) ;
       deg2rad(45) ; deg2rad(-45) ; deg2rad(45)]; %-0.0146
41 K_gain_p = 100; %gain for position error
42 K_gain_v = 10; %gain for velocity error
43 K = [K_gain_v*eye(6) K_gain_p*eye(6) zeros(6,4) ; zeros(6) zeros(6) zeros
       (6,4) ; zeros(4,6) zeros(4,6) zeros(4,4)];
44 big_F_eval = big_M_func(theta1,theta2,theta1_th,theta2_th)*(dots_des-K*(y
       (1:16)-s_des))-big_C_func(theta1,theta2,theta1d,theta2d,theta1_th,
       theta2_th,theta1d_th,theta2d_th)*y(1:16)+big_N_func(theta1,theta2,
       theta1_th,theta2_th);% + [0; +0.1*g; zeros(14,1)]; %the last term lets
        the controller think that the mass is higher
45
46 % Below the torques that correspond to the F_o are calculated
47 Torques_FC = J_hand_func(theta1,theta2,theta1_th,theta2_th)'*f_c; %
       Torques required to comply with the required friction cone
48 Torques_FGC = J_hand_func(theta1,theta2,theta1_th,theta2_th)'*pinv(G_eval
       )*big_F_eval(1:6); %Torques required to comply with the fundamental
       grasping constraint
49 Torques = Torques_FC + Torques_FGC;
50
51 dydt = pinv(big_M_func(theta1,theta2,theta1_th,theta2_th))*(big_F_func(T1
       ,T2,T1_th,T2_th,theta1,theta2,theta1_th,theta2_th)-big_N_func(theta1,
       theta2,theta1_th,theta2_th)+big_C_func(theta1,theta2,theta1d,theta2d,
       theta1_th,theta2_th,theta1d_th,theta2d_th)*y(1:16));
52 dydt(17) = dydt(13); %save the joint speeds for the next evaluation
53 dydt(18) = dydt(14);
54 dydt(19) = dydt(15);
55 dydt(20) = dydt(16);
56
57 % J*thetadot - G^T*xdot = 0. This is to check if the constraint is
       satisfied
58 constraint = J_hand_func(theta1,theta2,theta1_th,theta2_th)*dydt(13:16) -
        G_eval'*y(1:6)
59 end
```

# Bibliography


[1] G. Fantoni, D. Gabelloni, and J. Tilli, "Concept design of new grippers using abstraction and analogy," *Proceedings of the Institution of Mechanical Engineers, Part B: Journal of Engineering Manufacture*, vol. 227, no. 10, pp. 1521–1532, 2013.

[2] G. Fantoni, M. Santochi, G. Dini, K. Tracht, B. Scholz-Reiter, J. Fleischer, T. Kristoffer Lien, G. Seliger, G. Reinhart, J. Franke, H. Nørgaard Hansen, and A. Verl, "Grasping devices and methods in automated production processes," *CIRP Annals - Manufacturing Technology*, vol. 63, no. 2, pp. 679–701, 2014.

[3] SCHUNK GmbH Mobile Greifsysteme, "Mobile Gripping Systems- Tomorrow starts Today," *https://schunk.com/fileadmin/pim/docs/IM0012315.PDF, retrieved on 18-12-2017.*

[4] T. Takahashi, T. Tsuboi, T. Kishida, Y. Kawanami, S. Shimizu, M. Iribe, T. Fukushima, and M. Fujita, "Adaptive grasping by multi fingered hand with tactile sensor based on robust force and position control," in *Proceedings - IEEE International Conference on Robotics and Automation*, pp. 264–271, 2008.

[5] R. Suarez, M. Roa, and J. Cornella, "Grasp Quality Measures," *Systems Science*, vol. 24, no. 2, pp. 71–86, 2006.

[6] S. Baldi, P. Ioannou, and E. Mosca, "Discrete-time Adaptive Mixing Control with stability-preserving interpolation: The output regulation problem," in *IFAC Proceedings Volumes (IFAC-PapersOnline)*, vol. 18, pp. 102–107, 2011.

[7] K. J. Aström and B. Wittenmark, *Adaptive Control*, vol. 48. 1989.

[8] C. Zhang and R. Ordonez, *Extremum-Seeking Control and Applications, A Numerical Optimization-Based Approach.* Springer, 1 ed., 2012.

[9] K. B. Ariyur and M. Krstic, *Real-Time Optimization by Extremum-Seeking Control.* John Wiley & Sons, Inc, 2004.

[10] R. D. Howe, "Tactile Sensing and Control of Robotic Manipulation.," *Journal of Advanced Robotics*, vol. 8, no. 3, pp. 245–261, 1994.

[11] E. H. Grosse, C. H. Glock, and W. P. Neumann, "Human factors in order picking: a content analysis of the literature," *International Journal of Production Research*, vol. 55, no. 5, pp. 1260–1276, 2017.

[12] D. Battini, C. H. Glock, E. H. Grosse, A. Persona, and F. Sgarbossa, "Human energy expenditure in order picking storage assignment: A bi-objective method," *Computers and Industrial Engineering*, vol. 94, pp. 147–157, 2016.

[13] A. M. Mohan, "Labor shortages drive adoption of robotic carton loading," *Https://www.packworld.com/article/machinery/case-packing/case-packer/robotic-case-packer/labor-shortages-drive-adoption?utm_medium=Print&utm_source=pwgoto, retrieved on 19-08-2018*, 2018.

[14] T. Hebert, K. Valavanis, and R. Kolluru, "A Real-Time , Hierarchical , Sensor-Based Robotic System Architecture," *Journal of Intelligent and Robotic Systems*, no. 141640, pp. 1–27, 1998.

[15] GS1, "What we do," *https://www.gs1.org/about/what-we-do, retrieved on 13-08-2018.*

[16] GS1, "GS1 GPC standards June 2018," *https://www.gs1.org/standards/gpc/jun-2018, retrieved on 13-08-2018.*

[17] R. Lewis, "Development of a Universal E-commerce gripper," tech. rep., Fontys, 2017.

[18] C. C. Kessens and J. P. Desai, "Design, fabrication, and implementation of self-sealing suction cup arrays for grasping," in *Proceedings - IEEE International Conference on Robotics and Automation*, pp. 765–770, 2010.

[19] C. Huang, Y. Liu, and P. Yi, "Design and test of vacuum suction device for egg embryo activity sorting robot," *Nongye Gongcheng Xuebao/Transactions of the Chinese Society of Agricultural Engineering*, vol. 33, no. 16, pp. 276–282, 2017.

[20] A. M. Howard and G. A. Bekey, "Intelligent learning for deformable object manipulation," *Autonomous Robots*, vol. 9, no. 1, pp. 51–58, 2000.

[21] V. Duchaine, "Why Tactile Intelligence Is the Future of Robotic Grasping," *IEEE Spectrum, https://spectrum.ieee.org/automaton/robotics/robotics-hardware/why-tactile-intelligence-is-the-future-of-robotic-grasping, retrieved on 03-08-2018*, 2016.

[22] R. Hodson, "How robots are grasping the art of gripping," *Nature, https://www.nature.com/articles/d41586-018-05093-1, retrieved on 03-08-2018*, 2018.

[23] J. Sanchez, J. A. Corrales, B. C. Bouzgarrou, and Y. Mezouar, "Robotic manipulation and sensing of deformable objects in domestic and industrial applications: a survey," 2018.

[24] I. M. Bullock, T. Feix, and A. M. Dollar, "Workspace Shape and Characteristics for Human Two- and Three-Fingered Precision Manipulation," *IEEE Transactions on Biomedical Engineering*, vol. 62, no. 9, pp. 2196–2207, 2015.

[25] K. Shimoga, "Robot Grasp Synthesis Algorithms: A Survey," *The International Journal of Robotics Research*, vol. 15, no. 3, pp. 230–266, 1996.

[26] A. Bicchi, "Hands for dexterous manipulation and robust grasping: A difficult road toward simplicity," *IEEE Transactions on Robotics and Automation*, vol. 16, no. 6, pp. 652–662, 2000.

[27] R. Ozawa and K. Tahara, "Grasp and dexterous manipulation of multi-fingered robotic hands: a review from a control view point," 2017.

[28] M. Tichem, D. Lang, and B. Karpuschewski, "A classification scheme for quantitative analysis of micro-grip principles," *Assembly Automation*, vol. 24, no. 1, pp. 88–93, 2004.

[29] J. C. Trinkle, "On the Stability and Instantaneous Velocity of Grasped Frictionless Objects," *IEEE Transactions on Robotics and Automation*, vol. 8, no. 5, pp. 560–572, 1992.

[30] A. Bicchi and V. Kumar, "Robotic Grasping and Manipulation," *Ramsete Articulated and mobile robots for services and Technology*, vol. 270, pp. 55–74, 2001.

[31] S. Hogreve and K. Tracht, "Design and implementation of multiaxial force sensing gripper fingers," *Production Engineering*, vol. 8, no. 6, pp. 765–772, 2014.

[32] A. Wolf and H. Schunk, *Grippers in motion: The fascination of automated handling tasks*. 2018.

[33] A. Khurshid, A. Ghafoor, and M. A. Malik, "Robotic Grasping and Fine Manipulation Using Soft Fingertip," *Intech*, pp. 155–174, 2011.

[34] A. M. Okamura, N. Smaby, and M. R. Cutkosky, "An Overview of Dexterous Manipulation (Cited by: 203)," *The Hand*, vol. 1, no. April, pp. 255–262, 2000.

[35] R. R. Ma, A. Spiers, and A. M. Dollar, "M2 gripper: Extending the dexterity of a simple, Underactuated gripper," in *Mechanisms and Machine Science*, vol. 36, pp. 795–805, 2016.

[36] B. Ward-Cherrier, L. Cramphorn, and N. F. Lepora, "Tactile Manipulation With a TacThumb Integrated on the Open-Hand M2 Gripper," *IEEE Robotics and Automation Letters*, vol. 1, no. 1, pp. 169–175, 2016.

[37] S. Denei, P. Maiolino, E. Baglini, and G. Cannata, "Development of an Integrated Tactile Sensor System for Clothes Manipulation and Classification Using Industrial Grippers," *IEEE Sensors Journal*, vol. 17, no. 19, pp. 6385–6396, 2017.

[38] M. Cutkosky, R. Howe, and W. Provancher, "Handbook of Robotics, Chapter 19: Force and Tactile Sensors Chs.," *Handbook of Robotics*, no. November, p. 1611, 2007.

[39] A. Drimus, G. Kootstra, A. Bilberg, and D. Kragic, "Design of a flexible tactile sensor for classification of rigid and deformable objects," *Robotics and Autonomous Systems*, vol. 62, no. 1, pp. 3–15, 2014.

[40] J. Yin, V. J. Santos, and J. D. Posner, "Bioinspired flexible microfluidic shear force sensor skin," *Sensors and Actuators, A: Physical*, vol. 264, pp. 289–297, 2017.

[41] H. Yussof, J. Wada, and M. Ohka, "Object handling tasks based on active tactile and slippage sensations in a multi-fingered humanoid robot arm," in *Proceedings - IEEE International Conference on Robotics and Automation*, pp. 502–507, 2009.

[42] S. Teshigawara, T. Tsutsumi, S. Shimizu, Y. Suzuki, A. Ming, M. Ishikawa, and M. Shimojo, "Highly sensitive sensor for detection of initial slip and its application in a multi-fingered robot hand," in *Proceedings - IEEE International Conference on Robotics and Automation*, pp. 1097–1102, 2011.

[43] R. S. Johansson and G. Westling, "Roles of glabrous skin receptors and sensorimotor memory in automatic control of precision grip when lifting rougher or more slippery objects," *Experimental Brain Research*, vol. 56, no. 3, pp. 550–564, 1984.

[44] J. D. G. Fernández, J. C. Albiez, and F. Kirchner, "Bio-inspired robotic handling of heterogeneous logistics goods," in *Proceedings of the IEEE International Conference on Automation and Logistics, ICAL 2007*, pp. 192–197, 2007.

[45] R. Tomovic, G. Bekey, and W. Karplus, "A strategy for grasp synthesis with multifingered robot hands," *Proceedings. 1987 IEEE International Conference on Robotics and Automation*, vol. 4, pp. 83–89, 1987.

[46] J. R. Flanagan, M. C. Bowman, and R. S. Johansson, "Control strategies in object manipulation tasks," *Current opinion in neurobiology*, vol. 16, no. 6, pp. 650–659, 2006.

[47] M. a. Srinivasan, J. M. Whitehouse, and R. H. LaMotte, "Tactile detection of slip: surface microgeometry and peripheral neural codes.," 1990.

[48] J. Tegin and J. Wikander, "Tactile sensing in intelligent robotic manipulation âĂŞ a review," *Industrial Robot: An International Journal*, vol. 32, no. 1, pp. 64–70, 2005.

[49] R. S. Johansson and K. J. Cole, "Sensory-motor coordination during grasping and manipulative actions," *Current Opinion in Neurobiology*, vol. 2, no. 6, pp. 815–823, 1992.

[50] M. K. Burstedt, J. R. Flanagan, and R. S. Johansson, "Control of grasp stability in humans under different frictional conditions during multidigit manipulation.," *Journal of neurophysiology*, vol. 82, no. 5, pp. 2393–405, 1999.

[51] I. Birznieks, M. K. Burstedt, B. B. Edin, and R. S. Johansson, "Mechanisms for force adjustments to unpredictable frictional changes at individual digits during two-fingered manipulation.," *Journal of neurophysiology*, vol. 80, no. 4, pp. 1989–2002, 1998.

[52] P. Viviani and F. Lacquaniti, "Grip forces during fast point-to-point and continuous hand movements," *Experimental Brain Research*, vol. 233, no. 11, pp. 3201–3220, 2015.

[53] Y. Hiramatsu, D. Kimura, K. Kadota, T. Ito, and H. Kinoshita, "Control of precision grip force in lifting and holding of low-mass objects," *PLoS ONE*, vol. 10, no. 9, 2015.

[54] J. R. Flanagan and a. M. Wing, "The role of internal models in motion planning and control: evidence from grip force adjustments during movements of hand-held loads.," *The Journal of neuroscience : the official journal of the Society for Neuroscience*, vol. 17, no. 4, pp. 1519–1528, 1997.

[55] J. R. Flanagan and A. M. Wing, "The stability of precision grip forces during cyclic arm movements with a hand-held load," *Experimental Brain Research*, vol. 105, no. 3, pp. 455–464, 1995.

[56] J. R. Flanagan and A. M. Wing, "Modulation of grip force with load force during point-to-point arm movements," *Experimental Brain Research*, vol. 95, no. 1, pp. 131–143, 1993.

[57] D. M. Wolpert and J. Flanagan, "Motor prediction," *Current Biology*, vol. 11, no. 18, pp. R729–R732, 2001.

[58] Zexiang Li, P. Hsu, and S. Sastry, "Grasping and Coordinated Manipulation by a Multifingered Robot Hand," *The International Journal of Robotics Research*, vol. 8, no. 4, pp. 33–50, 1989.

[59] R. M. Murray, Z. Li, and S. S. Sastry, *A Mathematical Introduction to Robotic Manipulation*, vol. 29. 1994.

[60] G. Liu, J. Xu, X. Wang, and Z. Li, "On quality functions for grasp synthesis, fixture planning, and coordinated manipulation," *IEEE Transactions on Automation Science and Engineering*, vol. 1, no. 2, pp. 146–162, 2004.

[61] T. Yoshikawa, "Multifingered robot hands: Control for grasping and manipulation," *Annual Reviews in Control*, vol. 34, no. 2, pp. 199–208, 2010.

[62] M. A. Roa and R. Suárez, "Grasp quality measures: review and performance," *Autonomous Robots*, vol. 38, no. 1, pp. 65–88, 2014.

[63] R. Ball, "A Treatise on the Theory of Screws," *Cambridge University Press*, 1900.

[64] R. Brockett, "Robotic manipulators and the product of exponentials formula," *International Symposium on the Mathematical Theory of Networks and Systems*, 1983.

[65] S. Stramigioli, *Modern Robotics (Lecture slides)*. 2016.

[66] S. Ueki, H. Kawasaki, and T. Mouri, "Adaptive Coordinated Control of Multi-Fingered Robot Hand," *Journal of Robotics and Mechatronics*, vol. 21, no. 1, pp. 36–43, 2009.

[67] A. Delgado, C. A. Jara, D. Mira, and F. Torres, "A tactile-based grasping strategy for deformable objects' manipulation and deformability estimation," in *2015 12th International Conference on Informatics in Control, Automation and Robotics (ICINCO)*, vol. 02, pp. 369–374, 2015.

[68] A. Delgado, C. A. Jara, and F. Torres, "Adaptive tactile control for in-hand manipulation tasks of deformable objects," *Int J Adv Manuf Technol*, vol. 91, pp. 4127–4140, 2017.

[69] M. Kaboli, K. Yao, and G. Cheng, "Tactile-based manipulation of deformable objects with dynamic center of mass," in *IEEE-RAS International Conference on Humanoid Robots*, pp. 752–757, 2016.

[70] T. Wada, S. Hirai, H. Mori, and S. Kawamura, "Robust Manipulation of Deformable Objects Using Model Based Technique," in *Articulated Motion and Deformable Objects: First International Workshop, AMDO 2000, Palma de Mallorca, Spain, September 7-9, 2000. Proceedings*, pp. 1–14, 2000.

[71] L. Romdhane and J. Duffy, "Kinestatic Analysis of Multifingered Hands," *The International Journal of Robotics Research*, vol. 9, no. 6, pp. 3–18, 1990.

[72] Z. Li and S. S. Sastry, "Task-Oriented Optimal Grasping by Multifingered Robot Hands," *IEEE Journal on Robotics and Automation*, vol. 4, no. 1, pp. 32–44, 1988.

[73] J. Swevers, W. Verdonck, and J. De Schutter, "Dynamic model identification for industrial robots," *IEEE Control Systems Magazine*, vol. 27, no. 5, pp. 58–71, 2007.

[74] L. Sciavicco and B. Siciliano, *Modelling and Control of Robot Manipulators*. 2000.

[75] S. Baldi, *Adaptive and Predictive Control (Lecture notes SC4060)*. 2016.

[76] M. Benosman, *Learning-Based Adaptive Control: An Extremum Seeking Approach - Theory and Applications*. 2016.

[77] F. F. Khalil and P. Payeur, "Dexterous Robotic Manipulation of Deformable Objects with Multi-Sensory Feedback - a Review," *Robot Manipulators, Trends and Development*, pp. 587–621, 2010.

[78] N. McCrum, C. Buckley, and C. Bucknall, *Principles of polymer engineering*, vol. 39. 1988.

[79] V. L. Popov, "Contact Mechanics and Friction - Hertz force," *Contact Mechanics and Friction*, pp. 55–70, 2010.

[80] L. Zhang and R. Duuis, "Measurement and identification of dynamic properties of flexible polyurethane foam," *Journal of Vibration and Control*, vol. 1, no. 10, 2010.

[81] R. Ramsdale, "Reference Tables – Coefficient of Friction," *http://www.engineershandbook.com/Tables/frictioncoefficients.htm, retrieved on 15-08-18*.

[82] K. K. Singh, B. S. Reddy, A. C. Varshney, and S. Mangraj, "Physical and Frictional Properties of Orange and Sweet Lemon," *Applied Engineering in Agriculture*, vol. 20, no. 6, pp. 821–825, 2004.

[83] H. Culbertson, S. B. Schorr, and A. M. Okamura, "Haptics: The Present and Future of Artificial Touch Sensations," *Annu. Rev. Control Robot. Auton. Syst*, vol. 11225, no. 1, pp. 1–12, 2018.

# Glossary

## List of Acronyms

| | |
|---|---|
| **AC** | Adaptive Control |
| **APAs** | Anticipatory Postural Adjustments |
| **CM** | Center of Mass |
| **CNS** | Central Nervous System |
| **COP** | Center of Pressure |
| **DOA** | Degrees of Actuation |
| **DOF** | Degrees of Freedom |
| **ESC** | Extremum Seeking Control |
| **FGC** | Fundamental Grasping Constraint |
| **GPC** | Global Product Classification |
| **GQM** | Grasp Quality Measure |
| **MRAC** | Model Reference Adaptive Control |
| **SIR** | Smart Item Robotics |
| **TSU** | Transport Storage Unit |

## List of Symbols

| | |
|---|---|
| $n$ | Number of Fingers |
| $m$ | Number of Joints per Finger |
| $p_i$ | Contact point |
| $f_i$ | Contact force |
| $\tau_i$ | Torque around Center of Mass (CM) |
| $F_o$ | Object Wrench |
| $V_{CM}$ | Translational Velocity of CM |
| $\psi$ | Rotational Velocity of CM |
| $\zeta$ | Object Twist |
| $f$ | Contact Forces |
| $v$ | Contact Velocities |
| $r$ | Number of Contact Points per Finger |
| $T$ | Joint Torques |
| $\dot{\theta}$ | Joint Velocities |
| $J_h$ | Hand Jacobian |
| $G$ | Grasp Matrix |
| $H$ | Hand-Object Jacobian |
| $\omega_i$ | Rotational axis of finger $i$ |
| $q_{ij}$ | Position vector of joint $j$ of finger $i$ |
| $H$ | Homogeneous Matrix |
| $\tilde{\zeta}$ | Tilde Form of Twist |
| $\tilde{\omega}$ | Tilde Form of Wrench |
| $O$ | Object Reference Frame |
| $C_i$ | Contact Frame |
| $F_{C_i}$ | Wrench applied at $C_i$ |
| $B_{C_i}$ | Wrench Basis |
| $FC_{C_i}$ | Friction Cone Constraint |
| $f_t$ | Tangential Force |
| $\mu$ | Friction Coefficient |
| $f_n$ | Normal Force |

| | |
|---|---|
| $Ad_H$ | Adjoint Matrix Associated with Homogeneous Matrix $H$ |
| $P$ | Palm Frame |
| $\theta$ | Gripper Joint Angles |
| $T$ | Kinetic Energy |
| $V$ | Potential Energy |
| $M_g(\theta)$ | Gripper Inertia Matrix |
| $C_g(\dot{\theta}, \theta)$ | Gripper Coriolis and Centrifugal Matrix |
| $N_g(\theta)$ | Gripper Gravity |
| $M_o$ | Object Inertia Matrix |
| $C_o$ | Object Coriolis and Centrifugal Matrix |
| $N_o$ | Object Gravity |
| $\tilde{M}(q)$ | Combined Inertia Matrix |
| $\tilde{C}(q, \dot{q})$ | Combined Coriolis and Centrifugal Matrix |
| $\tilde{N}(q)$ | Combined Gravity |
| $\tilde{F}$ | Combined Wrench |
| $f_n$ | Reference Gripping Force |
| $\eta$ | Slip |
| $\sigma$ | Singular Value |
| $\mu_{stat}$ | Static Friction Coefficient |
| $\mu_{kin}$ | Kinetic Friction Coefficient |
| $K_p$ | Gain on Position Error |
| $K_v$ | Gain on Velocity Error |
| $J(z)$ | Measurement Function |
| $\gamma$ | Adaptation Gain |
| $F_n$ | Normal Force |
| $k$ | Penetration Stiffness |
| $b$ | Penetration Damping |
| $x_{pen}$ | Penetration |
| $\dot{x}_{pen}$ | Penetration Velocity |
| $F_f$ | Friction Force |